OPTICAL STUDIES OF THE GROWTH FROM SOLUTION OF SOME LONG-CHAIN ORGANIC CRYSTALS

Thesis presented for the degree of

Doctor of Philosophy

in the

University of London

by

PATRICIA MAY REYNOLDS

December 1956.

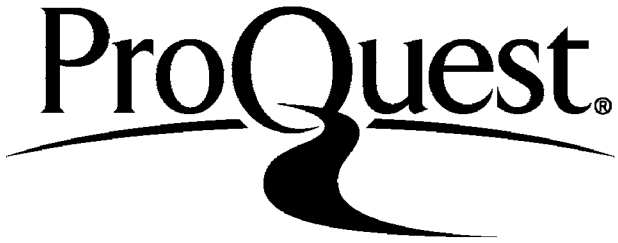

ABSTRACT

Growth patterns upon the (001) faces of crystals of stearic acid, $CH_3(CH_2)_{16}COOH$, and behenic acid $CH_3(CH_2)_{20}COOH$, are described. The crystals were grown from solution in chloroform at temperatures $\sim 268^{\circ}K$, and studied by optical, interferometric and electron microscopic techniques.

The crystals were found to be imperfect and to have grown by a spiral mechanism, in accordance with the theory proposed by Burton, Cabrera and Frank. Two independent methods were used to determine the height of the spiral steps. Interferometric measurements showed that the mean step-height was an integral multiple of $c \sin\beta$. There were four exceptions, in which the step-height was $\frac{1}{2} N c \sin\beta$, where N was an odd integer. Electron microscopic measurements on crystals of behenic acid revealed mainly bimolecular growth steps ($c \sin\beta$). Six examples of trimolecular steps ($\frac{3}{2} c \sin\beta$) were also found. These results showed that Frank's hypothesis that the normal component of the Burgers vector of a dislocation is equal to an interplanar spacing of the lattice was not always valid. An approximate calculation showed that many of these crystals had grown at supersaturations as low as 2%.

Evidence of unit slip and internal slip was given. It was shown that internal slip did not perfectly replicate the underlying surface structure; internal slip occurred through thicknesses as much as 1000 - 1500 A°. Patterns due to

internal slip also suggested that the dislocation lines were not necessarily parallel to the c-axis or perpendicular to (001).

The shape of the growth spirals was discussed. It was found to depend upon the crystal structure, the temperature at growth, and the inclination of the molecules to the basal plane.

It was shown that layer disorders occur in crystals of the fatty acids. These disorders were repeated by spiral growth, leading to polytypism or polysynthetic twinning, and characteristic interlaced growth patterns. The component layers were related by rotations through an angle $\phi = 180^\circ$, 106°, or 74°. When $\phi = 106^\circ$ or 74° the layers were in twinned orientation. Occasionally random values of ϕ occurred. This, together with observations of helicoidal crystals suggested that the dislocations were due to non-uniform distributions of stresses leading to buckle and shear of the thin crystal plates, as proposed by Frank.

To facilitate the comparison of the illustrations with the text, this thesis has been bound in two separate volumes. Volume I contains the text, and Volume II the illustrations.

CONTENTS : CHAPTERS

CONTENTS : SECTIONS

Page

Page

CHAPTER I.

THEORIES OF CRYSTAL GROWTH

1.1. Introduction.

The thermodynamical criteria which govern the nucleation of a crystalline phase from its vapour were derived by Gibbs [1] as early as 1878, but for many years the importance of this work was overlooked. The approach to the subject of crystal growth remained empirical, until some fifty years later when Stranski, [2,3] Kossel, [4] Becker and Doring, [5] and Volmer [6] introduced quantitative theories for the growth of a perfect homopolar crystal from its vapour. In 1949 these theories were critically re-examined by Burton, Cabrera and Frank [7] who proposed a new approach to the problem of crystal growth, which was based upon the concept of geometrical imperfections in real crystals. As the latter theory embodies many of the concepts and results of the earlier theories, it is proposed to briefly summarise the theory of the growth of a perfect crystal, and show how from it there developed the recent theory of the growth of an imperfect crystal.

1.2. Theory of the Growth of a Perfect Crystal.

A perfect crystal may be considered to be bounded by faces which are one of two types, low-index faces which are close-packed surfaces and perfectly plane, or high-index faces which are non-close packed surfaces and stepped; the

latter can also be regarded as formed from terraces which are sections of a close-packed face. Experimental observations show that whenever a crystal is in a supersaturated environment its high index faces are rapidly eliminated. The problem of the growth of a finite crystal therefore reduces to a consideration of the growth of its close-packed faces. Furthermore any incompleted, i.e. stepped, close-packed surfaces tend to extend to the boundary of the crystal face. Hence the rate of growth is governed by the rate at which fresh steps are created and advance on the close-packed faces. That is to say, in order that a crystal in a supersaturated environment may grow it is necessary to postulate a mechanism by which steps are continuously created upon its close-packed surfaces.

Frenkel[8] proposed that surface steps could result from thermodynamical fluctuations in surface level. Burton, Cabrera and Frank[7,9] have shown that this effect was only appreciable above a certain critical temperature, which, for close-packed surfaces on a simple or face-centred cubic crystal, was near or above the melting temperature. It is not therefore likely that fluctuations in surface level are significant in the growth of crystals from vapour or solution at ordinary temperatures, although they may be important in growth from the melt.

Observations on growing crystals by Volmer and

Estermann[10] suggested that the diffusion of molecules over the crystal surface played an important role in growth from the vapour. This hypothesis has since received theoretical confirmation. The structure of an infinite molecular step upon a crystal face has been discussed by Frenkel[8] and also by Burton, Cabrera and Frank[7,9] who showed that at finite temperatures the step would contain a high concentration of re-entrant angles or 'kinks' (see Fig.1) at which molecules would be preferentially deposited. The rate of growth of a step will depend upon the relative importance of the three methods by which a molecule may be deposited at a kink. Namely, direct deposition from the vapour, diffusion across the surface, and diffusion along step edges. According to Burton, Cabrera and Frank[7] the probability, $\frac{n}{n_o}$, that a molecule will be absorbed at a kink directly from the vapour is given by

$$\frac{n}{n_o} = \exp - \frac{Ws}{kT} \qquad \text{i)}$$

where W_s = energy of evaporation of a molecule from a kink.

k = Boltzmann constant

T = absolute temperature,

the mean distance, x_o , between kinks on a step in a close-packed direction was shown to be

Omitted sign

$$x_o \sim \frac{1}{2} a \exp \frac{w}{kT} \qquad \text{ii)}$$

where a = intermolecular distance

w = energy of formation of kink

and the mean displacement, x_s , of an absorbed molecule along the surface is given by

$$x_s = a \exp \frac{(W_s^1 - u_s)}{2kT} \qquad \text{iii)}$$

where W_s^1 = evaporation energy from the surface to the vapour per molecule.

and u_s = activation energy for diffusion.

Under typical experimental conditions at temperatures 0.5-0.8 times the boiling point it is estimated that

$\frac{W_s}{kT} \sim 12$, $\frac{W}{kT} \sim 2$, $\frac{W_s^1}{kT} \sim 12$, and $\frac{u_s}{kT} \sim 1.2$ (Mackenzie [20]).

Substitution of these values in the above formulae showed that

$$\frac{n}{n_o} \sim 10^{-6}$$

$$x_o \sim 4a$$

and $$x_s \sim 4 \times 10^2 a$$

It follows that in growth from the vapour the rate of arrival of molecules directly from the vapour is negligible compared with that due to surface migration.

The aggregation of adsorbed molecules into two-dimensional nuclei suggests a second method by which the steps necessary for continuous growth can be created upon the crystal surface. Under given conditions of supersaturation a two-dimensional nucleus will only have a finite probability of lateral extension if it exceeds a certain critical size. The energy of formation and critical size of a two-dimensional nucleus on the (001) face of a single Kossel cubic crystal

have been calculated by Becker and Doring[5], and their conclusions re-examined and revised by Burton, Cabrera and Frank[7,9]. In a crystal in which only nearest neighbour interactions need be considered, the activation energy, A_o, for the formation of a square nucleus of critical size, was shown to be given by

$$A_o = \frac{\phi^2}{kT \ln \alpha} \qquad \text{iv)}$$

where ϕ = energy of nearest neighbour interaction

α = supersaturation ratio.

and the length, ℓ, of the sides of the square critical nucleus by

$$\ell = \frac{a\phi}{kT \ln \alpha} \qquad \text{v)}$$

Assuming that $\frac{\phi}{kT} \sim 4$ (which is in accordance with the previous assumptions) for a supersaturation ratio $\alpha \sim 1.01$

$$\frac{A_o}{kT} = \frac{\phi^2}{(kT)^2 \ln \alpha} \sim 16 \times 10^2$$

hence $\frac{A_o}{kT} \gg \frac{u_s}{kT}$

and the activation energy for surface nucleation greatly exceeds that necessary for surface diffusion, resulting in a severe limitation upon the rate of growth. Equation iv) shows that the probability, $e^{\frac{-A_o}{kT}}$, for the formation of a two-dimensional nucleus of critical size is a very sensitive function of the supersaturation, but increases rapidly above

this value, when the rate of growth is no longer restricted by nucleation. Frank [11] estimates the critical supersaturation as 25-50%.

In contrast to the above theoretical considerations, Volmer and Schulze [12] have determined the rate of growth of crystals of napthalene, white phosphorous, and iodine from their vapours for different supersaturations at a temperature just below 0°C, and found finite growth rates at supersaturations as low as 3-4%. Furthermore, it is well known that in crystal growth quantitative results are seldom repeatable, even for apparently identical faces. Burton, Cabrera and Frank [7, 9] have proposed that these serious discrepancies can be explained if one realises that real crystals are seldom perfect.

1.3. The Imperfect Crystal.

Theoretical estimations of the strength of a perfect crystal indicate a critical tensile stress $\sim$ 0.1 Y, where Y is Young's modulus, and a critical shear stress $\sim$ 0.1 G, where G is the shear modulus. However, no macroscopic crystal has been found to possess this theoretical strength; the discrepancy may be several orders of magnitude. Griffith suggested that microscopic surface cracks would cause a reduction in mechanical strength, but X-ray investigations by Darwin indicated that real crystals are also internally disordered and have a mosaic structure. In 1934,

Taylor[16], Orowan[17] and Polanyi[18] were the first to attribute the mechanical weakness of crystalline solids to geometrical distortions of the perfect lattice which were termed 'dislocations'.

1.4. Definition of a Dislocation.

Consider a lattice plane in a perfect crystal; any path from one lattice point to the next (Fig.2) which forms a closed loop is termed a Burgers circuit. If the lattice is slightly deformed so that each lattice point can still be identified with its position in the perfect lattice, then to every Burgers circuit in the perfect lattice there corresponds a path in the deformed lattice. In general this path will be closed; when it fails to close it is said to surround a 'dislocation' in the deformed lattice. The vector required to close the path is defined as the Burgers vector of the dislocation. It is necessarily a lattice vector.

The lattice disorder which constitutes a dislocation is believed to have a lateral extension of a few atomic diameters. On a macroscopic scale a dislocation may be regarded as a line fault in the crystal. Since the Burgers vector of a dislocation line is invariant every line must either form a closed loop or terminate on the crystal surface.

The dislocation line, as defined above, can have any orientation with respect to its Burgers vector. Two important special cases arise when the dislocation line is

either perpendicular or parallel to its Burgers vector. Any dislocation can be expressed in terms of these two components.

1.5. The Edge Dislocation.

The edge dislocation, in which the dislocation line is perpendicular to the Burgers vector, was introduced by Taylor [16]. The special case in which the dislocation line terminates on crystal faces parallel to its Burgers vector is illustrated in Fig.3. Fig.4 shows the corresponding atomic disorder in a plane such as WXYZ, perpendicular to the dislocation line. In general the dislocation line will emerge upon faces inclined to its Burgers vector, and a terminated step occurs upon that face; the point of termination of the step marking the point of emergence of the pure edge dislocation, as shown in Fig.5.

1.6. The Screw Dislocation.

Burgers [19] first drew attention to the screw dislocation in which the dislocation line is parallel to its Burgers vector. Irrespective of whether the dislocation line is perpendicular or inclined to the surface upon which it emerges, a terminated step always occurs upon the crystal face. This is shown diagrammatically in Fig.6. Fig.7 shows the atomic arrangement in two successive lattice planes containing the dislocation line.

In general, it can be seen that whenever a dislocation, whether pure edge, pure screw, or compound emerges

upon a crystal face, there arises upon that face a terminated step whose height (measured perpendicular to the surface) is equal to the component of the Burgers vector perpendicular to the surface. The height of the step is equal to an interplanar spacing of the lattice. The necessary conditions for a step to terminate upon a crystal face are

i) a dislocation line emerging on the crystal face.

ii) a Burgers vector with a component normal to that face.

1.7. The Growth of an Imperfect Crystal from Vapour.

Frank [9] was the first to realise that dislocations might offer an explanation of the considerable discrepancies between observation and the current theory of the growth of a perfect crystal. The presence of a terminated step, due to the emergence of a dislocation upon the crystal face, provides a continuous site for the deposition of molecules and obviates the necessity for two-dimensional nucleation.

As in the case of the perfect crystal, the terminated step will generally contain kinks which will form sites at which molecules adsorbed and diffusing on the crystal surface will be preferentially deposited. However, this step is fixed at the point of emergence of the dislocation and can only advance by rotation about the dislocation point. Frank [9] has shown that, in growth from the vapour under steady conditions of supersaturation, the terminated step will assume a spiral form. When the velocity of advance is

independent of crystallographic orientation, each point of the step will initially advance with the same velocity. The section of the step nearest the dislocation will have the highest angular velocity and the step will develop a curvature which is greatest towards the centre. According to Burton, Cabrera and Frank [7], the radial velocity of advance, v_ρ, of a curved step, is related to its radius of curvature, ρ, by the equation

$$v_\rho = v_\infty \left(1 - \frac{\rho_c}{\rho}\right) \qquad \text{(vi)}$$

where v_∞ = velocity of advance of a straight step.
and ρ_c is the radius of the critical nucleus given by

$$\rho_c = \frac{a\phi}{2kT \ln \alpha} \qquad \text{(vii)}$$

It is apparent that as the curvature of the step increases its radial velocity of advance will decrease. The initial growth of the step will then be as shown in Fig.8. Eventually a steady state is reached when all sections of the step have the same angular velocity and the step has the spiral form of Fig.9. The distance, Y_o, between successive turns of the spiral at large distances from the growth centre ($r > \frac{1}{r^2}$) was estimated as

$$Y_o = 4\pi\rho_c \qquad \text{(viii)}$$

The same general formulae were expected to apply when the exchange of molecules between step and surface was slow, or if the velocity of advance depended upon the

orientation of the step. The critical nucleus would then be rectilinear, ρ_c half the diameter of the critical nucleus appropriately orientated and v_∞ the velocity in a slow-growing, close-packed direction.

It was also shown by Burton, Cabrera and Frank [7], that when two or more dislocations emerge upon a crystal face, the growth will depend upon the supersaturation and the separation of the dislocation centres. Two equal dislocations of opposite sign emerging near the centre of a crystal face cause continuous growth if the supersaturation is such that the critical nucleus (correctly orientated) will pass between them. Growth fronts in the form of closed loops then occur Fig.10 , with a separation of $\sim 4\pi\rho_c$ between successive loops. A pair of dislocations of like sign give a more complex situation, the growth patterns depending upon whether the separation of the dislocations is greater or less than $2\pi\rho_c$. The predicted growth patterns are illustrated in Figs. 11 and 12. Fig.13 shows the growth from a group of like dislocations of the same sign separated by a distance $< 2\pi\rho_c$.

1.8. Growth of an Imperfect Crystal from Solution.

The theory outlined above applies only to growth from the vapour, but in a qualitative approach there are no essential differences between growth from vapour or solution. In solution the diffusion of solute molecules towards kinks,

either through the solution or along the surface and step edges is expected to be much slower than on the free surface of the crystal. Consequently the velocity of advance of a step will depend upon its orientation, and rectilinear spirals will occur.

The quantitative theory of growth from solution is more difficult. According to Burton, Cabrera and Frank [7] the formula

$$Y_o = 4\pi\rho_c \qquad \text{viii)}$$

will still be approximately valid. If it is assumed that diffusion on the surface and in the step edge can be neglected

$$\rho_c = \frac{a\phi}{2kT\,\sigma(x_o)} \qquad \text{ix)}$$

where $\sigma(x_o)$ is a complicated function of the supersaturation and the mean distance between kinks x_o.

1.9. Growth from Melt.

It is possible, but not certain, that similar considerations apply to growth from the melt. In this case, the influence of thermodynamical fluctuations in surface level is probably significant, and the activation energy for two-dimensional nucleation lower than for growth from the vapour.

REFERENCES

1) GIBBS, J.W. Collected Works (1928) p.325 footnote. (London: Longman Green and Co.).

2) STRANSKI, I.N. Z. Phys. Chem. 136 259 (1928)

3) STRANSKI, I.N., and KAISCHEW, R. Z. Phys. Chem. B 26. 31. (1934)

4) KOSSEL, W. Nachr. Ges. Wiss. Gottingen, 135 (1927)

5) BECKER, R., and DORING, W. Ann. Phys. Lpz. 24 719 (1935)

6) VOLMER, M. Kinetik der Phasenbildung. (1939) Dresden and Leipzig. Steinkopff.

7) BURTON, W.K., CABRERA, N. and FRANK, F.C. Phil. Trans. Roy. Soc. (London) A 243 299 (1951)

8) FRENKEL, J. J. Phys. U.S.S.R. 9 392 (1945).

9) BURTON, W.K., CABRERA, N. and FRANK, F.C. Disc. Farad Soc. No. 5. (1949)

10) VOLMER, M., and ESTERMANN, I. Z. Phys. 7 13 (1921)

11) FRANK, F.C., Advances in Physics 1 91 (1952)

12) VOLMER, M., and SCHULTZE, W. Z. Phys. Chem. A 156, 1, (1931)

13) GRIFFITH, A.A. Phil. Trans. Roy. Soc. A. 221 163 (1921)

14) DARWIN, G.C. Phil. Mag. 27 315, 675 (1914)

15) DARWIN, G.C. Phil. Mag. 43 800 (1921)

16) TAYLOR, G.I. Proc. Roy. Soc. A. 145 362 (1934)

17) OROWAN, E. Z. Phys. 89 605, 614, 634 (1934)

18) POLANYI, M. Z. Phys. 89 660 (1934)

19) BURGERS, J.M. Proc. Kon. Ned. Akad. Wet. 42 293, 378 (1939)

20) MACKENZIE, J.K. Thesis. Bristol (1950).

CHAPTER II.

RECENT EXPERIMENTAL RESULTS OF CRYSTAL GROWTH

When the dislocation theory of crystal growth was introduced, Burton, Cabrera and Frank seem to have been unaware of existing reports by Mellor[21] as well as Menzies and Sloat[22] of spiral markings upon carborundum crystals. It was thought that many improvements in optical or electron microscope techniques would be necessary before growth spirals could be observed. In 1950, however, Griffin[23] described steps, revealed by a metallurgical microscope, upon the $(10\bar{1}0)$ faces of beryl crystals. The exact height of these steps could not be evaluated but was certainly less than 34 Å. Some of these steps had a spiral form and it was inferred that their point of termination marked the point of emergence of a 'screw' dislocation.

During the following year Dawson and Vand[24,25] published electron-micrographs of rectilinear spirals upon crystals of n-hexatriacontane, $C_{36}H_{74}$, grown from solution in petroleum ether. The steps were shadowcast and their height found to be equal to the c-spacing of the lattice. Verma[26-29] and Amelinckx[30,31] reported optical observations of spiral patterns upon the basal planes of silicon carbide crystals. Measurements of the step-heights by multiple-beam interferometry showed that some were equal to the c-spacing but others were multiples of this distance. In addition 'inter-

laced' spirals were observed in which portions of the step were only 7 Å high, i.e. half the c-spacing. Spirals of large Burgers vector were also found upon the (0001) faces of cadmium iodide by Forty [32]. A cine-film of the development of closed loops was obtained.

The interactions between curvilinear spiral growth fronts were found to closely agree with the theoretical predictions. Rectilinear spirals, in which the growth edges were parallel to close-packed planes were also observed. Verma [27] estimated from the spacing between successive turns of spirals upon silicon carbide that growth had occurred at supersaturations ~ 0.2%.

In 1952 there were many reports of growth spirals upon crystal faces. The most notable were those upon the basal plane of n-hectane, $C_{100}H_{202}$, grown from solution (Dawson [33]); (0001) faces of magnesium and cadmium (Forty [34, 35]); prism faces of fluor-apatite (Amelincx [36]); and the (111) faces of haematite (Verma [37, 38]). Many qualitative accounts of 'growth spirals' also appeared (Ref. 39 - 53), in which the height of the spiral step was not accurately known and frequently the structure of the spiral was not clearly resolved.

The theory put forward by Burton, Cabrera and Frank dealt with the growth of homopolar crystals from the vapour phase. Growth spirals were now reported upon the slower

growing faces of crystals bound by homopolar, van der Waals, ionic and metallic forces. These crystals had grown from vapour, from solution, by electrolytic deposition, and by precipitation, as well as under natural conditions.

This was the extent of experimental confirmation of the dislocation theory of crystal growth at the beginning of the present work. The above results indicated that dislocations of UNIT Burgers vector normal to the surface occurred in silicon carbide, n-hectane, n-hexatriacontane, magnesium, fluor-apatite and haematite. Only for silicon carbide was there precise evidence of dislocations of MULTIPLE Burgers vector, although observations of clearly visible spirals upon several crystals indicated dislocations of large Burgers vector. An unexpected result was the occurrence of 'interlaced' spirals upon polytypes of silicon carbide and biotite (Amelinckx [54]). It appeared that there was a close connection between the Burgers vector of the dislocation and the polytypism of the crystal. Forty [55, 56] had also reported interlacing upon another layer-type crystal, cadmium iodide. Here the spiral step-heights were found to be multiples of half the c-spacing.

Amongst the organic crystals spiral growth had been reported on n-hexatriacontane, n-hectane, salol (Amelinckx [41]) and graphite (Horn [47-48]). Brandstatter [46] had observed the growth and effects of temperature upon spirals and layers

on a number of organic crystals grown from vapour on a hot-stage microscope, but had not made any accurate measurements. Exact measurements were only available for n-hexatriacontane and n-hectane, in which all the dislocations were found to have unit Burgers vector. Except in the case of these latter substances all observations were made with optical microscopes.

In view of the paucity of quantitative information upon the growth of organic crystals it seemed desirable that a further study should be undertaken. Long-chain crystals, in which the thickness of a bimolecular layer was $\sim$ 50 Å, seemed to offer an opportunity to distinguish between unimolecular and bimolecular steps by using the techniques of multiple-beam interferometry. The purpose of the present work was threefold:

i) to establish whether spiral growth occurred in crystals of the fatty acids.

ii) to determine the elevation of the spiral steps, and their relationship to the crystal structure.

iii) to investigate whether 'interlaced' growth patterns occurred upon crystals of the fatty acids.

Initially optical and interferometric techniques were employed to study crystals of stearic and behenic acid. Towards the end of the investigation an electron microscope became available and it was possible to extend this study. In the following chapters the crystal structure of these fatty

acids and the experimental techniques which were used to to study their growth will be described.

REFERENCES

21) MELLOR, J.W. — A comprehensive treatise on Inorganic and Theoretical Chemistry. Vol.5. (1924) P.879.

22) MENZIES, A.W.C., and SLOAT, C.A. — Nature (Lond) 123 348 (1929)

23) GRIFFIN, L.G. — Phil. Mag. 41 196 (1950)

24) DAWSON, I.M., and VAND, V. — Nature (Lond) 167 476 (1951)

25) — Proc. Roy. Soc. A 206 555 (1951)

26) VERMA, A.R. — Nature (Lond) 167 939 (1951)

27) — Phil. Mag. 42 1005 (1951)

28) — Nature (Lond) 168 430 (1951)

29) — Nature (Lond) 168 783 (1951)

30) AMELINCKX, S. — Nature (Lond) 167 739 (1951)

31) — Nature (Lond) 168 431 (1951)

32) FORTY, A.J. — Phil. Mag. 42 670 (1951)

33) DAWSON, I.M. — Proc. Roy. Soc. A. 214 72 (1952)

34) FORTY, A.J. — Phil. Mag. 43 481 (1952)

35) — Phil. Mag. 43 949 (1952)

36) AMELINCKX, S. — Nature (Lond) 169 841 (1952)

37) VERMA, A.R. — Nature (Lond) 169 540 (1952)

38) — Proc. Phys. Soc. (Lond) B 65 806 (1952)

39) AMELINCKX, S. — Phil. Mag. 43 562 (1952)

40) — C. Rendus. (Paris) 234 971 (1952)

41) — Naturwiss. 39 547 (1952)

42)	AMELINCKX, S.	Nature (Lond)	170	760	(1952)
43)		Nature (Lond)	169	580	(1952)
44)		Comptes Rendus	234	1793	(1952)
45)	AMELINCKX, S., GROSJEAN, C.C., DEKEYSER, W.	Comptes Rendus	234	113	(1952)
46)	BRANDSTATTER, M.,	Zeitschr. fur Electrochemie	56	968	(1952)
47)	HORN, F.H.	Nature (Lond)	170	581	(1952)
48)	"	Phil. Mag.	43	1210	(1952)
49)	SEAGER, A.F.	Nature (Lond)	170	425	(1952)
50)	STEINBERG, M.A.	Nature (Lond)	170	1119	(1952)
51)	WEIL, A.R.	Comptes Rendus	235	256	(1952)
52)		Comptes Rendus	234	1068	(1952)
53)	WILLIS, B.T.M.	Nature (Lond)	170	115	(1952)
54)	AMELINCKX, S.	Natuurwet. Tijdschr.	34	73	(1952)
55)	FORTY, A.J.	Phil. Mag.	43	72	(1952)
56)		Phil. Mag.	43	377	(1952)

CHAPTER III.

THE CRYSTAL STRUCTURE OF SATURATED FATTY ACIDS

3.1. Introduction.

The saturated fatty acids form a homologous series of aliphatic compounds characterised by the formula $CH_3(CH_2)_n$ COOH. Each molecule may be regarded as composed of two parts, a long chain $CH_3(CH_2)_n$—— and an end group —— COOH. These substances crystallize in the form of fine-grained flaky powders. When the crystals are grown upon a substrate such as glass they tend to become orientated with the flake surface parallel to the surface of the substrate. The basal plane of the crystal is found to coincide with the flake surface.

The crystal structure of the fatty acids has been extensively investigated, beginning in 1923 with the work of Muller [57]. Successive workers have commented upon the difficulty of producing large single crystals of these substances. Consequently a majority of the X-ray diffraction studies have been devoted to polycrystalline layers upon substrates such as glass and metal foils. Prior to the recent work of Vand, Morley and Lomer [58] and also von Sydow [59-66] the only single crystal which had been analysed was of stearic acid, $CH_3(CH_2)16$ COOH, by Muller [67].

3.2. General Structure.

The results of the earlier work upon polycrystalline layers of fatty acids may be summarised as follows :

The fatty acids form molecular crystals; the molecules being arranged with their long axes all parallel and inclined to the basal plane at a constant angle. The a and b spacings are approximately constant for all members of the series. Laterally the molecules are close-packed and bound by residual van der Waals forces. Lengthwise the molecules are associated in pairs by hydrogen bonding at the carboxyl groups. The chain axis is parallel to the c-axis, hence the long-spacing, $c \sin\beta$, increases with the number of CH_2 groups in the molecule.

This general description is valid for all fatty acid crystals. However, Garner and Ryder[68] and also Francis, Piper and Malkin[69] have shown that if the long-spacing is plotted against the carbon content of the chemical molecule, the increment in chain length per carbon atom is different for acids containing an even number of carbon atoms and those containing an odd number of carbon atoms. Muller[70] and Malkin[71] have attributed this behaviour to the difference in packing of the —— COOH end groups necessitated by the geometry of the long chains.

In addition, the work of de Boer[72], Thibaud[73], and Francis, Piper and Malkin[69] has shown that the fatty acids are polymorphic. The polymorphic forms of the even acids are usually designated A, B and C, and of the odd acids A^1, B^1, C^1 and D^1, in order of decreasing long-spacing. The poly-

morphic forms differ primarily in the tilt of the chain axes relative to the basal plane. Fig.14, taken from a paper by Francis, Piper and Malkin [69], shows the relationship between the long-spacings of the different polymorphs and the carbon content of the chemical molecule.

The particular polymorphic form obtained in any preparation appears to depend upon the method of preparation, the temperature, and the purity of the material. Amongst the even acids the A-form is extremely rare, growth from non-polar solvents tends to produce the B-form, whilst growth from polar solvents or melt favours the appearance of the C-form. The C-form is the most stable. Irreversible transitions A $\longrightarrow$ C and B $\longrightarrow$ C have been reported as the temperature of the crystals is raised (Stenhagen and von Sydow [74]).

Since the present study has been entirely devoted to even fatty acids only the structure of these crystals will be described in detail. At present the only even fatty acids which have been fully analysed are the C-form of lauric acid, $CH_3(CH_2)_{10}COOH$ (Vand, Morley and Lomer [58]); the B-form of stearic acid, $CH_3(CH_2)_{16}COOH$ (Muller [67] and von Sydow [61, 64]); and the A-form of lauric acid (von Sydow [65]). The structures of behenic acid, and the A and C forms of stearic acid have not been studied in detail. Since the even fatty acids form such a closely related series it can be assumed that similar polymorphs of adjacent acids have similar structures.

3.3. The Structure of the B-form of Stearic Acid.

The results obtained by Muller [67] and von Sydow [62, 64] are compared in Table I. The unit cell is monoclinic.

	Muller	von Sydow
a	5.546 Å	5.591 ± 0.011 Å
b	7.381 Å	7.404 ± 0.008 Å
c	48.84 Å	49.38 ± 0.10 Å
β	116°21'	117°22' ± 7'
c sinβ	43.76 Å	43.85 ± 0.05 Å
No. of molecules in unit cell.	4	4
Space Group	C_{2h}	C_{2h}^5 - $P2_1/a$
(Calculated)	73°50'	74°6'

TABLE I.

The crystal molecule has a zig-zag chain of carbon atoms which is approximately planar. The chain deviates slightly from the ideal model of carbon atoms with diameter 1.54 Å (of diamond) linked at the tetrahedral angle 109°30'; this is probably due to lateral compression in the crystal. Fig.15 is an electron-density projection along the a-axis showing the packing of the hydrocarbon chains. The arrangement of successive layers of molecules is shown in projection in Fig.16. It may be seen that the c-spacing corresponds to the length of two molecules

associated by hydrogen bonds, and that the chain planes of these two molecules are parallel.

All hydrocarbon chains have their centrelines in (110) and ($1\bar{1}0$), hence the monoclinic angle, β , is a measure of the tilt of the chain axes relative to the basal plane. Half of the molecules have their chain planes almost in (110) and the other half have their chain planes almost in ($1\bar{1}0$). This affects the macrocrystalline shape. The faces of the crystals are usually (110), ($1\bar{1}0$) and (001), giving rhombic plates (Fig.17) in which the b-axis bisects the acute edge angle $\Psi \simeq 74^{\circ}$.

Twinning is very common.

3.4. <u>The Structure of the C-form of Lauric Acid.</u>

The unit cell is monoclinic with space group $C_{2h}^{5} - P2_1/a$

a =	9.524	±	0.02 Å
b =	4.965	±	0.01 Å
c =	35.39	±	0.07 Å
β =	$129^{\circ}13'$	±	$1'$
Ψ (calculated) =	$55^{\circ}\ 4'$		

There are ~~few~~ four molecules per unit cell.

The monoclinic angle β is greater than in the B-form of stearic acid, indicating that the chain axes are more steeply inclined to the basal plane. Otherwise the two structures are very similar. The chain planes of the molecules are approximately in (110) or ($1\bar{1}0$), and associated

pairs of molecules have their chain planes parallel. Figs.18 and 19 show the structure in projection. The packing of the carboxyl groups is shown in Fig.20. In lauric acid the hydrocarbon chain appears to be slightly bent. It can be assumed that in the higher members of this crystal form the chain axis is strictly linear.

The faces of the crystal are generally (110), $(1\bar{1}0)$ and (001), again giving rhombic plates (Fig.21). The b-axis bisects the obtuse edge angle and $\Psi \approx 56^{\circ}$.

Twinning is very common.

3.5. The Structure of the A-form of Lauric Acid.

Lomer [75] recently determined the unit cell dimensions of the A-form of lauric acid from X-ray powder photographs and concluded that the crystal was monoclinic. A more complete investigation by von Sydow [65] using rotation and Weissenberg photographs of a single crystal lead to the conclusion that this form is triclinic with space group $C_i^1 - P\bar{1}$ For convenience in describing the structure it was referred to the centred cell $C_i^1 - A\bar{1}$. The following data were given

$a = 5.41 \pm 0.01$ Å

$b = 26.27 \pm 0.07$ Å

$c = 35.42 \pm 0.13$ Å

$\alpha = 69^{\circ}36' \pm 30'$

$\beta = 113^{\circ}9' \pm 26'$

$\gamma = 121^{\circ}21' \pm 24'$

The structure is shown in projection in Fig.22. There are twelve molecules in the A-centred cell, arranged in dimers.

The carboxyl groups and methyl groups appear in the same planes in the crystal. All chain planes are parallel. This molecular arrangement affects the macrocrystalline shape as well as the cleavage properties of the crystal, since there are equal binding forces (hydrogen bonds and van der Waals forces) in every layer. Hence the A-form of lauric acid crystallises in elongated parallelopipeds. Its cleavage is difficult.

There is no evidence of twinning.

3.6. The Unit Cell of the C-form of Stearic Acid.

The results of the more recent determinations of the unit cell dimensions of the C-form of stearic acid are tabulated below.

a Å	b Å	c sin β Å	β	Reference.
9.46	4.96	39.85	126° 38'	(76)
9.357 ± 0.020	4.956 ± 0.004	39.87 ± 0.04	128° 14'	(77)
9.11 ± 0.04	4.82 ± 0.04	—	—	(78)
9.15	4.85	—	—	(79)

TABLE II.

The a parameter is definitely smaller than for the c-form of lauric acid, and the monoclinic angle β also somewhat less. Vand, Aitken and Campbell[80] have pointed out that long-chain compounds are not exactly homologous but all dimensions change

continuously with chain length. This change is, however, relatively small and it can reasonably be assumed that the C-forms of stearic and lauric acid are homologous.

3.7. The Unit Cell Dimensions of Behenic Acid.

Despite an extensive search through the literature no record of the a and b dimensions of the unit cell of the B-form of behenic acid has been found. Francis, Collins and Piper [21] reported

$$c \sin\beta = 52.95 \text{ Å}$$

A recent determination of the dimensions of the C-form of behenic acid by Abrahamsson and von Sydow [77] gave

$$a = 9.299 \pm 0.020 \text{ Å}$$

$$b = 4.953 \pm 0.004 \text{ Å}$$

$$c \sin\beta = 48.22 \pm 0.04 \text{ Å}$$

$$\beta = 127^{\circ}37'$$

REFERENCES

57) MULLER, A. J. Chem. Soc. 123 2043 (1923).

58) VAND, V., MORLEY, W.M., and LOMER, T.R. Acta. Cryst. 4 324 (1951)

59) VON SYDOW, E. Acta. Cryst. 7 529 (1954)

60) Acta. Cryst. 7 591 (1954)

61) Acta. Cryst. 7 823 (1954)

62) Acta. Cryst. 8 557 (1955)

63) Acta. Cryst. 8 810 (1955)

64) Acta. Cryst. 8 846 (1955)

65) Acta. Chemica Scandinaviea. 10 1 (1956)

66) Arkiv. fur Kemi 9 231 (1956)

67) MULLER, A. Proc. Roy. Soc. A 114 542 (1927)

68) GARNER, W.E. and RYDER, E.A. J. Chem. Soc. 721 (1925)

69) FRANCIS, F., PIPER, S.H. and MALKIN, T. Proc. Roy. Soc. A. 128 214 (1930)

70) MULLER, A. Proc. Roy. Soc. A. 124 317 (1929)

71) MALKIN, T. Nature. 127 126 (1931)

72) de BOER, G.M. Nature. 119 50 (1927)

73) THIBAUD, J. Comptes Rendus 184 96 (1927)

74) STEMHAGEN, E. and VON SYDOW, E. Arkiv fur Kemi 6 309 (1953)

75) LOMER, T.R. Nature. 176 653 (1953)

76) SCHOON, T. Zeit fur Physik Chemie B 39 385 (1938)

77) ABRAHAMSSON, S., and VON SYDOW, E. Acta. Cryst. 7 591 (1954)

78) ANDERSON, N.G., and DAWSON, I.M. Proc. Roy. Soc. A. 218 255 (1953)

79) TRILLAT, J.J., and HERSCH, Th. V. Comptes Rendus 195 215 (1932)

80) VAND, V., AITKEN, A., and CAMPBELL, R.K. Acta Cryst. 2 398 (1949)

81) FRANCIS, F., COLLINS, F.J.E., and PIPER, S.H. Proc. Roy. Soc. A. 158 691 (1937)

CHAPTER IV.

THE PREPARATION OF CRYSTALS AND THEIR OPTICAL PROPERTIES.

4.1. Materials.

Samples of pure stearic acid, $CH_2(CH_3)_{16}$ COOH, and behenic acid, $CH_2(CH_3)_{20}$ COOH, were kindly supplied by Price's (Bromborough) Ltd., The acids were subjected to repeated fractional distillation until temperature and pressure data and analytical characteristics indicated that the minimum purity was 99.5%. The characteristics of the acids were given as follows:

Stearic Acid.

Molecular weight	284.1
Iodine value	0.2
Unsaps	< 0.1%
Melting point	69.6°C.

Behenic Acid.

Molecular weight	340.2
Iodine value	0.01
Melting point	79.5°C.

The melting point of the stearic acid is 0.3°C lower than that generally quoted in the literature, but closely agrees with the value recently reported by Anderson and Dawson [82] and Stenhagen and Von Sydow [74]. Similarly the melting point of the behenic acid is 0.5°C. lower than

the generally accepted value. It seems unlikely that this indicates any serious impurity in the behenic acid since the iodine value is low. Also recent determinations of the melting point of stearic acid suggest that earlier values of the melting point of fatty acids are rather high.

4.2. The Preparation of Crystals of Stearic and Behenic Acid.

As previously stated the polymorphs obtained in any preparation depend upon the temperature and polarity of the solvent. Fortunately fatty acid crystals usually have a simple habit and it is possible to identify the polymorphic form of a single crystal by inspection under a microscope.

Single crystals with dimensions greater than 10^{-2} cm. could seldom be obtained. When larger crystals were occasionally obtained their surface structure was found to be too complex to be resolved with an optical microscope, and the crystals too thick for direct examination with an electron microscope. The factors which determined the most suitable method of preparation of crystals for examination with an optical microscope, were firstly the thickness of the crystals and secondly the regularity and spacing of the growth steps. It will be seen later that the thickness of the crystal should be less than 5λ if internal interference fringes, formed by reflexion between the (001) faces, are to be used. Furthermore the surface structure should be clearly resolved if ambiguities in interpretation of the growth sequence are to be avoided.

Crystals for direct examination with an electron microscope must be less than $\sim$ 2000 Å in thickness. Thicker crystals heavily absorb the incident electron beam and the specimen temperature increases. Phase changes, and even melting of the specimen then occur. The limitations imposed by the resolution of the instrument are relatively unimportant, since the electron microscope used in this study had an instrumental resolution $\sim$ 50 - 25 Å.

Growth from the melt was found to produce crystals with a very irregular surface structure. Only growth from solution produced crystals which satisfied the above conditions. Several different solvents such as carbon disulphide, petroleum ether, benzene and chloroform were tested. The most suitable solvent was found to be chloroform.

The crystals were prepared by the following method:

A solution of the acid in chloroform (concentration 0.3% by weight) was contained in a glass syringe (Fig.23). The substrate upon which the crystals were to be deposited was enclosed in a brass vessel, in which an almost saturated atmosphere of the solvent was maintained. This vessel communicated with the atmosphere through tubes containing calcium chloride which prevented water vapour entering the apparatus. As an additional precaution a side tube containing phosphorus pentoxide was also used. Droplets of the solution were placed upon the substrate, without opening the apparatus,

by means of a fine bore needle which projected into the brass vessel through a rubber stopper.

The entire apparatus was placed in a refrigerator at a temperature of $-6 \rightarrow -4^{\circ}C$. After the apparatus had attained the temperature of its surroundings a droplet of solution was placed upon the substrate and left to slowly evaporate.

This procedure produced rhombic plates with their (001) face approximately in contact with the substrate. The face under observation was (001); other faces developed were (110), $(1\bar{1}0)$, $(\bar{1}10)$ and $(\bar{1}\bar{1}0)$ and occasionally (010) and (100). Surfaces other than the basal plane were not accessible to study due to the small size and fragility of the crystals.

A majority of the crystals (Fig.24) had edge angles 74° and 106°. These angles and measurements of the optical properties identified these crystals as the B-form. Occasionally crystals with edge angles 56° and 124° occurred, whose optical properties agreed with the C-form of the crystal. The rare A-form was never observed.

4.3. <u>The Optical Properties of Fatty Acid Crystals.</u>

The optical properties of fatty acid crystals can readily be deduced from their crystal structure. Parallel arrays of long chain molecules are most polarisable for light vibrations parallel to their length. Hence the

maximum value of the refractive index, μ_γ , occurs for vibrations parallel to the c-axis. The minimum value of the refractive index, μ_α , occurs for vibrations parallel to the symmetry axis b , which is perpendicular to the chain axes. The third axis of the indicatrix, μ_β , lies in (010) perpendicular to the b and c axes.

Strong positive birefringence occurs.

4.4. The Refractive Indices of Stearic and Behenic Acid Crystals.

Thibaud and Dupre la Tour[83] determined the refractive indices of the B-form of stearic acid for vibrations parallel to the a and b axes. The wavelength of the incident light was not specified but was probably λ 5893. The values given were

$$\mu_b = 1.510$$

$$\mu_a = 1.535$$

In the present study it was necessary to know the refractive indices of the B-forms of stearic and behenic acid, and their variation with wavelength. For this purpose the Becke refractive index test was used. The immersion media were mixtures of pure liquid paraffin ($\mu_{NaD} = 1.4803$) and α-bromonapthalene ($\mu_{NaD} = 1.6574$). The refractive indices of the immersion media were determined with an Abbe refractometer.

The results of this investigation are shown in Table III.

λ Å	μ_a	μ_b
B-FORM STEARIC ACID.		
4358	1.548 ± 0.002	1.527 ± 0.002
5461	1.537 ± 0.001	1.517 ± 0.001
5893	1.536 ± 0.002	1.514 ± 0.002
B-FORM BEHENIC ACID.		
5461	1.543 ± 0.002	1.523 ± 0.001
5893	1.540 ± 0.001	1.520 ± 0.001

TABLE III.

The B and C forms of the fatty acids can be readily distinguished by their optical properties. The minimum value of the refractive index always occurs for vibrations parallel to the b axis. In the B-form of these crystals the b axis is parallel to the bisectrix of the acute edge angle ψ . In the C-form it is perpendicular to this bisectrix.

REFERENCES.

82) ANDERSON, G., and DAWSON, I.M. Proc. Roy. Soc. A 218, 255 (1953)

83) THIBAUD, J., and DUPRE LA TOUR, F. Comptes Rendus 191 200 (1930)

CHAPTER V.

OPTICAL TECHNIQUES.

In their natural state the surfaces of fatty acid crystals have a low reflectivity and only coarse surface structure is visible. In order to observe the details of the surface structure, the crystals were coated with a thin, highly reflecting, layer of spectroscopically pure silver and observed under a microscope with bright-field or phase contrast illumination.

5.1. Vacuum Deposition.

An Edwards Coating Unit Type E.3 was used to evaporate the molten silver in a suitable vacuum. The details of this unit are shown in Fig.25. A glass bell jar, 60 cm. high and 40 cm. in diameter, was evacuated by a silicon oil diffusion pump backed by a rotary pump. A Pirani gauge indicated the pressure in the backing line. The pressure in the chamber was shown by a Phillips cold-cathode ionisation gauge.

The silver was heated in a molybdenum filament placed at a distance of 30 cm. from the specimen. If α is the angle of incidence of the vapour stream, the thickness of the deposit is proportional to $\cos^3 \alpha$. Hence when the specimen-source distance is 30 cm. it can be assumed that the deposit is uniform to within 1% over an area 2 cm. square. Over the surface area of a small crystal ($\sim 10^{-2}$ cm. square)

the variation in the thickness of the deposit is negligible.

It was found that thermal radiation from the filament caused local melting of the surfaces of stearic or behenic acid crystals. To reduce this effect a boat-shaped filament was used with its minimum surface area towards the specimen.

Fatty acid crystals were silvered without cleaning. Glass surfaces were always thoroughly cleaned before silvering. The reagents used were the detergent Teepol (Shell Chemicals Ltd) and hydrogen peroxide. The glass was finally cleaned in a vacuum $\sim$ 0.02 cm. of mercury by ionic bombardment from a high tension discharge.

The silvering operation was as follows:

Initially the pressure in the specimen chamber was reduced to 5×10^{-6} cm. of mercury. A shutter was interposed between the specimen and filament. The silver was heated to its melting point to expel occluded gases. After a short interval of time, to allow these gases to be removed, the filament current was raised to 120 amps. The filament then became white hot. The shutter between the specimen and filament was withdrawn and the deposition of silver on the specimen commenced. During the deposition, the white hot source was viewed through a glass test plate placed alongside the specimen. By noting the apparent changes in the colour and brightness of the source the thickness of the deposit

could be estimated. With experience reflectivities could be reproduced with an accuracy $\sim 3\%$.

5.2. Phase Contrast Microscopy.

The silvered crystals were observed under a microscope with bright-field or phase contrast vertical illumination. The most sensitive method of observing steps ~ 50 Å high was found to be by reflexion phase contrast microscopy. Phase contrast microscopy is now a well-known technique and will not be described in detail. Its development may be traced in references (84-97).

A detailed mathematical treatment of the theory of a practical phase contrast microscope is extremely complicated cf. Philpot [93]. At present the theory of a transmission microscope with a finite source, annular condenser aperture and annular phase plate has not been developed. Zernicke [88, 89], Francon [94] and Barer [96, 97] have shown that the principles of a simple transmission microscope, with a point source of light and a point phase (Fig.26), can be illustrated by a simple vector treatment.

6.3. The Vector Theory of Phase Contrast.

Consider a parallel beam of light from a point source incident upon a single transparent particle. The incident vibration can be represented in amplitude and phase by a vector $\overrightarrow{OA}$ (Fig.27). On transmission through the transparent particle the amplitude of the vibration will be unaltered,

but its phase will be retarded by an angle ϕ relative to the incident light. The amplitude and phase of the light which has traversed the particle can therefore be represented by $\overrightarrow{OP}$. But this vector can be regarded as the sum of two vectors

$$\overrightarrow{OP} = \overrightarrow{OA} + \overrightarrow{AP}$$

where $\overrightarrow{OA}$ represents the undeviated incident wave and $\overrightarrow{AP}$, which originates from the particle, can be regarded as a deviated or diffracted wave. The deviated and undeviated waves are separated in the back focal plane of the objective. A point phase plate placed in this plane can be chosen to advance the phase of the undeviated wave by an amount Ψ, so that $\overrightarrow{OA}$ rotates to $\overrightarrow{OM}$. Hence when the deviated and undeviated waves recombine in the image plane their resultant is given by $\overrightarrow{ON}$ (since $\overrightarrow{AP} \equiv \overrightarrow{MN}$). The intensity in the image of the particle $(ON)^2$, is no longer equal to the background intensity $(OA)^2$ and the transparent particle is made visible.

In the most general case the object particle and the phase plate both produce absorption. The absorption of the particle reduces the transmitted vibration to $\overrightarrow{OP^1}$ (Fig.28), whilst absorption in the phase plate reduces the background illumination and the undeviated wave is represented by $\overrightarrow{OM^1}$. In this case the resultant vibration in the image plane is $\overrightarrow{ON^1}$. The intensity in the image of the particle is $(ON^1)^2$, and the background intensity is given by $(OM^1)^2$.

This elementary treatment shows that the difference

of intensity between the image of the particle and its surroundings depends both upon the phase change and absorption in the phase plate. The optimum values for the constants of the phase plate depend upon the phase difference and absorption introduced by the object. By a suitable choice of phase plate the particle can be made to appear dark against a bright background (positive phase contrast) or bright against a dark background (negative phase contrast). Baker estimated that with a pure phase object and a phase plate with $\psi = 90°$ and 70% absorption, positive phase contrast occurs for values of $\phi < 72°$ (i.e. path difference $< \frac{\lambda}{5}$).

For greater values of ϕ a reversal of contrast occurs. The system is very sensitive to small phase changes and has a maximum sensitivity when $\phi = 36°$ (path difference $\frac{\lambda}{10}$).

5.4. The Reflexion Phase Contrast Microscope.

The author used a vertical illumination phase contrast equipment manufactured by Cooke, Troughton and Simms Ltd., which could be attached to a Vickers Projection Microscope. The optical system, Fig.29, of this equipment is based upon a design by Taylor [92].

In principle, the reflexion phase contrast microscope and the transmission microscope are the same, but certain modifications of the optical system are necessary to obtain vertical incident illumination. The phase differences in the wavefront reflected from an almost opaque object arise from

differences in the general surface level, diffracting structure on the surface and any slight variations in the penetration of the incident light into the surface.

An image of the light source is formed upon the annular aperture A, Fig.29 . After passing through the projector lens L the light is partially reflected by the glass plate G . The objective lens O forms an image I_1 of the annulus just above the surface of the specimen. A virtual image of I_1 is formed at I_2 equidistant from the reflecting surface. After reflexion at the specimen the undeviated light passes through the objective to form an image I_3, of the annular aperture coincident in size and position with the annular phase plate P .

The phase plate produced a phase retardation $\Psi = 90^{\circ}$ and absorbed 70% of the incident light. It was placed slightly above the back focal plane of the objective to avoid loss of contrast due to light reflected from its surfaces.

5.5. The Examination of Crystal Surfaces with the Reflexion Phase Contrast Microscope.

In general reflexion phase contrast illumination was found to increase the visibility of discontinuities in surface level upon silvered crystals. The wavefronts between adjacent terraces separating steps of height t have equal amplitude, but differ in phase by an amount $\frac{2\pi}{\lambda}$ 2t., where λ is the wavelength of the incident monochromatic light. Hence it

appears that a uniformally reflecting surface is closely analagous to the pure phase object of the simple theory. Differences in contrast between adjacent terraces are therefore to be expected. In practice this did not occur.

If the terrace between parallel steps is compared with an infinite slit of width a, the first diffraction maximum occurs at an angle θ given by

$$\theta = \frac{3\lambda}{2a}$$

In the present case $\lambda = 5 \times 10^{-5}$ cm., and a has a typical value $\sim 10^{-3}$ cm., hence

$$\theta \sim 5 \times 10^{-4} \text{ radians.}$$

The simple vector theory of phase contrast assures a point phase plate. Consequently, however small the separation between the deviated and undeviated light, phase contrast conditions always occur. The elementary argument outlined above indicates that in a practical optical system with a phase plate of finite dimensions, the separation between the deviated and undeviated rays is so small that they both pass through the phase annulus. As a result no difference in contrast between adjacent terraces occurs.

Steps $\sim$ 50 Å high were readily detected under phase contrast illumination. Their visibility was due to diffraction at the step edges. When reflexion bright-field illumination was employed these steps were only visible if the field aperture was reduced to a minimum and the objective

slightly defocussed. Under these conditions there was a considerable risk of antefacts in the image. Steps $\sim$ 250 Å high were clearly visible under bright-field illumination. When phase contrast illumination was used a 'halo' occurred alongside the steps. This effect was probably due to a reversal of contrast. The optimum conditions of illumination therefore depended upon the surface structure of the specimen. Unfortunately difficulties of observation arose when large and small steps were in close proximity, since no single method of illumination proved completely satisfactory.

It will be seen later that thin crystals were often studied with a silvered film of 85% reflectivity on both (001) faces. One must then question whether reflexion phase contrast illumination revealed the structure of one or both of the crystal faces. A comparison was made between Photomicrographs of the same crystal, when both (001) faces had a reflectivity of 85%, and after the front surface of the crystal had been coated with an opaque layer of silver. It was shown conclusively that only the structure of the frontmost surface was revealed.

REFERENCES

84) CONRADY, A.E. Journ. Roy. Micr. Soc. 150 (1905)

85) RHEINBERG, J. Journ. Roy. Micr. Soc. 152 (1905)

86) ZERNICKE, F. Z. Tech. Phys. 16 454 (1935)

87) Phys. Z. 36 848 (1935)

88) Physica 9 686 (1942)

89) Physica 9 974 (1942)

90) JUPNIK, H., OSTERBERG, H., and PRIDE, G.E. J. Opt. Soc. Amer. 34 773 (1946)

91) J. Opt. Soc. Amer. 38 338 (1948)

92) TAYLOR, E.W. Journ. Roy. Micr. Soc. 69 49 (1949)

93) PHILPOT, J. St.L. Prog. in Biophysics 1 (1950)

94) FRANÇON, M. Le Contrast de Phase. (1950) Revue d'Optique, Paris.

95) JUPNIK, H., BENNETT, A.H., OSTERBERG, H., and RICHARDS, O.W. Phase Microscopy. (1951) Chapman and Hall, London.

96) BARER, R. Journ. Roy. Micr. Soc. 72, 10, 81, (1952)

97) Journ. Roy. Micr. Soc. 73, 30, 206, (1953)

CHAPTER VI.

INTERFEROMETRIC TECHNIQUES

Two independent methods were used to determine the height of growth steps upon crystals of the fatty acids. The first method utilised multiple-beam Fizeau fringes of equal thickness. The second method involved shadowcasting crystals for examination with an electron microscope.

Fizeau fringes have been used for many years to examine surfaces of low reflectivity. Tolansky was the first to recognise the advantages which arise from using highly reflecting surfaces in the interferometer. The theory and practice of multiple-beam interferometry have been discussed by Tolansky[98-104], Brossel[105], Wilcock[106], Faust[107], Holden[108] and many others. A brief review of the general theory of multiple-beam interferometry will now be given. The factors which affect the definition and shape of the fringes will be summarised, with particular reference to the reflection system of fringes and the method of internal interference, which were used in the present work.

6.1. The Parallel Plate Interferometer.

Multiple reflections between two plane parallel surfaces Fig.30 which have amplitude reflexion coefficients r, transmission coefficients t, and are separated by a distance x in a medium of refractive index μ, lead to the well-known Airy intensity distribution. The fringes are

localised at infinity.

The intensity distribution in the transmitted system is given by

$$I_T = \frac{\epsilon^4}{(1-r^2)^2} \frac{1}{1 + \frac{4r^2}{(1-r^2)^2} \sin^2 \frac{\delta}{2}} \qquad x)$$

where

$$\delta = \frac{2\pi}{\lambda} \cdot 2\mu x \cos\theta. \qquad xi)$$

and is the phase difference between successive beams reflected at an angle θ within the interferometer. Maxima and minima of intensity occur when

$$\delta = 2N\pi \quad \text{(max)} \qquad N\lambda = 2\mu x \cos\theta \qquad xii)$$

$$\delta = (2N+1)\pi \quad \text{(min)} \qquad N \text{ integer.} \qquad xiii)$$

In the absence of absorption the intensity distribution in the reflected system is given by

$$I_R = \frac{1}{(1-r^2)^2} \frac{4r^2 \sin^2 \frac{\delta}{2}}{1 + \frac{4r^2}{(1-r^2)^2} \sin^2 \frac{\delta}{2}} \qquad xiv)$$

and is complementary to the transmitted system.

Boulouch [110] has shown that the fringe shape is extremely sensitive to changes in the reflectivity r^2. At high reflectivities, Fig.31, the fringes become very sharp, and the positions of the fringe maxima (or minima) can be determined with great accuracy.

6.2. The Phase Condition.

The localisation of the interference phenomena

is altered if the interferometer plates are inclined at a small angle ε, and the incident light is normal, ($\theta = 0$). Brossel[105] has shown that at a point P (Fig.32) on the wedge surface the phase difference, δ_n, between a direct beam, A_0, and the beam which has suffered 2_n reflections, A_n, is to a first approximation given by

$$\delta_n = \frac{2\pi}{\lambda} \cdot 2nx \left(1 - \frac{2n^2+1}{3}\varepsilon^2\right) \qquad \text{xv)}$$

This equation shows that the intensity distribution of the fringes localised on the wedge surface differs from the Airy distribution. The fringes are assymmetrical due to the additional phase term $\frac{2\pi}{\lambda} \cdot 2nx \cdot \frac{(2n^2+1)}{3}\varepsilon^2$. If this term is made negligibly small an Airy-type distribution again results. For surfaces of high reflectivity the effective value, n_e, of n is necessarily large. Hence the additional phase term can only be made negligible if ε and x are extremely small. An acceptable practical limit is such that

$$\frac{4}{3} n_e^3 \varepsilon x < \frac{\lambda}{4} \qquad \text{xvi)}$$

6.2. <u>The Collimation Conditions.</u>

In the case of non-normal incidence equation (xv) becomes

$$\delta_n = \frac{2\pi}{\lambda} \cdot 2nx\cos\theta \left(1 - n\varepsilon\tan\theta - \frac{2n^2+1}{3}\varepsilon^2\right) \qquad \text{xvii)}$$

It is evident that deviations from normal incidence will also lead to assymmetrical fringe broadening.

Tolansky[103] and Brossel[105] have shown that when $\varepsilon \approx 1'$, which is a usual value for surface studies, precise

collimation is only necessary if $x > 1000\lambda$. When x is reduced to 50λ a collimation error of 3° can be tolerated.

Fringe broadening may also arise from the finite line-width of the source. This effect has been discussed by Tolansky [103] and Wilcock [106] who have shown that when equation (xvi) is satisfied the tolerable source line-width is never less than 2 Å.

6.4. The Viewing System.

Fig. 33 is a schematic diagram of the optical system used to view the reflexion fringes localised on the wedge surface. The lens L_1 concentrates monochromatic light from the source on to an aperture A. An image of this aperture is formed in the back focal plane F of the objective by lens L_2 , after reflexion at the glass plate G . The light is then incident normally on the interferometer. The reflected light passing through a point P on the wedge surface is brought to a focus in the image plane I of the objective lens.

6.5. The Linear and Angular Displacement Conditions.

The intensity at the point P (Fig.32) on the wedge can only be uniquely related to the wedge thickness, x, if all the beams contributing to the resultant intensity originate from an area below the lateral resolving power of the objective. Tolansky [103] has shown that to a first approximation the linear separation, d_n , along the wedge surface between the beams A_o and A_n (Fig.32) is given by

$$\alpha_n = 2n^2 x \varepsilon \qquad \text{xviii)}$$

The upper limit for the numerical aperture, N.A., of the objective is therefore given by

$$\frac{\lambda}{2N.A} > 2n_e^2 x \varepsilon \qquad \text{xix)}$$

The numerical aperture must also be sufficiently large for all the effective beams to enter the optical system. Since the n^{th} beam is inclined at an angle $(2n+1)\,\mathbf{E}$ to the incident beam, the lower limit for the numerical aperture of the objective is given by

$$\text{N. A.} > \mu \sin (2n+1)\,\mathbf{E}. \qquad \text{xx)}$$

6.6. Summary of the Conditions for Sharp Multiple-beam Fizeau fringes.

The most important optical conditions necessary to obtain sharp multiple-beam Fizeau fringes with a wedge interferometer with highly reflecting surfaces may be summarised as follows.

1) The phase condition $\frac{4}{3} n_e^3 x \varepsilon^2 < \frac{\lambda}{4}$
2) The linear displacement condition $2n_e^2 x \varepsilon < \frac{\lambda}{2NA}$.
3) The angular displacement condition $\mu \sin(2n+1)\varepsilon < N.A.$

The importance of these conditions in the present work will shortly be discussed.

6.7. The Effects of Phase Changes and Absorption upon the Reflexion Fringe System.

When, as in the present study, the medium between the interferometer surfaces is a dielectric, the effects of absorption and phase changes in the interferometer must be

considered.

A detailed examination of the reflection system by Faust[107] and Holden[108] has shown that in general

$$I_R = r_1^2 + \frac{\rho^2 t_1 t_2 + 2 r_1 \rho t_1 t_2 \cos(\psi+\delta) - 2 r_1 r_2 \rho^2 t_1 t^2 \cos\psi}{(1 + (\rho r_2)^2 - 2\rho r_2 \cos\delta)} \qquad \text{xxi)}$$

The symbols used in this expression are defined in Fig. 34. In the absence of absorption, and if $r_1 = r_2 = r$, this expression reduces to equation (xiv). Maximum or minimum values of I_R occur when

$$\delta + \phi = N\pi + (-1)^N \eta \qquad N \text{ integer,} \qquad \text{xxii)}$$

where $$\phi = f_1(r_1 r_2 t_1 t_2 \rho \psi) \qquad \text{xxiii)}$$

and $$\eta = f_2(r_1 r_2 t_1 t_2 \rho \psi) \qquad \text{xxiv)}$$

The fringes are usually assymmetrical, but the spacing between two successive maxima (or minima) is given by

$$\delta_1 - \delta_2 = \pm 2\pi \qquad \text{xxv)}$$

This is the same as for an Airy distribution and does not depend upon the fringe assymmetry. Consequently, provided that any assymmetry arises from phase change and absorption effects alone; multiple-beam fringes still give an exact representation of the topography of the interferometer surfaces.

Faust[107] has shown that the value of δ at which maxima or minima of intensity occur depends upon the value of

$$2 t_1 t_2 [\rho^2 r_2 (r_1 r_2 + t_1 t_2) - r_1] \qquad \text{xxvi)}$$

which involves the optical constants of both reflecting surfaces. The factor which governs the symmetry of the

fringes is the phase term

$$\psi = \beta_1 + \beta_2 - \alpha_1 - \alpha_2 \qquad \text{xxvii)}$$

which depends solely upon the optical constants of the front surface of the interferometer.

The only conditions under which the maxima of the transmitted system and the minima of the reflexion system coincide are when

$$\psi = (2N+1)\pi$$

and $$2t_1t_2\left[\rho^2 r_2(t_1t_2 + r_1r_2) - r_1\right] < 0$$

Symmetrical reflexion fringes then occur.

6.8. <u>The Use of Multiple-Beam Fringes for Surface Studies.</u>

When one plane surface of the wedge interferometer is replaced by a highly reflecting surface containing small irregularities, multiple beam Fizeau fringes accurately reveal the surface topography; (provided due attention is given to the limiting conditions summarised in 6.6) Brossel[105] and Tolansky[103] estimated that the fringes would reveal the true contour of the surface for details $> 10^{-3}$ cm. in extension.

Dielectric surfaces are usually coated with a thin film of high reflectivity, such as silver. If a correct interpretation of the fringe pattern is to be obtained, this film must accurately contour the underlying surface. By a study of cleavage steps on crystals Tolansky[104] has shown that evaporated silver films contour a surface to within molecular dimensions. Aggregation of the silver may occur near step

edges, but this effect is below the lateral resolving power of the optical microscope.

6.9. The Method of Internal Interference.

The ~~external~~ lateral dimensions of the crystals studied by optical methods were $\sim 10^{-2}$ cm. and their thicknesses 50 - 50,000 Å. These crystals were extremely fragile and could not be removed from the substrate. If a silvered microflat was matched against the silvered crystals, sharp multiple-beam Fizeau fringes could seldom be obtained. This was due to the fact that the separation between the interferometer surfaces and the wedge angle could not be made sufficiently small for the limiting conditions (6.6) to be satisfied. Furthermore the surface structure of the crystals was only revealed in the vicinity of a fringe maximum (or minimum). It was then difficult to correlate the fringe pattern with the surface details of a given crystal. To overcome these difficulties fringes formed by internal interference between the (001) and (00$\bar{1}$) faces of the crystal were used. Tolansky[104] has employed a similar technique to examine inclusions in thin mica sheets. Two-beam internal interference fringes have also been used by Forty [111] to study the growth of cadmium iodide crystals.

In the present work tabular fatty acid crystals were grown upon a silvered glass substrate ($r^2 \sim 0.85$), and the upper surfaces of the crystals were also silvered. An

examination of the multiple-beam reflection fringes formed between the silvered substrate and the silvered surface of the crystals showed that the $(00\bar{1})$ face of some crystals was in intimate contact with the substrate. The interference fringes then accurately contoured the growth layers on the upper surface of the crystal (Fig.35). If there was an air-gap between the crystal and the substrate the fringes failed to contour the surface structure. The interferometric measurements in the present work were confined to crystals whose $(00\bar{1})$ face was in contact with the substrate.

In a typical case, the crystals were observed with a 4 mm. objective of numerical aperture 0.95. Successive fringes contouring a growth spiral of step-height $h = 200$ Å were separated by a distance $d_1 = 10^{-2}$ cm. The optical thickness of the crystal was 5λ (λ 5461) and its refractive index $\mu = 1.5$. The validity of the limiting conditions for the use of multiple-beam Fizeau fringes formed by internal interference for this crystal will now be considered.

The wedge angle ε_1, parallel to AB (Fig.36) is given by

$$\varepsilon_1 = \frac{\lambda}{2\mu d_1} \approx 2 \times 10^{-3} \text{ radian} \qquad \text{xxviii)}$$

when $r^2 = 0.85$ the number of effective beams $n_e = 35$ (Brossel [105]). Substitution of the above values in eqn.(xvi) gives for the phase lag

$$\frac{4}{3} n_e^3 \varepsilon_1^2 x = 1.2\lambda$$

whilst the linear displacement is given by

$$2 n_e^2 x \varepsilon_1 = 17\lambda.$$

Hence it appears that both the phase and linear displacement conditions were violated. However this analysis neglects the essential nature of the crystal, which consists of parallel layers of molecules. The slope along A B is not continuous but decreases step-wise. Hence, in a crystal growing by plane layers, $E = 0$ and the conditions for the use of multiple-beam Fizeau fringes are satisfied.

In a crystal having a spiral surface structure it is more relevant to consider the slope along A' B' parallel to the step-edges. If the distance, d_2, around one complete turn of the spiral 2×10^{-2} cm, the wedge angle ε_2 is given by

$$E_2 = \frac{h}{d_2} \approx 10^{-4} \text{ radians.} \qquad \text{xxix)}$$

whence $\frac{4}{3} n_e^3 \varepsilon_2^2 x = 0.17 \quad 0.003 \lambda$

and $2 n_e^2 \varepsilon_2 x = 0.85 \lambda$

Hence the phase condition was satisfied, but the linear displacement condition was not quite fulfilled. The angular displacement condition was always satisfied. In practice the fact that the linear displacement condition was not quite fulfilled was not a serious difficulty. It was unlikely that the objective reached its theoretical resolving power when the incident illumination was normal. Every effort was made to study extremely thin crystals, and hence to reduce x.

It may be concluded that the method of internal interference using highly reflecting surfaces may be used to

to study extremely thin crystals, even at high magnifications ($\sim \times 200$); however, care must be taken to select suitable crystals, and the reflectivities employed should not exceed ~ 0.85. The method of internal interference had the following advantages:

i) the surface structure and interference pattern could be viewed simultaneously.

ii) high magnifications could be used.

iii) the sensitivity of the fringes to changes of geometrical thickness was increased by a factor μ.

The disadvantages of the method were

i) crystals for study must be judiciously selected.

ii) the interferometric gap and wedge angle are invariable, only the wavelength of the incident light can be varied.

iii) unsuitable for the study of disordered crystals in which the value of the refractive index is unknown.

6.10. <u>The Effects of Phase Changes. Internal Interference.</u>

Since fatty acid crystals have a refractive index $\mu = 1.5$ it can be assumed that the optical constants of a silver-crystal-silver system are similar to those for a silver-glass-silver system. Faust[112] reported that for a glass-silver interface when $r^2 = 0.85$, $t^2 = 0.09$. Substitution of these values in equation (xxvi) shows that if $r_1 = r_2 = \rho = r$ and $t_1 = t_2 = t$

$$2t_1t_2[\rho^2 r_2(r_1r_2 + t_1t_2) - r_1] < 0$$

The phase factor ψ cannot be determined experimentally, since the phase changes on transmission are not known. Dufour[113] estimates that for a thin film of low absorption

$$\psi = (2N+1)\pi \pm \Delta\psi \qquad \text{xxx)}$$

where $$\tan \Delta\psi \leq \frac{A}{\sqrt{r^2(1-r^2)}} \qquad \text{xxxi)}$$

and the absorption $A = 1 - r^2 - t^2$.

Hence, in the present case

$$\Delta\psi \leq 0.03 \text{ radians.}$$

The fringes should therefore be symmetrical, and the maxima of the transmission system coincide with the minima of the reflexion system. This was confirmed by experimental observations upon fringes formed by internal interference.

It is therefore unlikely that any assymmetry in these fringes can be attributed to absorption effects.

6.11. Fringes of Equal Chromatic Order.

In addition to multiple-beam Fizeau fringes formed by internal interference, the related fringes of equal chromatic order (Tolansky[104]) were also occasionally used to study silver-crystal-silver films. The optical arrangement is shown in Fig.37.

Light from a white light source is collimated by the lenses L_1 and L_2 and falls at normal incidence upon the film. The objective lens L_3 and projector lens L_4 form

an image of this film upon the slit S of a prism spectrograph. Hence the multiple reflected beams from a narrow line section of the interferometer are isolated and brought to a focus after dispersion by the prism. Chromatic multiple-beam fringes appear in the focal plane of L_6.

Provided that due attention is paid to the limiting conditions which have previously been discussed, these fringes have an Airy intensity distribution. The position of the fringe maximum (or minimum) is governed by the equation

$$n\lambda = 2\mu x \qquad \text{xxxii)}$$

where for each fringe of the system

$$n = \text{const.} = \frac{2\mu x}{\lambda} \qquad \text{xxxiii)}$$

The number of fringes in the field of view depends upon the optical separation of the interferometer surfaces. For quantitative measurements there must be at least two fringes between $\lambda 5790$ and $\lambda 4358$, i.e. μx must exceed 10^{-4} cm. It has already been shown that, under the optical conditions necessary to study small crystals of the fatty acids, $\mu x \neq 2.5 \times 10^{-4}$ cm. if sharp multiple beam fringes are to be obtained. Fringes of equal chromatic order formed by internal interference can therefore only be used over a very limited range of thicknesses. Also, since the medium between the reflecting surfaces was dispersive, the variation of the refractive index and phase changes with wavelength restricted the wavelength range over which the fringes could be used for quantitative results.

REFERENCES

98) TOLANSKY, S. Phil. Mag. 34 555 (1943)

99) Phil. Mag. 35 120 (1944)

100) Phil. Mag. 35 179 (1944)

101) Phil. Mag. 36 225 (1945)

102) Phil. Mag. 37 390 (1946)

103) Proc. Phys. Soc. 58 654 (1946)

104) Multiple-Beam Interferometry. O.U.P. (1948) London.

105) BROSSEL, J. Proc. Phys. Soc. B 59 234 (1947)

106) WILCOCK, W.L. Thesis. Manchester. (1951).

107) FAUST, R.C. Thesis. Manchester. (1949).

108) HOLDEN, J. Thesis. London (1951).

109) Proc. Phys. Soc. B 62 405 (1949)

110) BOULOUCH Journ. de Phys. 5 789 (1906)

111) FORTY, A.J. Phil. Mag. 43 377 (1952)

112) FAUST, R.C. Phil. Mag. 41 1239 (1950)

113) DUFOUR, C. Les Proprietes Optiques des lames Minces Solides. P.24. Centre National de la Recherche scientifique. FRANCE. 1950.

CHAPTER VII.

ELECTRON MICROSCOPE TECHNIQUES.

The lateral resolution of an electron microscope greatly exceeds the resolution of an optical microscope. In the present study a Metropolitan-Vickers Electron Microscope, Type E.M.3. was used. This instrument had a lateral resolution 50 - 25 Å. As a result, the growth patterns upon extremely small crystals ($\sim 10^{-4}$ cm) which were unsuitable for optical examination, could be studied. The height of surface steps could also be determined by shadowcasting these crystals at known angles of incidence.

The evolution of the electromagnetic electron microscope and the progressive achievement of high instrumental resolutions have been described by Busch, Ruska, Knoll and Von Borries (References 114-128). The mathematical treatment of electron optics is extremely cumbersome. In the current study an adequate appreciation of the electron-optical system could be obtained by regarding the electro-magnetic lenses as equivalent to thick optical lenses of variable power.

The mechanism of image formation in the electron microscope differs from that in an optical microscope. Image contrast in the electron microscope arises from the scattering of electrons by the specimen. An aperture in the image space of the objective lens limits the angular width of the imaging beam. Thus electrons scattered through angles greater than a

limiting value fail to reach the image. The intensity in the image of a highly scattering particle is therefore less than the background intensity.

7.1. The Metropolitan-Vickers Electron Microscope, E.M.3.

The E.M.3. Electron Microscope has been fully described by Haine, Hirst, Page and Garfitt (Ref. 129-131). A vertical section of this instrument is shown in Fig.38. There were four electromagnetic lenses, a condensor, and objective and two projector lenses. The system was aligned by lateral and tilt adjustments of the electron-gun and condensor unit, and the objective lens.

The pressure in the microscope column was reduced to 0.5×10^{-5} cm. of mercury by an oil diffusion pump backed by a rotary pump. A Geissler tube indicated the pressure in the backing line. The pressure in the microscope column was indicated by a Pirani gauge having a range $10^{-1} \longrightarrow 10^{-6}$ cm. of mercury.

The electron gun consisted of three electrodes; a hair-pin tungsten wire mounted centrally in a biassed anode shield, and an earthed anode cup. Accelerating voltages of 50, 75 or 100 k.v. could be supplied to the shield. The bias voltage between filament and shield could be varied to allow for slight differences in the position of the filament.

A condensor lens of variable power collimated the electron beam from the gun. The maximum angular aperture of

the illuminating beam was defined by an 0.5 mm. condensor aperture. Below the condensor was the specimen and movable specimen stage. This stage nested upon the upper face of the objective lens. When necessary a prespecimen aperture could be used to localise the illumination and reduce heating effects at the specimen. The objective power was continuously variable. In the image space of the objective lens was the objective aperture which controlled the image contrast. Interchangeable copper discs with an aperture of diameter 40, 20, 10, or 5 μ were used. The axial and lateral position of this aperture could be adjusted to obtain optimum contrast. The two projector lenses were constructed as a single coaxial unit, and their position was fixed. These lenses could be operated under a number of conditions to produce low magnifications, high magnifications on electron diffraction. The power of the first projector lens was continuously variable, but that of the second projector lens had three fixed values.

7.2. Operation of the E.M.3. Electron Microscope.

When the electron microscope had been correctly aligned there were three distinct methods of combining the lens system.

Method I.

In normal operation, Fig. 39a, the first projector lens acted as a converging lens. Two intermediate images, I_1 and I_2, were formed. The second intermediate image I_2

was in the object plane of the second projector lens. The magnification range was 2,000 → 100,000.

Method II.

When the power of the first projector lens was sufficiently reduced an image of the back focal plane of the objective was formed in the object plane of the second projector lens. The electron diffraction pattern from the specimen was then seen. Usually the objective aperture was removed and a small diffraction aperture placed at I_1, Fig.39b. The diffraction pattern from selected areas of the specimen could then be studied.

Method III.

When the power of the first projector lens and objective were further reduced a single intermediate image was formed, as shown in Fig. 39c. The system then acted as a two-stage microscope and magnifications 1000 → 2000 were obtained.

Electron lenses suffer from the same defects as unconnected optical lenses; namely, spherical and chromatic aberrations and astigmatism. In addition there are several defects due to the rotation of the electron paths in the lens field. When the present instrument was correctly aligned most of these defects were negligible except at low magnifications. At magnifications $<$ x 5000 there was noticeable spherical aberration.

7.3. Specimen Support Films.

Thin films to support specimens for examination with an electron microscope must have a low atomic scattering power, be free from resolvable structure, and be stable in the electron beam. Carbon films $\sim$ 50 Å thick were found to satisfy these conditions extremely well.

The carbon was deposited upon a clean glass plate by sputtering spectroscopically pure carbon in a vacuum $\sim 10^{-5}$ cm. of mercury. The apparatus was similar to that used for the vacuum deposition of silver. The circuit supplying the carbon electrodes is shown in Fig.40. The time of deposition and hence the thickness of the carbon film was controlled by a fuse in the d-c supply. It was found that with a source-specimen distance of 10 cm, and a 12 - 15 amp fuse the carbon deposit was just visible, and of suitable thickness.

7.4. Preparation of Specimens.

Crystals of behenic acid were grown from solution upon the carbon coated glass. The composite layer was examined under an optical microscope and selected areas were then stripped on to a clean water surface. This proved a difficult operation. It was found that the film stripped more readily if the glass was wetted with a trace of Teepol and polished dry before the carbon film was deposited.

Whilst the film floated upon the water surface an L-shaped mesh was placed beneath it. Upon the mesh several

A.E.I. specimen grids were placed. The required regions of film were carefully manipulated into position above the grids, and the L-shaped mesh gently raised above the water surface. The carbon film and crystals thus settled upon the specimen grids.

7.5. Shadowcasting.

To reveal the surface structure of these crystals they were shadowcast with a layer of 60% gold - 40% palladium ~15 Å thick. The coating unit described in 5.1. was employed. The technique of shadowcasting was similar to that of the vacuum evaporation of silver. Some modifications were however necessary and these will be described.

The filament was a U-shaped tungsten wire. Around the U-bend a suitable length of gold-palladium wire of uniform diameter was coiled. The length of wire, ℓ , required to produce a deposit of thickness t at a shadowing angle θ was calculated from the formula

$$\ell = \frac{3 s^2 t}{r^2 \sin\theta} \qquad \text{xxxiv)}$$

where s = source - specimen distance (10 cm).

and r = radius of the wire.

The shadowing angles used were ~ 12°. To reduce variations in the shadowing angle θ due to the finite size of the source, the filament was placed with its smallest dimension in the plane of incidence.

The source - specimen distance was 10 cm. It was therefore necessary to place a shield over the filament to prevent unwanted thermal radiation causing local melting of the crystals.

The approximate shadowing angle was indicated by an angular scale attached to the rotatable specimen mount. The local shadowing angle upon the specimen grid was also determined. For this purpose accurately spherical particles of polystyrene latex were scattered over the specimen grids by spraying a 3% solution of the latex in distilled water from a fine atomiser. The latex particles and crystals were then shadowed simultaneously. Hence the local shadowing angle, θ, could be determined from the ratio of the diameter of the particles, D, to the shadow length s, since

$$\tan \theta = \frac{D}{s} \qquad \text{(Fig.41.)} \qquad \text{xxxv)}$$

It was essential to shadowcast the crystals after stripping and not before. For firstly, a carbon-crystal-metal layer was extremely difficult to strip; and secondly, during stripping the latex particles were displaced from their 'shadows', and an accurate measurement of the shadowing angle became impossible.

7.6. Magnification Calibration.

The magnification of the electron microscope used had not previously been determined. The instrument was therefore calibrated by using spherical polystyrene latex

particles kindly supplied by I.C.I. (Plastics) Ltd., The mean diameter of these particles, which as may be seen from Fig. 4c, were extremely uniform, was $(0.54 \pm 0.01) \times 10^{-4}$ cm. There was a small amount of contaminant, which could usually be recognised.

Several independent calibrations of the magnifications were made and the lens currents noted. The centre of the range calibrated with polystyrene latex was compared with a calibration using a shadowed Formvar replica of a metal diffraction grating. All the calibrations were found to agree within the limits of error, which were 3 - 5%.

REFERENCES

114)	BUSCH, H.	Ann. Phys. Lpz.	81	974	(1926)
115)		Arch. Elektrot.	18	583	(1927)
116)	RUSKA, E.	Z. Phys.	83	492	(1933)
117)		Z. Phys.	87	580	(1934)
118)		Z. Phys.	89	90	(1934)
119)		Arch. Electrotechn	36	431	(1942)
120)		Arch. Electrotechn	38	102	(1944)
121)	BORRIES, B. VON	Z. Tech. Phys.	20	225	(1939)
122)	BORRIES, B. VON., and RUSKA, E.	V.D.I.	79	519	(1935)
123)		Wiss. Ver. Siemens-Werk	17	99	(1938)
124)		Z. Tech. Phys.	20	225	(1939)
125)		Ergeb. Naturwiss	19	237	(1941)
126)		Phys. Z.	45	314	(1944)
127)	KNOLL, M., and RUSKA, E.	Ann. Phys. (5)	12	607	(1932)
128)	KNOLL, M., and STARK, M.	Fiat Review of German Science. Electronics I 57 (1943).			
129)	HAINE, M.E., PAGE, R.S., and GARFITT, R.G.	Journ. App. Phys.	21	173	(1950)
130)	HAINE, M.E.	Journ. Sci. Inst.	24	61	(1947)
131)	HAINE, M.E., and HIRST, W.	Brit. Journ. App. Phys.	4	239	(1953)

CHAPTER VIII.
OBSERVATIONS UPON THE GROWTH OF CRYSTALS OF STEARIC ACID AND BEHENIC ACID.

8.1. Introduction.

Although the advance of molecular growth layers upon the (001) faces of fatty acid crystals could not be directly observed, an insight into the dynamic processes of growth could be gained from a study of the crystal surfaces after growth had been arrested.

Initially only the B-form of stearic acid was examined. Later, when an electron microscope became available, it was found that stearic acid crystals decomposed in the electron beam. It was therefore necessary to study a fatty acid with a higher melting point. Behenic acid, which was the highest melting point acid which could be obtained in a pure state, was found to be relatively stable in the electron beam. Before proceeding to an electron microscopic study of this acid, the growth of the B-forms of stearic acid and behenic acid was compared using optical techniques. No significant differences were found between growth features on crystals of these acids. All optical observations upon stearic acid were confirmed by similar observations upon crystals of behenic acid. This was not unexpected since the crystal structures are homologous, and the molecules of these acids differ by only four CH_3 groups. As a result, examples of growth features could be chosen from either acid

without any loss in generality.

8.2. Layer Growth.

Many crystals showed no visible surface structure even after silvering or shadowcasting. Fig.42 shows an internal interferogram (reflexion) of a group of tabular crystals illuminated by unfiltered mercury light. Each crystal is an area of uniform tint. The reflectivity of the silver surfaces was $\sim$ 85%. Hence in the region of a fringe minimum a change in optical thickness of 72 Å should cause a 50% increase in the fringe intensity. Since the fringe intensity is uniform it can be concluded that the crystal surfaces were molecularly plane. The crystals had settled with (001) in intimate contact with the silvered glass substrate.

It may also be seen from Fig.42 that where two lamella crystals were superimposed they coalesced in parallel orientation. This is of particular interest when considering the growth of disordered crystals.

Incompleted layers were also observed upon the (001) faces of fatty acid crystals. Fig.43 shows an example of several island nuclei upon a large crystal of stearic acid. On this particular crystal it was possible to determine the thickness of individual growth layers by using a small external optical flat and multiple beam Fizeau fringes. The thickness of the elevation marked A was found to be

(88.1 ± 4.5) Å. Since $c \sin \beta = 43.9$ Å, this nucleus consisted of two bimolecular layers. Other growth layers upon this crystal were found to have thicknesses of (43.9 ± 3.6)Å; (89.5 ± 5.3) Å and (84.5 ± 5.0) Å. The later results arose from pairs of closely spaced steps. It is clear that this crystal grew by the nucleation and advance of groups of bimolecular layers.

8.3. Spiral Growth.

Stearic and behenic acid crystals were frequently found to have grown by a spiral mechanism. A preliminary report of spiral growth upon stearic acid crystals was given by Verma and Reynolds (1953)[132]. The growth patterns varied in complexity from the simple multiple spiral in an early stage of development, illustrated in Fig.44 to the complex spiral pattern shown in Fig.45. Fig.46 is an example of a well developed single spiral upon a crystal of behenic acid.

According to the theory proposed by Burton, Cabrera and Frank[7,9], if a growth spiral forms upon one face of a tabular crystal, the thickness of the crystal will decrease continuously along the spiral terrace. The regular change in the fringe intensity in the internal interferogram of a single spiral, Fig.47, reveals this continuous change in the thickness of the crystal.

An approximate value of the supersaturation at which a single bimolecular spiral grew can be calculated from the

spacing, Yo , between successive turns of the spiral. According to equations xiii) and ix)

$$y_o \sim \frac{2\pi a \phi}{k T \sigma(x_o)} \qquad \text{xxxiv)}$$

The magnitude of the energy of interaction between neighbouring molecules, ϕ , can be estimated from the heat of solution of the acid. The heat of solution of stearic acid in a non-polar solvent $\sim$ 70 kilojoules mole^{-1} , and of behenic acid $\sim$ 90 kilojoules mole^{-1} , (Int. Crit. Tables) . Hence the energy of solution for a pair of molecules, E, is approximately 24 x 10^{-13} erg for stearic acid and 30 x 10^{-13} erg for behenic acid. This may be regarded as the energy needed to remove a pair of molecules from a kink in a bimolecular step. If only nearest neighbour interactions are considered

$$E = 2\phi_1 + \phi_2 \qquad \text{xxxv)}$$

where ϕ_1 = energy of interaction between adjacent dimers, and ϕ_2 = energy of interaction between CH_3 and groups in adjacent lattice planes. Clearly, $\phi_1 >> \phi_2$, hence $\phi_1 \leq \frac{1}{2} E$ i.e. $\phi_1 \leq$ 12 x 10^{-13} erg for stearic acid and $\phi_1 \leq$ 15 x 10^{-13} erg for behenic acid. The mean intramolecular spacing a = 6.5 x 10^{-8} cm. The temperature at which the crystals grew was T $\approx$ 270^{o} K.

y_o $\times 10^{-4}$ cm	$\sigma(x_o)$	α
STEARIC ACID		
5.1	0.02	1.02
2.6	0.04	1.04
6.9	0.02	1.02
4.0	0.03	1.03
3.4	0.03	1.03
BEHENIC ACID		
1.3	0.12	1.12
1.7	0.09	1.09
1.7	0.09	1.09
4.3	0.03	1.03
1.5	0.10	1.10
1.2	0.15	1.15
1.4	0.11	1.11
0.5	0.30	1.30
0.8	0.19	1.19

Table 4.

Table 4 gives the mean value of Yo for several bimolecular single spirals. The approximate value of $\sigma(x_o)$ obtained by substituting the above values of ϕ, τ and a in equation (xxxiv) is also tabulated.

The function $\sigma(x_o)$ is given by

$$\sigma(x_o) = \sigma \left[1 + \frac{2\pi a (\delta - y_o)}{x_o y_o} + \frac{2a}{x_o} \ln \frac{y_o}{x_o} \right]^{-1} \quad \text{xxxvi)}$$

where σ = supersaturation ratio

and δ = thickness of the unstirred layer at the surface of the crystal (Burton, Cabrera and Frank [7]). Since the magnitudes of the quantities involved in this expression are $a \sim 10^{-7}$ cm, $x_o \sim 10^{-6}$ cm, $y_o \sim 10^{-4}$ cm and $\delta \sim 10^{-6}$ cm the bracketed term has a magnitude of the order 1.3. To a first approximation

$$\sigma(x_o) \longrightarrow \sigma$$

Therefore, since

$$\sigma = (1 - \alpha) \quad \text{xxxvii)}$$

a value of the supersaturation ratio, α, can be estimated. The approximate values of α are shown in the third column of Table 4.

These results indicate that the supersaturation seldom exceeded 30%. A majority of the crystals grew at supersaturations below 10%. Under these conditions the probability of growth by two-dimensional nucleation was small $(\sim e^{-10^4})$.

8.4. Interactions between Growth Spirals.

The growth spirals found upon crystals of the fatty acids grown at temperatures $-267 \rightarrow -269^{\circ}$ K were generally

rectilinear. There was a close analogy between the interactions between many of these rectilinear growth spirals and the curvilinear growth patterns anticipated by Burton, Cabrera and Frank.[7, 9]

Figs. 48 and 49 illustrate the interaction between two spirals of the same sense when the separation between the growth centres is less than $2\pi\rho_c$. These may readily be compared with Fig. 12 .

In Fig. 50 three co-operating growth spirals of the same sense appear to emerge from a common origin. Whereas the group of rectilinear spirals shown in Fig. 51 originate from a group of growth centres disposed along a straight line. This growth pattern is clearly analogous to the theoretical pattern shown in Fig. 13 .

When two spirals of equal step-height but opposite sign emerged from centres separated by a distance, d , where $4\pi\rho_c < d < 8\pi\rho_c$, closed loops were generated, as may be seen from Fig. 52. If the separation between the growth centres exceeded $\sim 8\pi\rho_c$ each spiral developed several turns before the growth steps merged, as illustrated in Fig. 53.

The growth centres were generally found to occur near the centre of the (001) face. Occasionally, Fig. 54, at least two distinct centres of growth occurred.

Spiral growth patterns were also observed upon crystals of the C-form of both stearic and behenic acid crystals.

An example is shown in Fig.55. However, the growth of this polymorph was not extensively investigated in the present work, since the structure of the B and C forms of the fatty acids are so similar. Few fundamental differences in the growth of these polymorphs were to be expected, except in effects which depend upon the tilt of the molecules relative to the basal plane. In the course of the detailed investigation of the B-form, several hundred crystals of the C-form were seen. No significant differences in the growth of these polymorphs were found.

These observations show that a spiral mechanism plays an important part in the growth of fatty acid crystals from solution at low supersaturations. This indicates that fatty acid crystals are often imperfect and contain dislocations. The interactions between most of the growth spirals, which were generally rectilinear, were closely analagous to the growth patterns foreseen by Burton, Cabrera and Frank[7,9]. There were some exceptions which will be described shortly.

8.5. <u>The Shape of the Growth Spirals.</u>

The step edges in crystals grown at temperatures between 267°k and 269°k were generally parallel to $\langle 110 \rangle$ in (001), which are the most close-packed directions in this plane. Occasionally growth edges parallel to $[010]$ or $[0\bar{1}0]$ were observed. These are the next most close-packed

directions in (001). In a bimolecular step the step edge must also have been parallel to the chain axes of the molecules i.e. the c-axis.

Assymetrical growth spirals were frequently observed in which the velocity of advance, v , of the growth edges was not equal in all close-packed directions. Although this velocity could not be determined absolutely, the relative velocities of advance could be estimated, since v is proportional to Yo, the spacing between successive steps.

The vector diagram for the velocities v for a single bimolecular spiral or a crystal of the B-form of behenic acid (Fig.46) are shown by Fig.56. It can be seen that this diagram is symmetrical about (010), which is the plane of maximum tilt of the molecules. A section through the crystal in the directions AOB or $A'OB'$, perpendicular to the growth edges is illustrated in Fig.57. The difference in the velocities of advance, v_1 and v_2, was associated with a difference in the inclination of the step-edge to the layer over which it was advancing. The velocity was greater (or less) when the step edge overhung the underlying layer. It has been assumed that this velocity was greater when the step edge made a re-entrant angle with the underlying layer.

The assymetry of simple growth spirals was more marked in crystals of the B-form of behenic acid than in crystals of the B-form of stearic acid grown under similar

conditions. This indicated that the relative velocity ($v_1 - v_2$) increased as the length of the molecule increased.

Bimolecular growth spirals upon the C-form of these acids were also frequently assymetrical. An example is shown in Fig.55. The a-axis is parallel to the bisectrix of the acute edge angle. The vector diagram, Fig.58, is again found to be symmetrical about (010), which is the plane of maximum tilt of the molecules. The difference in the velocity of growth of a bimolecular step, therefore corresponds with a difference in the inclination of the step-edge relative to the underlying layer.

When $v_1 \neq v_2$ the locus of turning points of growth edges along $[1\bar{1}0]$ and $[110]$ was inclined to the b-axis (Fig.46) ; the pair of lines linking the intersections of $[1\bar{1}0]$ with $[110]$ and $[\bar{1}\bar{1}0]$ with $[\bar{1}10]$ were inclined to each other. The angle between these two locii was less than 180° towards the side of crystal on which the velocity of advance of the growth edges was greatest. Fig.59 shows a crystal of the B-form of stearic acid grown at about 276°k. The locii are clearly marked by a bright diffraction pattern. It can be seen that the small increase in the temperature of growth has accentuated the difference between v_1 and v_2. In addition the growth edges have become slightly curved and more irregular.

The space group of the B-form of these fatty acids

is $P2_1/a$. Hence the vector diagram for growth upon (001) and (00$\bar{1}$) should be related by a two-fold rotation about the b-axis. This effect is illustrated by the growth pattern upon a crystal of the B-form of stearic acid grown at $\sim 276^{\circ}k$, shown in Fig.60. The brighter diffraction lines clearly mark the turning points of the growth edges on the upper face of the crystal. A fainter pair of diffraction lines is also visible. This probably marks the turning point of growth edges upon the lower face of the crystal. The two pairs of locii are related by rotation about the diad axis.

These observations show that one of the factors which determines the shape of growth spirals upon the (001) face of fatty acid crystals is the tilt of the molecules. This conclusion has recently been confirmed by Amelinckx [133]. The dependence of the velocity of growth upon the tilt of the molecules is extremely important when considering the growth patterns due to layer disorders.

8.6. Spiral Growth and Related Steps.

Generally the (001) face had a rhombic shape, and the dislocation occurred near the centre of the face. When the growth origin was not at the centre of the face, or $v_1 \neq v_2$, modifications of the growth pattern occurred. Three possible modifications are shown in Fig. 61. In each case the spiral growth leads to 'related' steps, such as RR ; which have the same height as the spiral step but are not directly

linked with it.

The density of stearic acid crystals is 0·85 $gm.cm^{-3}$, and of behenic acid is 0·84 $gm.cm^{-3}$, which is less than the density of chloroform, 1·50 $gm.cm^{-3}$. Hence some of the crystals must have floated on the crystal surface. The question now arises, what effect would this have upon a spiral growth hill.

Consider the growth pattern shown in Fig.61. If all growth upon (001) was arrested but growth on other $\{001\}$ faces continued, steps such as RR which extended to an edge of the (001) face would lengthen in a direction normal to that edge (Fig.62). It is unlikely that all growth on (001) would cease, since the edges of the face would be in contact with the solution. Then, as the lateral growth continued, RR would gradually change direction, as shown by the dotted lines in Fig.62. In either case, the boundary of the (001) face at the time when growth on this face was arrested would be revealed by the sudden deviation of these steps.

Figs. 48 and 63 show growth patterns which can be interpreted in this manner. The spacing and doubling of the 'related' steps in Fig.48, clearly corresponds with that of the spiral step. This indicates that the spiral steps and related steps are all due to the spiral growth. Since the related steps have not become normal to the crystal edges it appears that as the crystal extended laterally some deposition

of molecules occurred at the step edges.

Fig. 64 shows an internal interferogram (reflexion) of a crystal of the B-form of stearic acid in which growth upon (001) was arrested at an early stage. The reflexion fringes are parallel to the step edges. If this growth pattern is compared with Fig.62, it will be seen that the area A should be an elevation. An examination of the fringe displacement in Fig.64 confirms this deduction.

The fringes of equal chromatic order for a line section SS across this crystal are shown in Fig.65. Since the crystal was birefringent these fringes were originally double; but one plane polarised component of the fringe system has been suppressed by using an analyser. For each fringe of order n ,

$$n = \frac{2\mu x}{\lambda}$$

The internal interferogram therefore shows that the thickness of the crystal was greatest at its centre. The growth pattern is a spiral hill. The mean height of the spiral step was found to be (429 ± 34) Å. The height of the related steps was also determined and found to be (423 ± 29) Å. and (406 ± 45) Å. The height of the spiral step and related steps was therefore equal, within the limits of error. Thus observations of growth patterns Fig.48 and measurements of step-height both show that the related steps arose from the spiral growth.

These considerations are useful when studying complex growth patterns similar to Fig.66. Only the central region of the growth pattern was due to growth on (001). The outer growth steps developed after growth on (001) had ceased.

REFERENCES

132) VERMA, A.R., REYNOLDS, P.M. Proc. Phys. Soc. 66 414 (1953)

133) AMELINCKX, S. Acta Cryst. 9 217 (1956)

CHAPTER IX.

MEASUREMENTS OF THE HEIGHT OF SPIRAL GROWTH STEPS

9.1. Interferometric measurements.

The mean height of a continuous spiral step or set of closed loops was determined from Fizeau fringes of equal thickness formed by internal interference, which contoured the growth steps.

Fig. 67a shows the central area of a single spiral on a crystal of behenic acid. The reflexion internal interference fringes are shown in Fig. 67b. The region to the left of the central dividing line was photographed with phase contrast illumination, and was used to determine the position of the steps. The region to the right shows one component of the reflexion fringes formed by internal interference, and enables the position of the fringe minima to be located. Superimposed upon this figure are faint two-beam fringes which originated from the glass reflector used to obtain normal incident illumination.

The Fizeau fringes (Fig. 67) are contouring the surface steps. Hence if the number of steps between successive fringe minima having the same place of polarisation is n, the mean step-height, h, is given by

$$h = \frac{\lambda}{2\mu n} \qquad \text{xxxviii)}$$

where μ is the appropriate value of the refractive index. In

this case $n = 34 \pm 2$, $\mu = 1.543 \pm 0.002$ and $\lambda = 5780 \pm 10$. Å
Hence

$$h = (52.1 \pm 3.2)\ \text{Å}.$$

Since the (001) spacing of the B-form of behenic acid is 53.0 Å, this growth step was bimolecular.

The optical thickness of a crystal changes discontinuously along any radius of a growth hill. Hence the fringe minimum may not occur upon a terrace between steps, and n is not an exact integer. In the above example, the growth steps were so closely spaced that the error in neglecting the fractional part of n was small compared with the error in locating the approximate position of the fringe minimum. When the growth steps were more widely spaced the fractional part of n could be estimated by visual inspection to $\pm \frac{1}{2}$.

Fig. 68 shows a single spiral on a crystal of stearic acid. Here $n = 13 \pm \frac{1}{2}$, $\lambda = 5461$ Å and $\mu = 1.517 \pm 0.001$. The mean step-height was given by

$$h = (138.4 \pm 5.3) = 3(46.1 \pm 1.8)\ \text{Å}.$$

i.e. the spiral step was probably composed of three bimolecular layers each of thickness $c \sin\beta = 43.8$ Å.

The growth pattern shown in Fig.69 appears to be due to a set of closed loops. It can be seen that $2n = 32 \pm 1$. The wavelength of the incident light was 5461 Å and the refractive index of this stearic acid crystal $\mu = 1.527 \pm 0.010$.

Hence

$$h = (110 \pm 4) = 2\tfrac{1}{2} \quad (44.0 \pm 1.6)\,\text{Å}$$

It was essential that these measurements should be confined to single spiral steps on sets of closed loops. Otherwise two co-operating spirals of step-height $2\,c \sin\beta$ and $3\,c \sin\beta$ would lead to an apparent (mean) step-height $2\tfrac{1}{2}\,c \sin\beta$. Since the steps were not always clearly resolved and diffraction effects occurred at their turning points it was extremely difficult to avoid errors in interpreting the growth pattern.

The results of several of the interferometric measurements on crystals of stearic and behenic acid are shown in Table 5.

STEARIC ACID $c \sin\beta = 43.8$ Å		BEHENIC ACID $c \sin\beta = 53.0$ Å	
Step height Å	Multiple	Step height Å	Multiple
45.9 ± 1.2	1 (45.9 ± 1.2)	52.1 ± 3.2	1 (52.1 ± 3.2)
45.9 ± 3.0	1 (45.9 ± 3.0)	82.6 ± 8.1	$1\tfrac{1}{2}$ (53.4 ± 5.4)
43.6 ± 2.2	1 (43.6 ± 2.2)	104 ± 6	2 (52.0 ± 3.0)
44.7 ± 1.6	1 (44.7 ± 1.6)	105 ± 7	2 (52.5 ± 3.5)
94.1 ± 5.0	2 (47.0 ± 2.5)	136 ± 11	$2\tfrac{1}{2}$ (54.4 ± 4.2)
94.1 ± 5.0	2 (47.0 ± 2.5)	155 ± 11	3 (51.7 ± 3.6)
86.6 ± 4.4	2 (43.3 ± 2.2)		
84.6 ± 6.0	2 (43.3 ± 3.0)		
110 ± 4	$2\tfrac{1}{2}$ (44.0 ± 1.6)		
138 ± 5	3 (46.0 ± 1.8)		
155 ± 7	$3\tfrac{1}{2}$ (44.6 ± 1.9)		
173 ± 9	4 (43.4 ± 2.2)		

Table 5.

A majority of the step-heights were multiples of $c \sin\beta$, i.e. an even number of molecules high. There were four exceptions, in which the step-height corresponded to an odd number of molecules. In each case the growth patterns appeared to be due to single spiral steps or sets of closed loops.

9.2. Measurements with the Electron Microscope.

To overcome the difficulties due to the limited resolution of the optical microscope and to verify the above observations, crystals of behenic acid were studied with an electron microscope. The height of individual growth steps was found by shadowcasting the crystals. When the shadowing angle was θ , and the shadowlength in the shadowing direction ℓ , the step-height h was given by

$$h = \frac{\ell \tan\theta}{M} \qquad \text{xxxix)}$$

where M was the magnification.

In a typical case the error in M was $\sim 3.7\%$, and in θ $\sim 4.5\%$. It was found that the shadowing metal, gold-palladium, tended to aggregate. This caused irregularities in the background intensity which tended to increase the measured values of ℓ . The estimable error in ℓ was $\sim 4.5\%$.

h Å	h Å	h Å
53 ± 12	56 ± 11	55 ± 7
57 ± 9	54 ± 11	60 ± 8
56 ± 9	53 ± 11	61 ± 7
60 ± 9	53 ± 11	
61 ± 10	55 ± 13	
58 ± 12	54 ± 11	75 ± 13
62 ± 11	56 ± 13	77 ± 15
59 ± 9	55 ± 12	84 ± 11
56 ± 9	59 ± 12	79 ± 12
56 ± 6	58 ± 12	74 ± 8
56 ± 8	53 ± 13	85 ± 12

$c \sin\beta = 53.0$ Å $\qquad \frac{3}{2} c \sin\beta = 79.5$ Å

Table 6. (Behenic Acid)

The results of measurements with the electron microscope are shown in Table 6. The height of a growth step was either $c \sin\beta$ or $\frac{3}{2} c \sin\beta$. There was no evidence of monomolecular growth steps. In the case of the optical measurements this was not surprising. A crystal would have to be exceptionally well-developed for seventy successive growth steps to be resolved. Usually not more than forty steps were observed. With the electron microscope several steps < 50 Å high were found. These steps had not grown.

It seems that monomolecular growth steps rarely occurred.

Large growth steps were observed with the electron microscope, and it was seen that these steps tended to dissociate into groups of smaller steps. These crystals were usually too thick for detailed examination. After a few seconds in the electron beam the heat absorbed by a thick crystal caused the support film to rupture.

Fig. 70 shows a spiral growth from a single dislocation of large Burgers vector. The height of the main spiral step exceeds 80 Å. It was impossible to make exact measurements on this crystal owing to the irregularity of the step edges and the proximity of the crystal to the support grid (which altered the local shadowing angle). Fig.44 also shows that single dislocations of large Burgers vector occurred. It can be seen that the growth step is tending to dissociate. Under phase-contrast illumination the 'halo' around large steps generally prevented the observation of any finer detail on the terraces between these steps. Consequently the growth patterns illustrated in Figs.44 and 70, would probably appear, under phase-contrast illumination, to arise from single spiral steps.

The fact that optical measurements showed single spiral steps of height as much as $\sim$ 400 Å (Fig. 64), whereas electron microscopic measurements revealed only steps less than $\sim$ 80 Å high was due to the limitations of the two techniques.

9.3. Conclusions.

Within the limitations of the respective techniques, the electron microscopic measurements confirmed the optical measurements. The height of spiral growth steps upon crystals of stearic and behenic acid was found to be a multiple (greater than unity) of $\frac{1}{2}$ c $\sin\beta$. Even multiples of this unit occurred more frequently than odd multiples. Large growth steps tended to dissociate into smaller steps (which were probably bimolecular).

When the height of a spiral growth step was $\frac{(2N+1)}{2}$ c $\sin\beta$, where N was an integer, the component of the Burgers vector of the parent dislocation normal to (001) was not an interplanar spacing. The dislocation was therefore IMPERFECT.

9.4. Imperfect Dislocations.

The next point to be considered was whether the normal component of the Burgers vector of the parent dislocation was also a multiple of $\frac{1}{2}$ c $\sin\beta$, or whether it was $\frac{1}{2}$ N c $\sin\beta$ + ε , where $\varepsilon < \frac{1}{2}$ c $\sin\beta$.

Energy considerations suggest that perfect dislocations (N c $\sin\beta$) will occur more frequently than dislocations whose Burgers vector has a normal component $\frac{(2N+1)}{2}$ c $\sin\beta$; and that dislocations with Burgers vector $\frac{1}{2}$ N c $\sin\beta$ + ε will be least frequent.

In a molecular crystal the height of spiral growth steps must depend upon the Burgers vector of the parent dis-

location and the units in solution. Since chloroform is a non-polar solvent the fatty acids tend to associate into dimers in solution (Broughton [134]), but the association is probably incomplete. This suggests that bimolecular steps will grow more readily than monomolecular or trimolecular steps. Furthermore, if a dislocation produces a terminated step of height $\frac{1}{2}$ N c sin$\beta + \varepsilon$, one expects that during growth this will dissociate into a single growth step or group of steps of height $\frac{1}{2}$ N c sinβ and a residual step of height ε which does not grow.

In a majority of crystals the height of a single spiral step was a multiple of c sinβ and there was no evidence of a residual step (Fig.71, N = 1). The parent dislocation was therefore perfect.

Fig.72 shows a set of closed loops of step-height (75 ± 13) Å. There is no evidence of a residual step. The normal component of the Burgers vector was therefore $\frac{3}{2}$ c sinβ.

Fig.73 illustrates a crystal of the C-form of behenic acid. The height of the two innermost growth steps was found to be (67±12) Å, i.e. $\frac{3}{2}$ c sinβ. There are also faint steps emerging from the growth centres whose height was less than 48 Å. Because the molecules exist as units in solution it could be assumed that the growth step was trimolecular. This reasoning could not be extended to the residual steps which had not grown. The errors in measuring the step-height were

then so high that it was impossible to draw any conclusions from measurements on residual steps. These steps could be monomolecular, or be of random height, or be due to internal slip (cf Chap. X).

Hence it has been shown that perfect dislocations and imperfect dislocations whose Burgers vector had a normal component $\frac{(2N+1)}{2} c \sin\beta$ occurred in these crystals. It was not possible to show that the normal component of the Burgers vector was <u>always</u> an exact multiple of $\frac{1}{2} c \sin\beta$. On the contrary it was possible that dislocations of random Burgers vector were occasionally present.

These observations show that in molecular crystals, in which the molecules are bound by residual van de Waals forces, the hypothesis that the normal component of the Burgers vector of a dislocation is equal to an interplanar spacing, is not valid.

9.5. <u>Recent Reports of Spiral Growth in Molecular Crystals.</u>

Since the commencement of the present study, further evidence has been presented of spiral growth on the basal planes of long-chain crystals.

Dawson [135] and Anderson and Dawson [136, 137] studied crystals of the orthorhombic paraffins n-hectane, n $C_{100} H_{202}$, and n-nonatriacontane, n $C_{39} H_{80}$, stearic acid, $CH_3 (CH_2)_{16} COOH$, and the fatty acid ester n-propyl n-pentacontanoate, n $C_{53} H_{166} O_2$ with an electron microscope.

The height of spiral growth steps upon these crystals was compared with the association of the molecules in the solution. The results of these investigations, together with the earlier work by Dawson and Vand [138] on n-hexatriacontane, $C_{36}H_{74}$ are summarised in Table 7.

Substance	Solvent	c parameter (molecules)	unit in solution (molecules)	Spiral step heights (molecules)
n-hexatriacontane	Petroleum Ether	1	1	1
n-hectane	Xylene	1	1	1
n-nonatriacontane	Petroleum Ether	2	1	1
Stearic acid	"	2	2	2
n-propyl n pentacontanoate	"	1	1	1

Table 7.

No evidence of growth steps greater than the unit in solution was found. It appeared that growth steps from dislocations of high Burgers vector tended to dissociate into a succession of smaller steps. A similar observation has been made in the present study. It was concluded that the height of the growth steps depended upon the association of the molecules in solution and not upon the Burgers vector of the parent dislocation. This conclusion was at variance with Frank's [139] hypothesis that the Burgers vector of the dislocation determines the height of growth steps.

Upon stearic acid a step which was apparently unimolecular was reported. This step had not grown Since the errors of measurement were ± 20% it is not clear whether this step was definitely unimolecular.

It is interesting to note that in the case of n-nonatriacontane, if the height of a single spiral step is equal to the length of one molecule, the parent dislocation must be imperfect.

Later Anderson, Dawson and Watson [140] investigated the effect of the solvent upon the height of growth steps on n-pentacontanol, n C_{50} H_{101} OH. It was found that a majority of crystals of this alcohol grown from polar solvents had both monomolecular and bimolecular growth steps; those grown from a non-polar solvent showed monomolecular growth steps. These results differ from those reported by Amelinckx [141] for the crystallisation of C_{26} H_{53} OH from benzene. Here no monomolecular steps were observed.

Verma [142] has studied the growth of palmitic acid crystals from benzene by optical and interferometric methods. A majority of the growth steps were found to be multiples of $c \sin\beta$. Amongst some fifty measurements two exceptions were found in which the spiral step-heights were $\frac{5}{2}$ $c \sin\beta$ and $\frac{3}{2}$ $c \sin\beta$ respectively,

Optical and interferometric methods were also used by Amelinckx [143, 144] to study the growth of crystals of the

n-alcohols $C_{22}H_{45}OH$, $C_{24}H_{49}OH$ and $C_{26}H_{53}OH$. These crystals exist in both an orthorhombic and monoclinic form. The height of spiral steps was generally found to be equal to the (001) spacing. Growth patterns from dislocations of multiple Burgers vector were also described. To explain some of the growth patterns it was necessary to introduce imperfect dislocations.

Later Amelinckx [145, 146] studied the growth of behenic acid, $CH_3(CH_2)_{20}COOH$, cikosanoic acid $CH_3(CH_2)_{18}COOH$, and lignoceric acid $C_{23}H_{47}CO_2H$, from solution in xylene and benzene. The height of the growth steps was measured by multiple-beam fringes formed by internal interference. On behenic acid most of the growth steps were bimolecular. Single growth steps of height $4c\sin\beta$ were also reported. Evidence of layer disorders and imperfect dislocations was also found.

From these reports it may again be seen that whereas optical studies revealed growth steps whose height was a multiple of the (001) spacing, electron microscopic examinations showed only monomolecular or bimolecular growth steps. Steps whose height exceeded the molecular unit in solution tended to dissociate.

Verma [142], Amelinckx [143–146] and also Anderson and Dawson [136] have also found evidence of imperfect dislocations in long-chain crystals. It is clear that

molecular crystals are often imperfect, and that their spiral growth depends upon both the Burgers vector of the parent dislocation and the association of the molecules in the solution.

REFERENCES

134) BROUGHTON, G. Trans. Faraday Soc. 30 367 (1934)

135) DAWSON, I.M. Proc. Roy. Soc. A. 214 72 (1952)

136) ANDERSON, N.G., and DAWSON, I.M.
Proc. Roy. Soc. A. 218 255 (1953)

137) Proc. Roy. Soc. A. 228 539 (1955)

138) DAWSON, I.M., and VAND, V.
Proc. Roy. Soc. A. 206 555 (1951)

139) FRANK, F.C. Disc. Faraday Soc. No.5.
(Crystal Growth) p. 67.

140) ANDERSON, N.G., DAWSON, I.M., and WATSON, D.H.
Naturwiss. 41 211 (1954)

141) AMELINCKX, S. Naturwiss 40 620 (1953)

142) VERMA, A.R. Proc. Roy. Soc. A. 228 34 (1955)

143) AMELINCKX, S. Acta Cryst. 8 530 (1955)

144) Acta Cryst. 9 16 (1956)

145) Natuurw. Tijdschr (Gent) 36
p.p. 3 - 206 (1954) (published 1955)

146) Acta Cryst. 9 217 (1956)

CHAPTER X.

SLIP AND INTERNAL SLIP

10.1. Introduction.

Slip in real crystals has long been attributed to the movement of dislocations in planes of easy glide. The height of the slip step raised on a growth face is expected to be a multiple of the interplanar spacing.

According to Forty and Frank[147] a slip step is essentially similar to a growth step, but is initially straighter. There is, however, one important difference, for whereas growth steps cannot intersect, slip lines can cross other surface steps without interruption.

Consider now a crystal face with a set of parallel growth steps of equal height h. If a slip step, also of height h, intersects these growth steps the terraces A, B, C, etc., (Fig.74) are elevated by an amount h. Thus the level of B and A', C and B', etc., becomes the same. A slip step of height $2h$ would raise the terrace C to the same level as A'. In general slip through a height mh will bring the n^{th} terrace on one side of the slip plane to the level of the $(n+m)^{th}$ terrace on the opposite side.

If growth continues after slip has occurred, the two terraces at the same level will merge into one, and the re-entrant corners in the step-edge will become rounded. When $m = 1$ the step edges will appear as shown in Fig.75, where the

trace of the slip plane is indicated by a series of kinks in the step edges. Eventually preferred deposition at the re-entrant corners will eliminate all evidence of the slip process.

10.2. Slip in crystals of Stearic Acid.

Fig. 76. shows the surface of a large, thick crystal of stearic acid. Two types of step may be identified. Firstly, serrated steps whose spacing alters in a regular manner; these are characteristic features of growth steps. Secondly sharp irregularly spaced steps which intersect the growth steps; these steps appear to be due to slip in the later stages of growth.

An internal interferogram of this crystal is shown in Fig. 77. The correspondence between areas of uniform tint shows that the height of many of the slip steps is equal to the height of the growth steps. There were over twenty-seven resolvable growth steps between successive internal interference fringes, i.e. most of the steps were probably bimolecular.

A further case of slip is illustrated in Fig.78. Here it is quite clear that the serrated steps originated from a growth centre. Intersecting the growth hill are two clearly defined steps which branch into sets of parallel steps which are irregularly spaced and intersect the growth steps. There can be no doubt that these are slip lines. In addition

there is a series of kinks in the step edges. An enlargement of this region of the crystal is shown in Fig.79. It can be seen that in this case, slip occurred before growth had ceased. The interaction between the slip step and growth step shows that all the growth steps were of equal height, and had the same height as the slip step. In Fig.78 at least thirty-four steps occur between successive interference fringes, hence the growth steps were bimolecular. Since $m = 1$ this is an example of unit slip in a crystal of stearic acid.

Unit slip lines have also been observed by Forty and Frank [147] upon crystals of silver grown at a temperature close to their melting point.

The slip lines shown in Figs. 76 and 78 are slightly curved and are not in strictly crystallographic directions. This is not surprising, since the lateral binding forces in these crystals are extremely weak.

An unusual type of terminated slip line was occasionally found upon these crystals (Fig.80). These slip lines were usually in crystallographic directions. It was not possible to accurately determine the height of these steps, since they did not cause any apparent deviation in the interference fringes. Their height was probably less than 50 Å.

These results, together with the observations of spiral growth, show that slip readily occurs in crystals of stearic and behenic acid.

10.3. Internal Slip. Introduction.

A striking proof of the ease with which fatty acid crystals are deformed at ordinary temperatures was given by the phenomena of internal slip. Anderson and Dawson[148] found that when thin crystals of the long-chain paraffins settled upon a support film, steps on the lower surface of the crystal became imprinted on to its upper surface. This phenomena was called 'internal slip.' Internal slip also occurs when two crystals settle on top of each other. Verma[149] has shown that in crystals of palmitic acid the underlying growth pattern can be imprinted through thicknesses $\sim$ 1000 Å.

Before proceeding to discuss examples of internal slip in crystals of stearic and behenic acid, it must be emphasised that it has been repeatedly confirmed that when the uppermost surfaces of these crystals were coated with a highly reflecting silver film, phase contrast illumination did not reveal the structure of the lowermost surface. This conclusion has been supported by Verma[149].

10.4. The inclination of a dislocation line.

In general, the energy of a dislocation line is proportional to its length. Hence, to obtain stable equilibrium the dislocation lines will tend to make themselves as short as possible. This consideration will probably overcome the tendency for a dislocation line to follow a preferred

direction in the lattice. Consequently the dislocation lines will probably emerge more or less normal to a crystal face (Frank [150]).

In the case of molecular crystals such as the fatty acids, the energy of unit length of a dislocation line cannot depend strongly upon its orientation. Therefore since the lateral dimensions greatly exceed the thickness of the crystal, one expects most of the dislocation lines to terminate on (001) and $(00\bar{1})$.

10.5. Internal Slip in Crystals of Stearic and Behenic Acid.

Fig.81 shows two superimposed growth spirals due to a single dislocation which terminates on (001) and $(00\bar{1})$. The two growth spirals appear to be of opposite hand. The reason for this may be understood from Fig.82. A single dislocation has led to an anti-clockwise growth spiral upon each face of the crystal. Yet if these growth patterns are viewed from the same side of the crystal the spirals appear to be of opposite sense.

Since internal slip has occurred, the thickness of the crystal must be less than 2000 Å. Hence, if it is assumed that the lateral resolution of the optical microscope was $\sim$ 6000 Å, the dislocation line must be inclined to the crystal face at a mean angle θ where $18^\circ \leq \theta \leq 90^\circ$. Since the lateral resolution was probably better than 6000 Å, the most likely values were $30^\circ \leq \theta \leq 90^\circ$.

The two superimposed spirals of opposite hand shown in Fig. 83 do not emerge from coincident growth centres. The two growth centres are linked by a faint irregular line. The two spirals appear of opposite hand, and since there is no other structure visible upon this crystal, it can reasonably be assumed that they are due to the same dislocation. The mean inclination of the dislocation line to the (001) face must therefore be extremely small.

Figs. 84 and 85 show internal interferograms of two similar superimposed growth patterns. To reveal the growth steps, phase contrast illumination was used. This slightly altered the fringe intensities but did not modify the interpretation of the fringe pattern. The areas of uniform tint show that the growth steps on either face of these crystals had the same height. The steps were probably bimolecular, and due to the same dislocation.

Although these results are not conclusive, they strongly suggest that in fatty acid crystals the dislocation lines are not necessarily parallel to the chain axes, or normal to (001).

When there were steps radiating from the centre of a spiral growth pattern, it was seldom possible to determine whether they were due to residual steps which had not grown, or steps revealed by internal slip. Fig.86 illustrates a crystal in which the radial lines were clearly due to internal

slip. On one face of the crystal there were two closely co-operating spirals. On the other face were two steps with a similar separation, which had just begun to assume a spiral form.

It has been suggested that certain growth patterns can be interpreted by assuming that the crystal floated to the surface of the solution and growth on (001) was arrested. Further evidence in support of this hypothesis is given by Fig.87. Growth upon (001) was arrested, but the growth spiral upon $(00\bar{1})$, which was in contact with the solution, extended to the boundaries of the crystal face.

These observations clearly show that internal slip occurs in crystals of stearic and behenic acid. However, there must be an upper limit to the thickness of the crystals in which internal slip occurs. Furthermore, the ease with which internal slip occurs must depend upon the temperature of the crystals.

10.6. The Mechanism of Internal Slip.

Fig. 88 shows an internal interferogram of two superimposed crystals of stearic acid. One crystal has developed a growth spiral with steps of height $\sim$ 300 Å. The other crystal shows no surface structure and has a thickness $\sim$ 1500 Å. These crystals were opaquely silvered, Fig.89, and it was found that the spiral step had been imprinted through the hexagonal crystal plate. In this process the

step became more diffuse.

The single spiral step on a crystal of stearic acid shown in Fig.68 had a height $\sim$ 140 Å. Across the centre of this spiral lies a small crystal of thickness $\sim$ 1000 Å. If it is assumed that the smaller crystal had settled upon the larger one, internal slip occurred through a thickness $\sim$ 1000 Å.

These optical observations indicated that internal slip could occur in layers $\sim$ 1500 Å thick. However, the electron micrograph, Fig.90, proves that internal slip cannot be regarded as slip in a crystallographic sense. Here the upper crystal was only $\sim$ 300 Å thick, yet the steps revealed by internal slip were not as clearly defined as the growth steps. Thus, in the process of internal slip the underlying structure was not perfectly replicated even when the crystals were extremely thin. The perfection of replication depended upon the thickness of the crystal through which the underlying steps are imprinted. Optical observations did not reveal this unless the crystal thickness exceeded 1000 Å. This was due to the limited resolution of the phase contrast microscope.

REFERENCES

147) FORTY, A.J., and FRANK, F.C.
Proc. Roy. Soc. A. 217 262 (1953)

148) ANDERSON, N.G., and DAWSON, I.M.
Proc. Roy. Soc. A. 218 255 (1953)

149) VERMA, A.R. Proc. Roy. Soc. A. 228 34 (1955)

150) FRANK, F.C. Disc. Faraday Soc. No.5.
(Crystal Growth) p. 76.

CHAPTER XI.

INTERLACING AND GROWTH FROM IMPERFECT DISLOCATIONS.

11.1. Interlacing.

A growth spiral is said to be interlaced if the growth edges in one (or several) orientation(s) dissociate in a regular manner. Hexagonal interlaced spirals were first reported by Verma [151] upon a crystal face of carborundum Type II. Later, interlaced spirals were observed upon cadmium iodide (Forty [152]) and biotite (Amelinckx [153], Amelinckx and Dekeyser [154]). An explanation of this phenomenon has been given by Frank [155].

11.2. The origin of interlacing.

Suppose that a dislocation leads to a terminated step of height $(h + h')$ upon a crystal face. Let this step be composed of two layers, L and L', of thickness h and h' respectively. The velocity of advance of a composite step is governed by the velocity of its lowermost component. Consequently this step will tend to dissociate whenever L has a greater velocity of advance than L'. For example, suppose the vector diagrams for the velocity of advance, v, of L and L' are as shown in Fig.91. In sectors 1 and 2, $V_1 < V_1'$ and $v_2 < v_2'$, and the step cannot dissociate. In sectors 3 and 4, $v_3 > v_3'$ and $V_4 > V_4'$. The step therefore dissociates into layers of thickness h and h' and the growth pattern shown in Fig.92 is obtained. The separation between

the growth edges in sectors 3 and 4 increases as the distance from the growth centre increases. Eventually the n^{th} turn of L coincides with the $(n + 1)^{th}$ turn of L' and the advance of L again becomes restricted. As a result, the two layers reform into a single step of height $(h + h')$. The corners of these growth edges are 'interlaced' by layers of thickness h.

11.3. Interlacing in Stearic and Behenic Acid Crystals.

Figs. 93 and 94 are examples of interlaced spirals upon crystals of stearic acid. These growth patterns closely agree with the theoretical pattern (Fig.92) and show the way in which the steps gradually regroup as the distance from the growth centre increases. It can be seen that the vector diagrams for the two component layers were related by a relative notation $\phi = 180^{\circ}$.

When $v_3 >> v_3'$ and $V_4 >> V_4'$ the component layers regrouped within a few turns of the spiral. The only evidence of interlacing was faint steps linking the acute corners of the main spiral, as shown in Fig. 95.

Fig. 96 illustrates a complex growth pattern due to at least five disordered layers.

Despite prolonged efforts it was not possible to determine the height of the main growth fronts of an interlaced spiral by interferometry. Clearly resolved interlaced spirals were seldom found with the optical microscope. In the few cases observed the internal interference fringes were not

suitable for step-height measurements. One example of interlacing (on a crystal of behenic acid) was found with the electron microscope, and is shown in Fig.97. The growth edges were extremely irregular. The two outermost growth steps each had a height (48 ± 20) Å, and were probably bimolecular.

Fig.98 shows an electron micrograph of a large crystal of behenic acid. The grouping of the growth edges was probably due to multiple interlacing. The growth steps were all equal and had a height (49 ± 12) Å.

These results suggested that interlacing in crystals of stearic and behenic acid grown from solution was due to stacking faults between successive (groups of) bimolecular layers. It has already been shown that the vector diagram for the velocity of bimolecular growth steps is assymetrical and depends upon the tilt of the molecules relative to (001). The example of interlacing given in 11.2 shows the result of the growth of two bimolecular layers which are misoriented by a rotation of $\phi = 180^{\circ}$. This immediately yields an explanation of the interlacing observed upon crystals of stearic and behenic acid.

The spiral growth from these misoriented bimolecular layers generates a helical fault surface. The positions of the CH_3 end groups in a (001) plane are shown in Fig.99. It can be seen that after a rotation $\phi = 180^{\circ}$ the CH_3 groups are

almost in their normal stacking positions. Consequently the increase in the potential energy of the crystal due to the fault surface is small.

The structure of an interlaced crystal is a POLYTYPE of the normal structure. The c-spacing of the polytype is a multiple of the thickness of a bimolecular layer. X-ray and electron diffraction examinations of fatty acid crystals have not yet shown any evidence of polytypism.

11.4. Related Work.

The preceding conclusions were supported by an earlier observation by Verma [156] of interlacing upon a crystal of palmitic acid, $CH_3(CH_2)_{16}COOH$ grown from solution in benzene. The height of the main growth fronts was measured from multiple-beam internal interference fringes and found to be $2c \sin\beta$ i.e. two bimolecular layers. Verma [156] suggested that interlacing in fatty acid crystals was due to growth from an imperfect dislocation. This hypothesis was not confirmed by the experimental observation.

Whilst the present investigation of interlacing was in progress Amelinckx [157] reported interlacing upon crystals of behenic acid grown from solution in xylol or benzol. Optical and interferometric methods were used. The main growth fronts were found to be bimolecular. It was concluded that the interlacing was due to the grouping of monomolecular

layers. The vector diagrams for the two component layers were related by a rotation $\phi = 180^{\circ}$. The following explanation of interlacing was given:

The crystal structure consists of molecules associated in bimolecular layers. Hence when a bimolecular layer dissociates into two monomolecular layers, one monomolecular layer advances with CH_3 - CH_3 bonding to the substrate, whilst the other has COOH - COOH bonding. It was assumed that the vector diagram for a monomolecular layer was assymetrical, and that the relationship between the vector diagrams for the two component layers was as shown in Fig.100. The resultant interlaced growth pattern is also shown in this figure. After the monomolecular layers had regrouped into bimolecular layers, the bonding between the advancing growth front and the substrate was of the COOH - COOH type on one half of the crystal (shaded), and the CH_3 - CH_3 type on the other.

There were two points in this explanation which were questionable. Firstly, why was the velocity of advance of a monolayer different in different sectors. Secondly, since the carboxyl bond was the strongest bond between adjacent molecules, the helical fault surface must lead to a large increase in the potential energy of the crystal. Thus energy considerations suggested that this type of interlacing would be extremely rare. The present study was therefore continued.

Recently Amelinckx[158] withdrew this explanation of interlacing in fatty acid crystals. He concluded that interlacing in these crystals arose from stacking faults between successive bimolecular layers. These conclusions were substantiated by accurate measurements of the height of the main growth fronts. Interlaced spirals with main growth fronts at height up to 4 c sinβ were reported.

Previously Amelinckx[157, 159, 160] studied the monoclinic and orthorhombic forms of the n-alcohols $C_{22}H_{45}OH$, $C_{24}H_{47}OH$ and $C_{26}H_{53}OH$, by optical methods. Interlacing was found. An analysis of the growth patterns upon the monoclinic form of these alcohols revealed stacking faults between successive bimolecular layers. The layers were related by a rotation $\phi = k \times 60^{\circ}$. The orthorhombic form of these alcohols showed two types of interlacing which were due to stacking faults between monomolecular layers. In the first type the polar diagrams for the velocities of growth were related by a mirror line; whereas in the second type they were related by a rotation $\phi = 180^{\circ}$.

Collectively these reports show that stacking faults occur in crystals of many long chain compounds. In the case of the fatty acids and the monoclinic form of the n-alcohols, spiral growth in disordered crystals leads to polytypism.

11.5. Growth from an Imperfect Dislocation.

If an imperfect dislocation whose Burgers vector has

a normal component $\frac{2N+1}{2}$ c $\sin\beta$ occurs in an otherwise perfect crystal, the exposed ledge contains an odd number of monomolecular layers. This is shown in Fig.101 for the case when $(2n+1) = 3$. It has been assumed that the surface layer consists of CH_3 groups. The slip surface is a fault surface.

Both Verma [156] and Amelinckx [157, 159] have discussed the growth from an imperfect dislocation. When growth occurs on the exposed ledge two possibilities arise.

i) the stacking in the growth step is determined by the stacking in the exposed ledge

ii) the stacking in the growth step is determined by the stacking in the substrate.

In the first case a helical fault surface is generated, and the crystal is a polytype of the normal structure.

In the second case the normal structure is maintained but the growth is extremely complicated. Each time the spiral growth step crosses the fault surface, the stacking sequence in the growth edge must be reversed. As a result alternate terraces have COOH (or CH_3) groups uppermost, as shown by the shaded regions in Fig.102. The original fault surface is extended. Apparently nothing will reveal the presence of the fault surface. If the layer with COOH - COOH bonding to the substrate advances with a different velocity from the layer with CH_3 - CH_3 bonding, the growth pattern shown in Fig.103 will result. The trace of the fault surface is revealed by

alternating kinks in the step edges. Two imperfect dislocations of opposite sign would result in the growth pattern shown in Fig. 104. Amelinckx [160] has reported that differences in the velocity of growth of successive layers from an imperfect dislocation also leads to interlacing (Fig. 105).

The observations of growth from an imperfect dislocation recorded in Table 6 are shown in Figs. (106-111). The growth steps are trimolecular. There is no evidence of dissociation of these steps or interlacing.

The sets of closed loops shown in Figs. 106 and 107 are evenly spaced, i.e. successive terraces advanced with the same velocity. These results therefore differ from those reported by Amelinckx [160].

These crystals show many examples of residual steps of height less than 50 Å. These residual steps may be described as a) loops terminating at the crystal edges, and b) steps terminating on the (001) face. Their effect upon the growth pattern must depend upon whether they arose before or after growth had ceased. The steps marked a' (Fig. 108) were clearly due to slip, or internal slip, after the cessation of growth. The hindrance of the growth steps at a (Fig. 110) shows that the residual step was present before the growth of the crystal was arrested.

If a residual step of type b) extends to within a distance $\sim 4\pi\rho_c$ of the centre of a growth spiral, the innermost turn of the spiral will be delayed each time it

crosses the residual step, as shown in Fig.112. However, each time a new growth layer crosses the residual step one expects that the residual step will become less sharp. Hence as the thickness of the crystal increases the residual step will produce less retardation of the innermost turn of the spiral. The resulting growth pattern is shown in Fig.113. Eventually the residual step will recede until it appears to terminate beyond the first turn of the growth spiral. In this position it no longer seriously impeded the advance of rectilinear growth steps. The kinked steps b in Fig.110, can be interpreted in this manner. The kinks marked ab (Fig.109) show the results of a combination of the retardation due to two steps of type a extending to within the first turn of a spiral and the delay due to a step loop of type b. The kinks marked c were due to slip, or internal slip, in the last stage of growth. It is probable that the original dislocation was cancelled by internal slip of an undeveloped step on the opposite face of the crystal (cf. Anderson and Dawson [161]).

These observations show that in these crystals there was a profusion of slip, imperfect slip and internal slip. They yield no positive evidence of the structure of a trimolecular growth step. On crystals grown from solution in chloroform the trimolecular steps did not dissociate in the manner described by Amelinckx [160] for crystals grown from solution in xylol or benzol.

REFERENCES

151) VERMA, A.R. Phil. Mag. 42 1005 (1951)

152) FORTY, A.J. Phil. Mag. 43 72 (1952)

153) AMELINCKX, S. Comptes Rendus. 234 971 (1952)

154) AMELINCKX, S. and DEKEYSER, W.
Comptes Rendus de la 19e Session du Congres Geologique international
18 9 (1952)

155) FRANK, F.C. Phil. Mag. 42 1014 (1951)

156) VERMA, A.R. Proc. Roy. Soc. A. 228 34 (1955)

157) AMELINCKX, S. Natuurw. Tijdschr. (Gent) 36.
pp. 3 - 206 (1954) Published (1955).

158) Acta Cryst. 9 217 (1956)

159) Acta Cryst. 8 530 (1955)

160) Acta Cryst. 9 16 (1956)

161) ANDERSON, N.G. and DAWSON, I.M.
Proc. Roy. Soc. A. 218 255 (1953)

CHAPTER XII.

THE SPIRAL GROWTH OF CONTACT TWINS

12.1. Introduction.

It is well known that twinning readily occurs in crystals of the fatty acids. Fig.114 shows an electronmicrograph of three contact twins. The contact plane is (001) and the twin axis is either parallel or perpendicular to [110]. This twinning can also be described as a relative rotation of the individual crystals about the normal to (001) through an angle $\phi = 74^{\circ}$ or 106°.

12.2. Spiral Growth in Twinned Crystals.

When a dislocation occurs in a twinned crystal, the subsequent growth depends upon the structure of the initial step. Consider a twinned crystal composed of two individual crystals of thickness h_1, and h_2, where $h_2 > h_1$. If (Fig.115) the normal component of the Burgers vector of the dislocation, d_n, is less than h_1, simple growth spirals develop on the upper and lower faces of the crystal. The spirals are in twinned orientation. When $h_2 > d_n > h_1$ a more complex growth occurs. The growth spiral on the upper face results from two layers in twinned orientation, but the spiral on the lower face is simple. A consideration of the growth patterns which arise from two bimolecular layers misoriented by angles $\phi = 74^{\circ}$ or 106°, shows that it is possible to distinguish between the two types of twinning.

Case i) $\phi = 74^{\circ}$.

The twin axis is parallel to [110] . The relationship between the vector diagrams for the two component layers, L_1 and L_2 , of the growth spiral is shown in Fig.116. Fig.117 shows the resulting growth patterns. Parallel to $\overrightarrow{OA}$ and $\overrightarrow{OB}$ the component layers advance with the same velocity, i.e. the growth steps do not dissociate.

Case ii) $\phi = 106^{\circ}$.

The twin axis is perpendicular to [110] . Fig.118 shows the derivation of the resultant growth pattern. Growth edges advancing along $\overrightarrow{OB}$ tend to dissociate. Eventually the n^{th} turn of L_2 overtakes the $(n+1)^{th}$ turn of L_1 . This growth pattern can therefore be distinguished from that shown in Fig.117.

12.3. Observations of the Spiral Growth of Twinned Crystals.

Fig.119 shows an electronmicrograph of a twinned crystal of behenic acid. The growth spiral is simple and has the same orientation as the uppermost crystal. The spirals in twinned orientation on opposite faces of a crystal in which $d_n < h_1$, were sometimes revealed by internal slip. An example is shown in Fig.120. It may be noted that the two spirals appear to be of opposite sense.

The second type of growth pattern in which $h_2 < d_n < h_1$ is shown in Fig.121 (stannic acid). Here, the two interleaving spirals are of the same sense but in twinned orientation.

Consequently this growth pattern cannot be due to internal slip. A closer examination of the twinned spirals suggests that the component layers were misoriented by an angle $\phi = 106^{\circ}$. Figs. 122 and 123 show growth patterns which are clearly due to a misorientation $\phi = 106^{\circ}$ and 74° respectively. These crystals were not simple contact twins; as a consequence of the repetition of layer disorders by the spiral growth mechanism POLYSYNTHETIC TWINS were generated.

A notable feature of the growth spiral shown in Fig.122 is the manner in which the non-parallel growth edges have extended beyond the boundaries of the underlying layers. The trace of the underlying step is revealed by the collapse of the projecting growth edges. This phenomenon was only found when the component layers were several molecules thick. It was not observed in normal crystals or in interlaced crystals.

Fig.124 shows an unusual crystal of stearic acid. The crystal was opaquely silvered (Fig.125) and it was found that the growth steps were entirely on the upper surface. Since the two component spirals were of the same sense, the growth pattern could not be due to internal slip. This growth pattern could only be explained by assuming that the individual layers extended beyond the boundaries of the underlying layer and collapsed. A further example of this effect is illustrated in Fig.126. The central region of this growth pattern shows that $\phi = 106^{\circ}$.

A single case of a second type of twinning in behenic acid crystals was found; this is shown in Fig.127. It appears to be an example of spiral growth in an interpentrant twin.

Since the refractive index of a twinned crystal does not have a unique value, internal interference fringes could not be used to study these crystals. The relationship between the misoriented layers in twinned crystals was confirmed by studying the transmission electron diffraction patterns.

12.4. Electron Diffraction. Introduction.

The electron microscope was used to study the electron diffraction patterns from small crystals of the B-form of behenic acid. The accelerating voltage was 75 kV, and the equivalent wavelength, λ , of the electrons 0.045 Å. The incident electron beam was normal to (001), i.e. effectively parallel to [hol].

Fig.128 shows a transmission electron diffraction pattern from a single crystal of behenic acid. The condition for a diffracted beam can be regarded as being made up of two parts. Firstly the condition that wavelets from scattering points in (hol) should reinforce. This condition alone tends to a two-dimensional cross-grating pattern. Secondly, the condition that wavelets from lattice points along [hol] should be in phase. Hence the two-dimensional diffraction pattern will be strong where the second condition is also satisfied and weak, or absent, where it is not. It is only necessary to consider

the three-dimensional lattice to interpret the intensities of the reflexions. Trillat and Hersch[162, 163] have shown that the most intense reflexions were (020). The (010) reflexion was absent, since the space group extinctions are (0k0) when k is odd and (h0l) when h is odd.

It is more convenient to describe the reflexions with the aid of the reciprocal lattice, whose parameters are a^*, b^*, and c^*, where

$$a^* = \frac{1}{d_{100}} \quad \text{(direction} \perp (100)\text{)}$$

$$b^* = \frac{1}{d_{010}} \quad \text{(direction} \perp (010)\text{)}$$

$$\text{and } c^* = \frac{1}{d_{001}} \quad \text{(direction} \perp (001)\text{)}$$

For this purpose it is necessary to introduce the concept of a sphere of reflexion with radius $r = \frac{1}{\lambda}$.

Fig. 129 shows the (010) plane of the reciprocal lattice of the B-form of stearic acid. The c^* axis is parallel to the incident beam and is also a diameter of the sphere of reflexion. The b^* axis coincides with the b-axis and is normal to the plane of the diagram. The third axis of the reciprocal lattice a^* is perpendicular to the b c plane. Since the B-forms of stearic and behenic acid are homologous the reciprocal lattice of the B-form of behenic acid will be similar to that shown in Fig.128, but the c^* spacing will be slightly smaller. Also, since the crystals were extremely thin the reciprocal lattice points will tend to be elongated in the direction of the c^* axis. The radius of the sphere

of reflexion is large compared with the parameters of the reciprocal lattice. Hence the sphere of reflexion is effectively a plane perpendicular to the c^* axis, and is represented by SOS (Fig.129). The sphere of reflexion intersects the (100) plane of the reciprocal lattice at a distance x from the origin, where

$$x = a^* \sin\beta = \frac{1}{a} \qquad \therefore \quad a^* = \frac{1}{a \sin\beta} \ .$$

and the (010) plane of the reciprocal lattice at a distance y from the origin, given by

$$y = b^* = \frac{1}{b}$$

i.e. the intersection of the sphere of reflexion with the reciprocal lattice leads to a rectangular network with parameters $\frac{1}{a}$ and $\frac{1}{b}$. The diffraction pattern recorded upon a flat photographic plate normal to the incident beam is a linear projection of this rectangular network. The h and k indices of the reflexions can be indexed by inspection. The third index, ℓ , is only zero for reflexions lying on the $\frac{1}{b}$ axis, otherwise ℓ is indeterminate. However, since a knowledge of ℓ is only necessary to interpret the intensities of the reflexions, for the present purposes all reflexions can be regarded as (hKO).

12.5. Electron diffraction patterns from Behenic Acid Crystals.

It was found that crystals of behenic acid were not stable even with a very low intensity electron beam. Nevertheless, when these crystals were studied in the intense electron

beam necessary for examination of the surface structure, there were no visible changes in the crystals. Only thick crystals showed any distortion. This observation has been confirmed by Thibaud and Dupre la Tour [164]. Fig.130 shows the transmission electron diffraction patterns from a single crystal of behenic acid. The photographs were taken at ten second intervals; the exposure time was two and a half seconds. Initially the strong (020) reflexions appeared and weaker (040) and (200) reflexions. As the temperature of the crystal rose the (020) reflexions became less sharp and (110), $(1\bar{1}0)$, $(\bar{1}10)$ and $(\bar{1}\bar{1}0)$ reflexions appeared. The latter reflexions increased in intensity until the intensities of the six most prominent reflexions were equal. The $\frac{1}{b}$-axis could then no longer be identified. The final stage of the diffraction pattern is shown in Fig.131. This transition was irreversible.

The detailed interpretation of this phenomenon was not pursued, since it was not relevant to this study of crystal growth. Trillat and Hersch [163] have reported similar observations, but were not able to identify the final form of the crystal. It can be seen that there was only a small change in the lattice parameters.

The position was then as follows: When the crystals were examined directly and disordered crystals selected for study by electron diffraction, in the few seconds which elapsed between selecting the crystals and adjusting to electron diffraction

conditions, the crystal had already undergone a transition. Alternatively, if the crystals were first scanned under electron diffraction conditions and disordered diffraction patterns photographed, it was generally found that the patterns merely arose from crystal aggregates.

Fig. 132 shows the diffraction pattern from the twinned crystal of behenic acid illustrated in Fig. 133. The diffraction rings were due to the shadowcasting metal. Owing to the thickness of the crystal, a rapid transition occurred, and the b-axis could not be identified. This diffraction pattern shows that amongst the possible angles of misorientation between the component crystals were the values $\phi \sim 74^\circ$ or 106°. Thus this observation appears to confirm the deductions based upon a study of the growth patterns.

It is interesting to note that from transmission electron diffraction patterns it would be impossible to distinguish between $\phi = 74^\circ$ and $\phi = 106^\circ$. However, an examination of the growth patterns in twinned crystals indicates that both types of twinning occurred.

12.6. The Packing in the Plane of Contact.

The mean values of the a and b parameters of the B-form of stearic acid given in Table I, are

$$a = 5.57 \text{ Å}$$

$$b = 7.39 \text{ Å}$$

whence $\Psi = 74^\circ\ 2'$.

It can be assumed that the a and b parameters of the

B-form of behenic acid are similar.

The arrangement of the CH_3 end groups of the molecules in (001) is shown in Fig.134. The distance OA = 9.13 Å and OB = 9.13 Å. Since the angle $\hat{COB} = 76°61'$, after a clockwise rotation $\phi = 74°$ about O the lattice point C will almost coincide with the position formerly occupied by B. Similarly a rotation $\phi = 106°$ in an anticlockwise direction will bring C almost to the position formerly occupied by D. The positions of the lattice points after rotations $\phi = 74°$ or 106° about O are shown by the asterisks (Fig.134). It can be seen that alternate rows of CH_3 groups are almost in their normal stacking positions. For simplicity the translation of CH_3 groups on opposite sides of a (001) plane has been ignored. The CH_3 end groups are in an approximately close-packed arrangement, so that the upper CH_3 groups occupy a 'hollow' between three lower CH_3 groups.

12.7. Related Work.

The spiral growth of twinned crystals of behenic acid has also been described by Amelinckx [165]. The present analysis of twinned spirals was almost complete when this work was published. Amelinckx reported crossed growth edges but gave no explanation of this phenomenon. The differences between growth patterns due to misorientation $\phi = 74°$ and $\phi = 106°$ were not discussed.

Amelinckx [166] has also reported twinned spirals in crystals of the monoclinic form of the n-alcohols.

REFERENCES

162)	TRILLAT, J.J. and HERSCH, Th. V.	Comptus Rendus	195		215	(1932)
163)		J. Phy. Radium Ser.7.	4		38	(1933)
164)	THIBAUD, J., DUPRÉ LA TOUR, F.	J. de Chemie Phys.	29		153	(1932)
165)	AMELINCKX, S.	Acta Cryst.	9		16	(1956)
166)		Acta Cryst.	8		530	(1955)

CHAPTER XIII.

THE ORIGIN OF DISLOCATIONS IN FATTY ACID CRYSTALS.

13.1. Introduction.

Two suggestions have been put forward to explain the origin of dislocations in thin molecular crystals. Frank[167] suggested that dislocations are created by a buckling of the thin crystal plate followed by slip of the molecules. However, Dawson[168] put forward a suggestion that in the orthorhombic paraffins the stacking fault which is responsible for lattice dislocations occurs in the original crystal nucleus, when adjacent molecules fail to align in exact juxtaposition but condense in a position such that the ends of the molecules project above or below the plane of the normal orthorhombic molecular layer (Fig.135). By a succession of small stacking faults of this type a final stage is reached where a molecule has been translated above the (001) plane through a distance equal to the molecular length. This argument was extended by Anderson and Dawson[169]. it was pointed out that small stacking faults might combine to form a partial step on the crystal surface. This would form a point of anchorage around which molecules could condense to give a screw dislocation. It was found that crystals of n-hectane, n C_{100} H_{202}, grown from solution at an initial temperature of 60°C formed monomolecular sheets without dislocations. As the temperature fell a point

was reached at which small stacking faults were stable. Screw dislocations were then formed around the crystal periphery.

13.2. Random Disorders in Fatty Acid Crystals.

It was shown in Chapter IX that fatty acid crystals often coalesce with their (001) planes parallel. However, the relative rotation ϕ between the component crystals has a random value. If a dislocation occurs after the crystals have coalesced two types of growth may occur. The special cases when $\phi = 74^{\circ}$ and 106° have been discussed in 12.2. It is clear that similar considerations apply when the component crystals are randomly misoriented. Either single spirals will develop on opposite faces of the component layer or on one face a pair of interleaved spirals in random orientation will develop.

Fig.136 shows a growth pattern revealed by internal slip in a crystal of behenic acid. There are two pairs of co-operating spirals; each pair is of opposite sense. It is improbable that the superposition of the growth centres and similarity of the two superimposed growth patterns was accidental. The growth patterns clearly arise from a pair of dislocations, separated by a distance $< 2\pi\rho_c$, which intersected both component crystals. This suggests that the dislocations occurred after the component crystals had coalesced.

In Fig.137, which is an electronmicrograph, it is clear

that the two component crystals coalesced before the dislocation was created. Two further examples of interleaved spirals in random orientation are illustrated in Figs. 138 and 139.

13.3. Spiroidal Crystals.

When the normal component of the Burgers vector of a 'dislocation' exceeds the thickness of the crystal a spiroidal crystal is formed. The use of the term 'dislocation' to describe such a macroscopic lattice disorder is questionable. The two halves of the crystal on opposite sides of the slip plane are only in contact in the vicinity of the 'dislocation' and there is not necessarily a unique relationship between lattice points on either side of this plane. The development of growth spirals from the 'dislocation' is modified since only the innermost region of the exposed ledges provide sites for the nucleation of new layers on (001).

The crystal of stearic acid shown in Fig.140 was photographed with the dark-slit microscope illumination described by Tolansky [170]. The vertical dark line represents a profile of the crystal thickness. It can be seen that the crystal plate was helical. Spiral growth steps have developed from the central region of the terminated ledge created by the dislocation. Fig.141 is an electronmicrograph of a spiroidal crystal of behenic acid.

It is highly improbable that macroscopic lattice disorders of this type can be attributed to an accumulation

of small scale lattice defects. They indicate that non-uniform stresses on the crystal plate, resulted in catastrophic slip.

13.4. The origin of Non-Uniform Stresses.

The growth of fatty acid crystals from solution in petroleum ether was observed under an optical microscope. It was found that even when the rate of evaporation was severely restricted the crystals were in violent motion. As the crystals twisted across the field of view it was seen that many of the crystal plates were distorted. This suggested that even when the crystals were grown from a droplet of solution currents in the solution would lead to a motion of the microcrystals which would result in a non-uniform distribution of stresses on the microcrystallic plates.

13.5. Conclusion.

It was shown earlier that steps less than two molecules high, due to imperfect or partial dislocations, do not promote growth. On the contrary, the present study showed that these steps hinder growth. Hence it seems unlikely that partial steps on the crystal surface can form a point of anchorage around which molecules would condense to give a screw dislocation; as suggested by Anderson and Dawson [169]. The occurrence of randomly misoriented spirals and spiroidal crystals shows that dislocations are often formed in a later stage of growth, and are due to catastrophic events affecting

groups of coalescing crystals and single crystals. There is evidence that thin crystals growing in solution are subject to non-uniform distributions of stresses. It is therefore concluded that in crystals of stearic and behenic acid grown from solution at temperatures below $0^{\circ}C$, a majority of the dislocations are due to the buckling of the crystal plate followed by slip of the molecules. The appearance of internal slip shows that these crystals are easily distorted.

It is not however suggested that the layer disorders leading to interlaced spirals and the spiral growth of contact twins are entirely due to the coalescence of single crystals, followed by terminated slip. These layer disorders may also arise from the nucleation of new layers in incorrect orientation.

REFERENCES

167) FRANK, F.C. Phil. Mag. 42 809 (1951)

168) DAWSON, I.M. Proc. Roy. Soc. A. 214 72 (1952)

169) ANDERSON, N.G., and DAWSON, E.M. Proc. Roy. Soc. A. 228 539 (1955)

170) TOLANSKY, S. Nature (Lond) 169 455 (1952)

CHAPTER XIV.

CONCLUSION.

This work was undertaken in order to establish whether dislocations and spiral growth occurred in crystals of the fatty acids, and to determine the relationships between the growth patterns and the crystal structure. Most of the crystals studied were of the B-form of either stearic or behenic acid. These crystals were grown from solution in chloroform at temperatures $\sim$ 268°K. Abundant evidence of spiral growth upon (001) was found, but no significant differences were observed between the growth of stearic and behenic acid crystals.

It has been shown that there was a close analogy between the rectilinear growth spirals observed on these acids and the interactions between the curvilinear spirals predicted by Burton, Cabrera and Frank for the growth of imperfect homopolar crystals from the vapour phase. The detailed shape of the growth spirals was found to depend upon the structure of the parent crystal, the temperature, and the inclination of the long-chain molecules relative to the basal plane.

According to Burton, Cabrera and Frank spiral growth can occur at low supersaturations, when the probability of growth by two-dimensional nucleation is negligible. This deduction has been confirmed by the present observations; an

approximate calculation indicated that many of the growth spirals upon fatty acid crystals had developed at supersaturations as low as 2%.

The dimensions of the crystals studied ranged from 10^{-2} to 10^{-3} cm. in lateral extension, and 25,000 Å to 50 Å in thickness. Consequently certain difficulties of observation arose. For interferometric study it was necessary to use multiple-beam fringes formed by internal interference. Two independent methods were used to determine the height of the spiral steps, the first method utilised internal interference fringes, the second method involved shadowcasting the crystals and examining them with an electron microscope. Steps $\sim$ 50 Å high were rendered visible by phase contrast illumination after the crystals had been silvered. Reflexion bright-field illumination revealed these steps only when the field aperture was reduced to a minimum and the objective slightly defocussed. The possibility of artefacts in the image could not then be excluded. On the contrary, steps $\sim$ 250 Å high were more readily revealed by reflexion bright-field illumination, since phase contrast illumination produced an intense 'halo' around these steps. Consequently, when large and small steps were in close proximity, or if a large step tended to dissociate, optical observation was not satisfactory. Steps $\sim$ 250 Å high usually occurred on large, thick crystals. These crystals were found to be too thick for

examination by transmission methods in the electron microscope. In addition, the crystals usually extended over one or more support grid apertures, and were too large even for study by replica methods. These limitations of the optical and electron microscope techniques were significant when the results of measurements of spiral step-heights were considered.

Optical measurements revealed that the mean height of most of the spiral steps was an integral multiple of c sin . There were four exceptions in which the step-height was found to be $\frac{1}{2}$ N c sin β , where N was an odd integer. Measurements with the electron microscope were confined to crystals of behenic acid. Most of the spiral steps were bimolecular (c sin β), but six cases of trimolecular steps ($\frac{3}{2}$ c sinβ) were also found. There was no evidence of monomolecular growth steps. Also the trimolecular growth steps did not tend to dissociate. Occasionally larger growth steps were observed with the electron microscope; these steps tended to dissociate. Both electron microscopic and optical measurements showed that Frank's hypothesis that the normal component of the Burgers vector of the parent dislocation is equal to an interplanar spacing of the lattice was not entirely valid in the case of fatty acid crystals. Imperfect dislocations also occurred.

It was not possible to decide whether steps of height N c sinβ were stable, or whether they dissociated into bimolecular steps. Optical evidence suggested that they were

stable, whereas electron microscopic examination indicated that these steps tended to dissociate. It is probable that both situations occur, depending upon the exact supersaturation and temperature of growth.

It has also been shown that when a dislocation arises in a crystal composed of two or more misoriented layers, the spiral growth leads to a repetition of the disorder, and polytypic crystals or polysynthetic twins were generated. The component layers were generally related by rotation through an angle $\phi = 180^{\circ}$, 106° or 74°. These three cases could be distinguished by the growth patterns. The spiral growth of these crystals generated a low energy helical fault surface. Occasionally random values of ϕ also occurred, and the component crystals grew as interpenetrant helicoids.

There was reason to believe that the dislocations in fatty acid crystals were not necessarily parallel to the c-axis or perpendicular to (001).

Observations of helicoidal crystals and spiral growth in randomly misoriented layers gave strong support to Frank's hypothesis that in thin crystal plates dislocations arise from non-uniform distributions of stresses, which lead to a buckling of the crystal followed by slip. Evidence of unit slip in fatty acid crystals has been put forward and it has been shown that internal slip also occurred.

Collectively these results proved that fatty acid

crystals are readily deformed and are subject to both perfect and imperfect slip. The dislocation mechanism plays an important role in their growth from solution. Since the lateral binding between the molecules is due to residual van de Waal's forces, the ease with which the molecules are displaced from their normal stacking positions was not unexpected.

It is interesting to note that no evidence of interpenetrant growth of two different polymorphic forms was found.

ACKNOWLEDGEMENTS

I wish to express my thanks to my supervisor, Professor S. Tolansky, F.R.S., for the assistance and encouragement which he has given me during this work. I am also indebted to Dr. A. R. Verma, Dr. V. G. Bhide, Dr. J. Ramage and many of my other colleagues in this laboratory for much useful discussion. The workshop Staff including Mr. A. Grant and Mr. J. Henley, have shown much patience and skill in making apparatus and providing numerous other necessities. I also wish to thank Mr. R. V. Williams, who instructed me in the use of the electron microscope and gave valuable assistance in its maintenance. Finally I would like to acknowledge the help of my friend, Miss J. Steel, in reading and correcting the manuscript.

The latter part of this work was facilitated by a postgraduate research grant from the Royal Holloway College and the Ministry of Education.

OPTICAL STUDIES OF THE GROWTH FROM SOLUTION OF SOME LONG-CHAIN ORGANIC CRYSTALS

Thesis presented for the degree of

Doctor of Philosophy

in the

University of London

by

PATRICIA MAY REYNOLDS

December 1956.

To facilitate the comparison of the illustrations with the text, this thesis has been bound in two separate volumes. Volume I contains the text, and Volume II the illustrations.

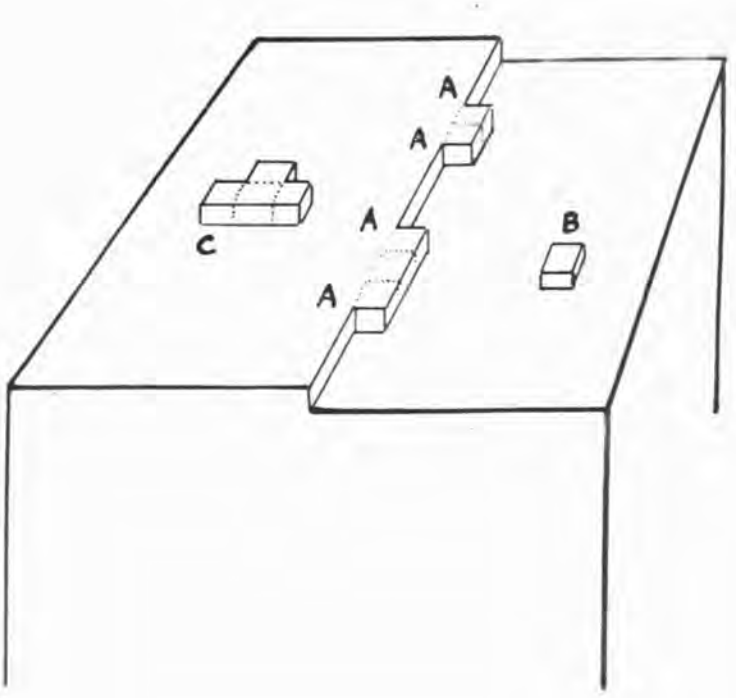

Fig. 1. The Structure of a Monomolecular Step at a Finite Temperature.

A.....kink in step.
B.....adsorbed molecule.
C.....aggregate of adsorbed molecules.

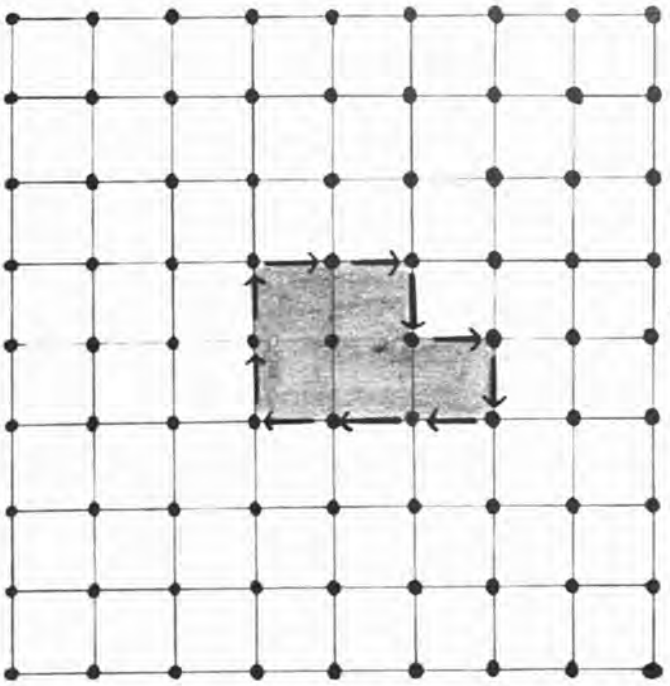

Fig.2. Burgers Circuit in a Perfect Crystal.

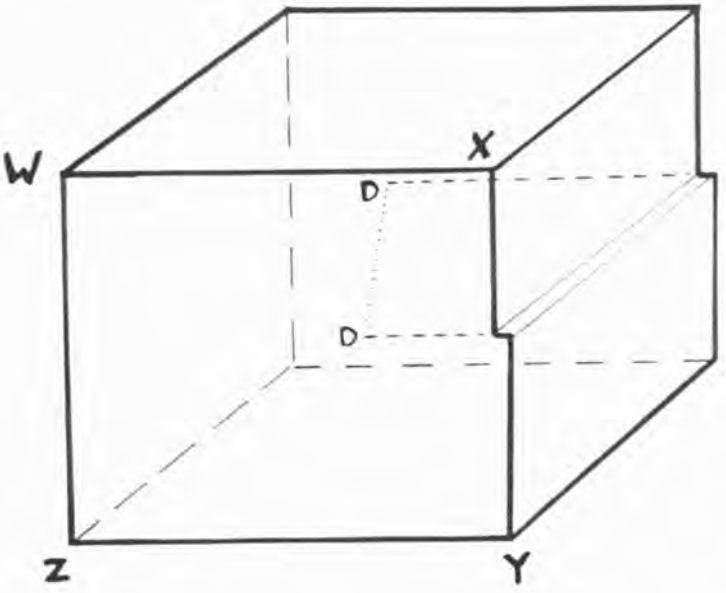

Fig.3. Edge Dislocation. Burgers Vector Parallel to Crystal Face.
DD...Dislocation line.

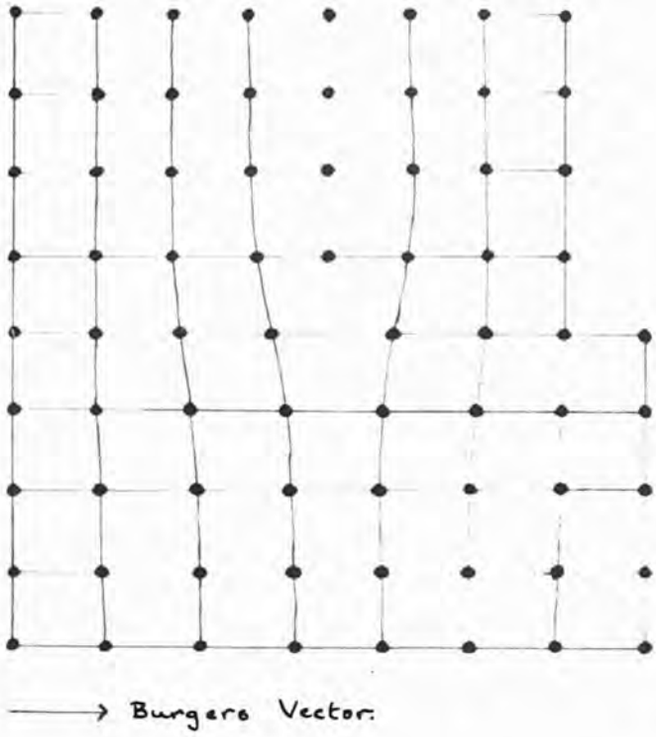

Fig.4. Atomic Disorder in Plane WXYZ (Fig.3) Parallel to Burgers Vector.

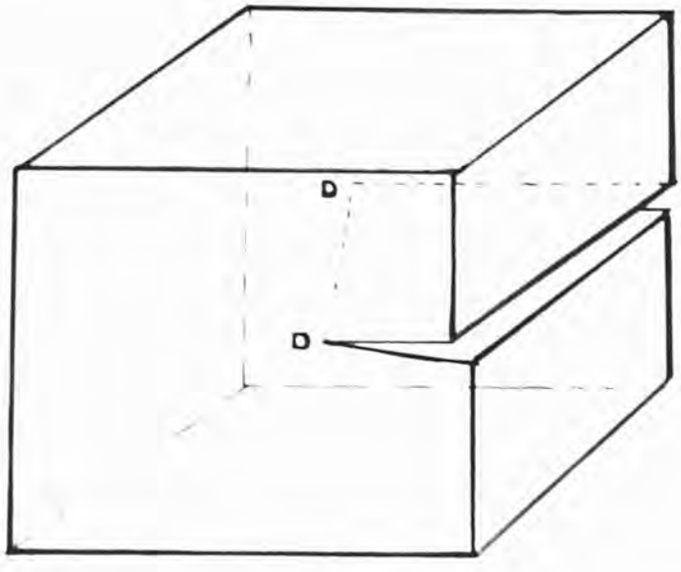

Fig.5. Edge Dislocation: General Case.
DD...Dislocation Line.

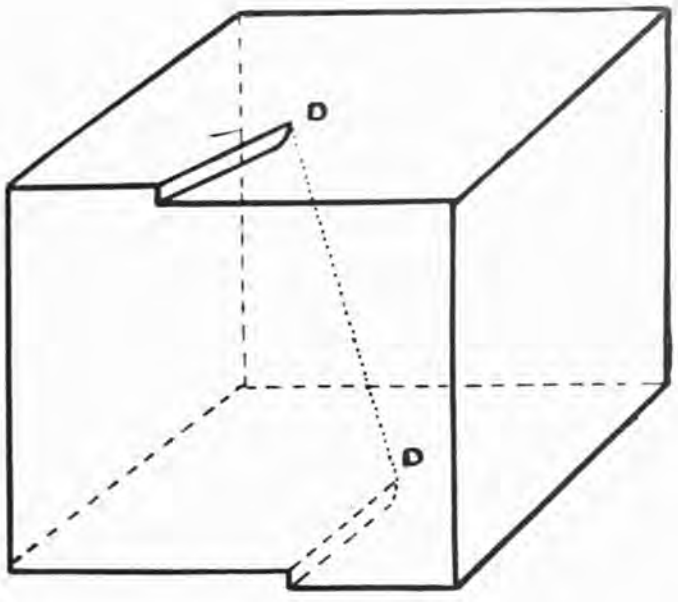

Fig.6. Screw Dislocation: General Case.
DD...Dislocation line.

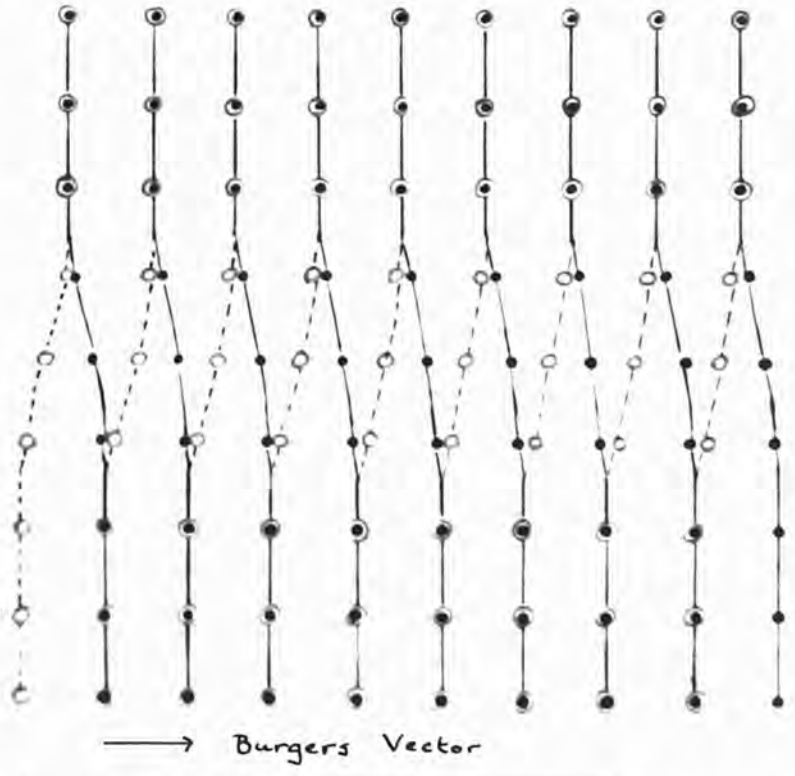

Fig.7. Atomic Disorder around Screw Dislocation.
upper lattice plane.
lower lattice plane.

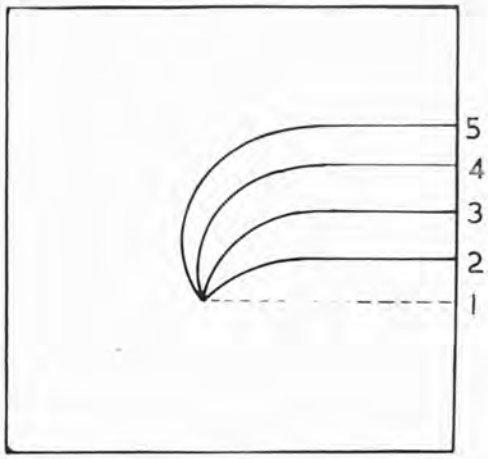

Fig.8. The Initial Growth of a Terminated Step.

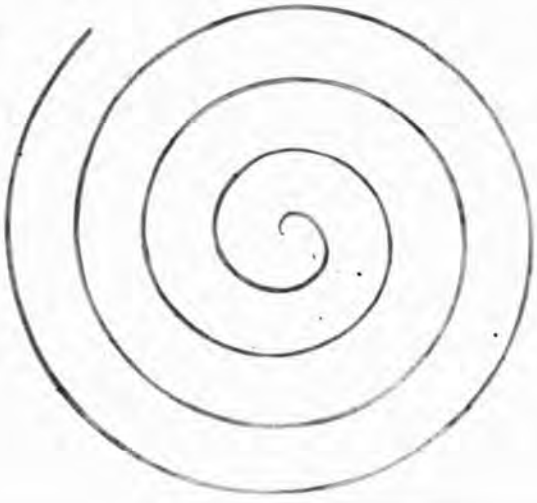

Fig.9. Growth Spiral (steady state).

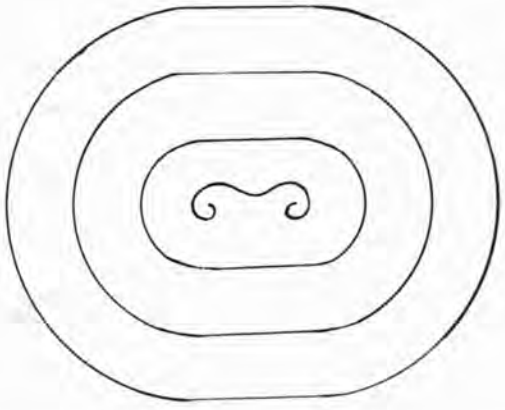

Fig.10.
Equal Dislocations of Opposite Sign. Seperation $> 4\pi\rho_c$.

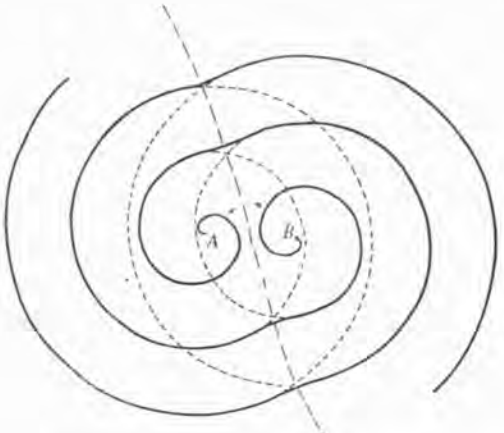

Fig.11.
Two Dislocations of Like Sign. Seperation $> 2\pi\rho_c$.

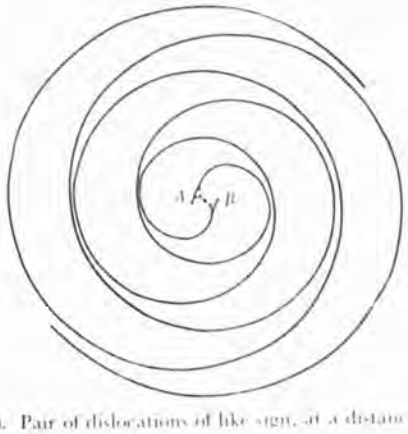

Pair of dislocations of like sign, at a distance $d > 2\pi\rho_c$.

Fig.12.
Two Dislocations of Like Sign. Seperation $< 2\pi\rho_c$.

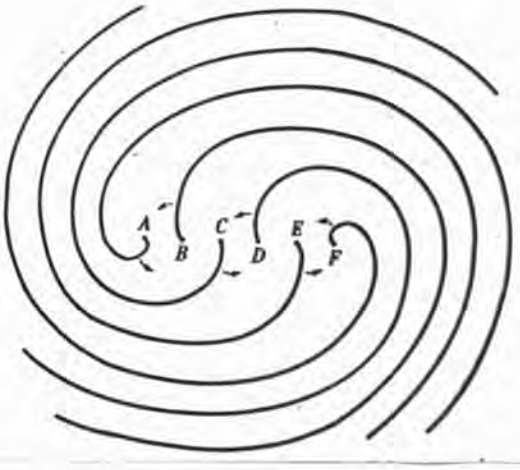

Fig.13.
Group of Dislocations of Same Sign. Seperation $< 2\pi\rho_c$.

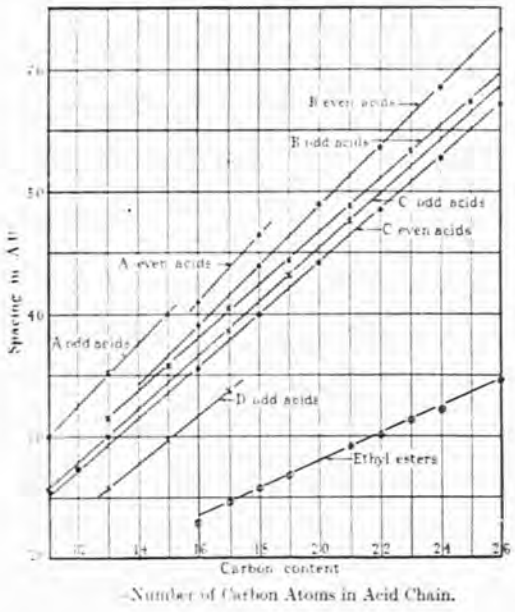

Fig.14. Polymorphic Forms of the Fatty Acids. Long-spacing against Carbon Content.

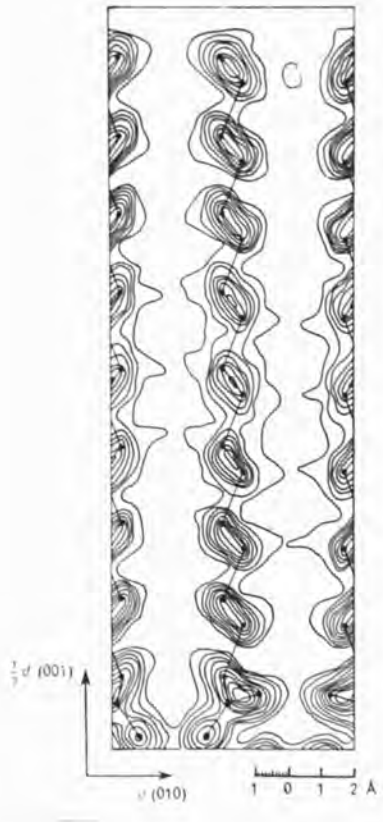

Fig.15. B-Form Stearic Acid. Electron Density Projection along the a-axis.

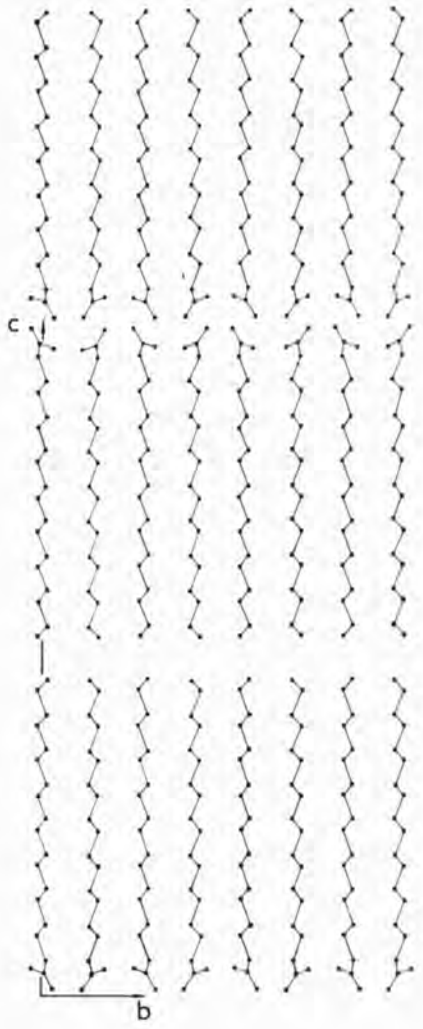

Fig.16. B-Form Stearic Acid.
Projection along a-axis.

Fig.17. B-Form Stearic Acid.

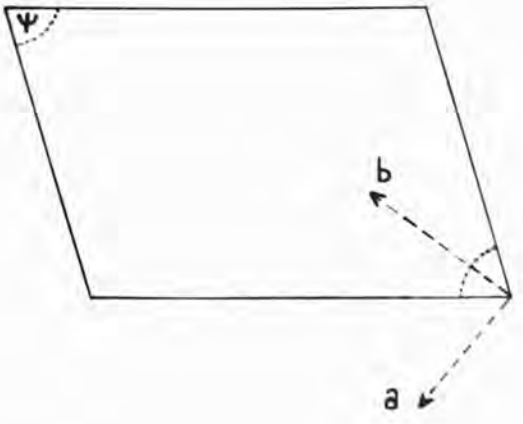

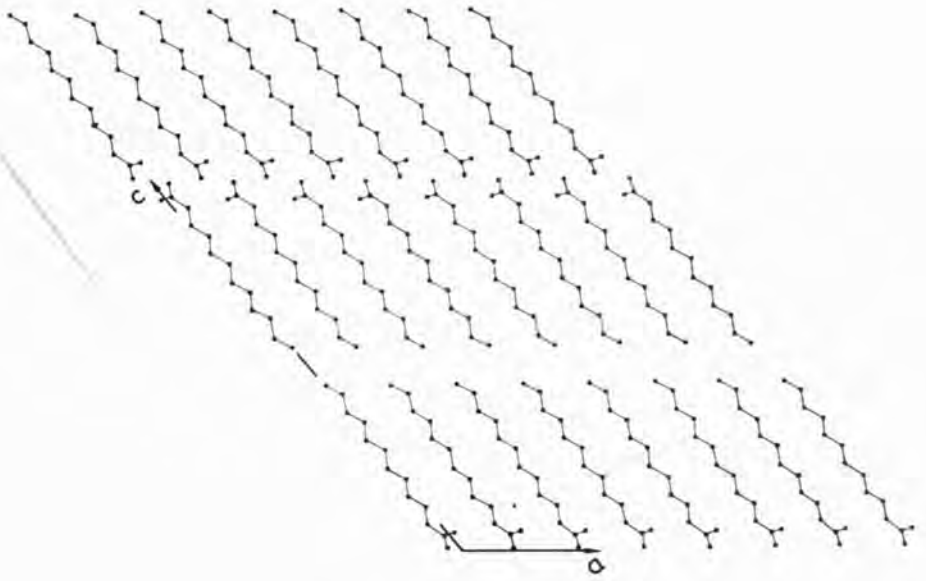

Fig.18. C-Form Lauric Acid. Projection along a-axis.

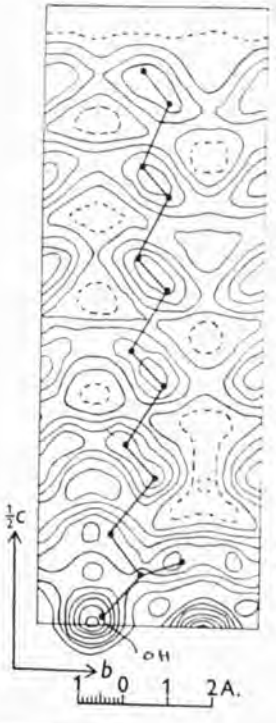

Fig.19. C-Form Lauric Acid. Electron Density projection along a-axis.

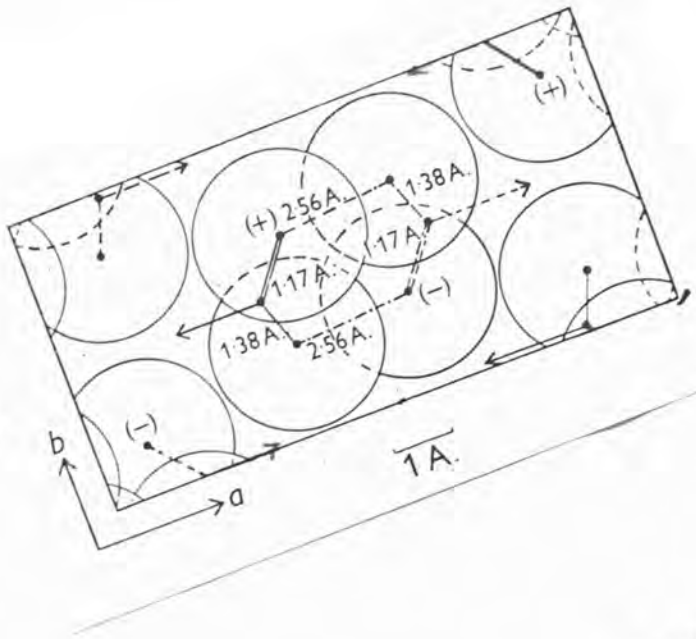

Fig.20. C-Form Lauric Acid. Packing of Carboxyl Groups.

Fig.21. C-Form Lauric Acid.

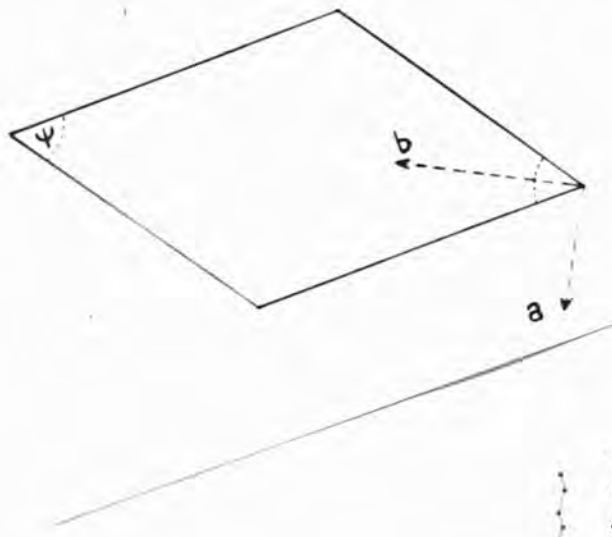

Fig.22. A-Form Lauric Acid. Projection along a-axis.

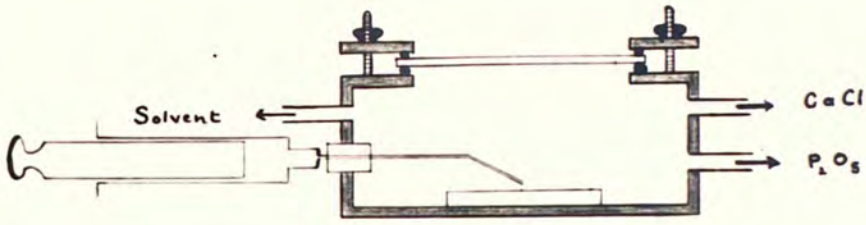

Fig.23. Apparatus for Preparation of Crystals.

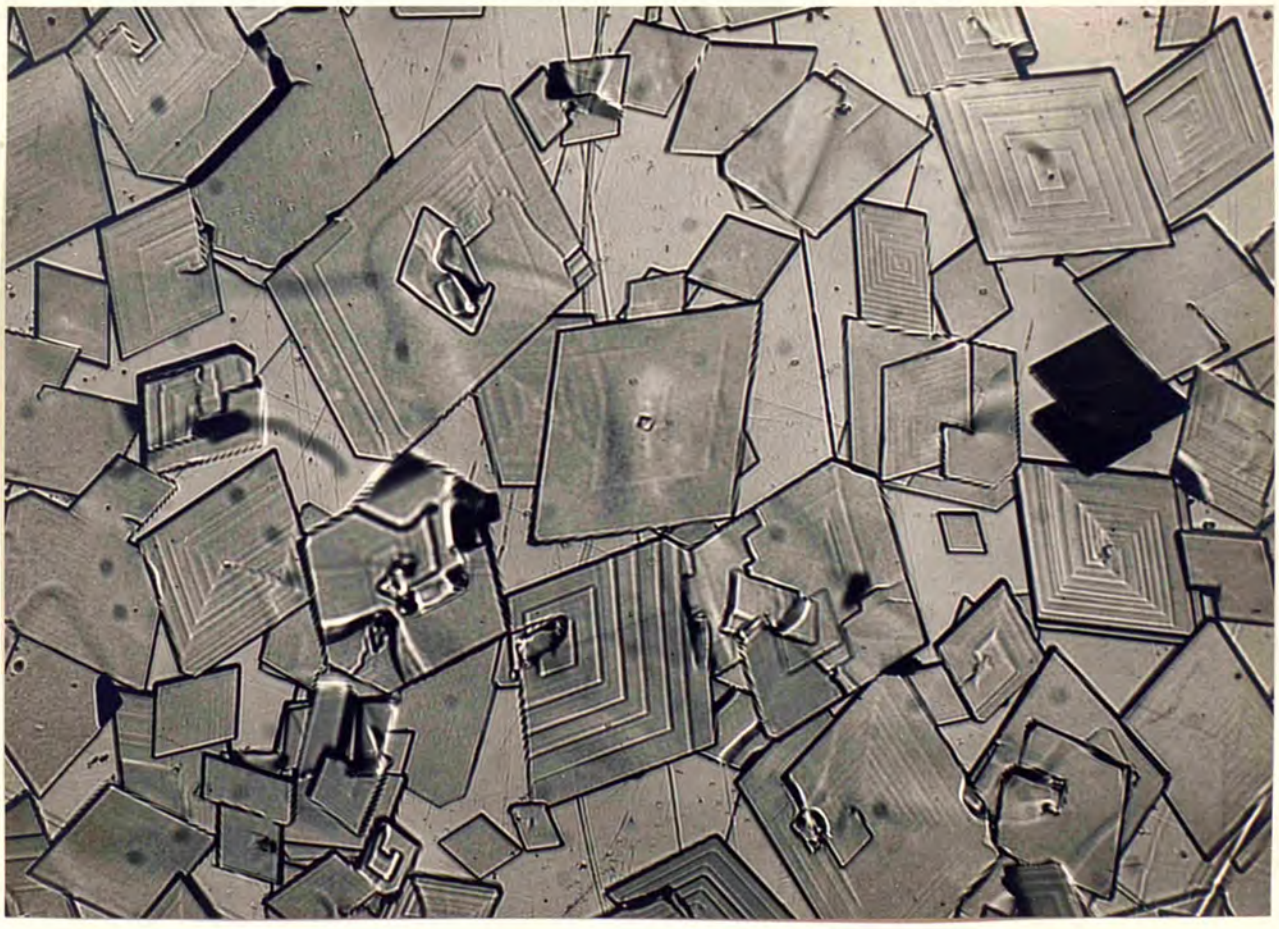

Fig.24. Stearic Acid Crystals: B-form.
Reflexion Bright-field. x350.

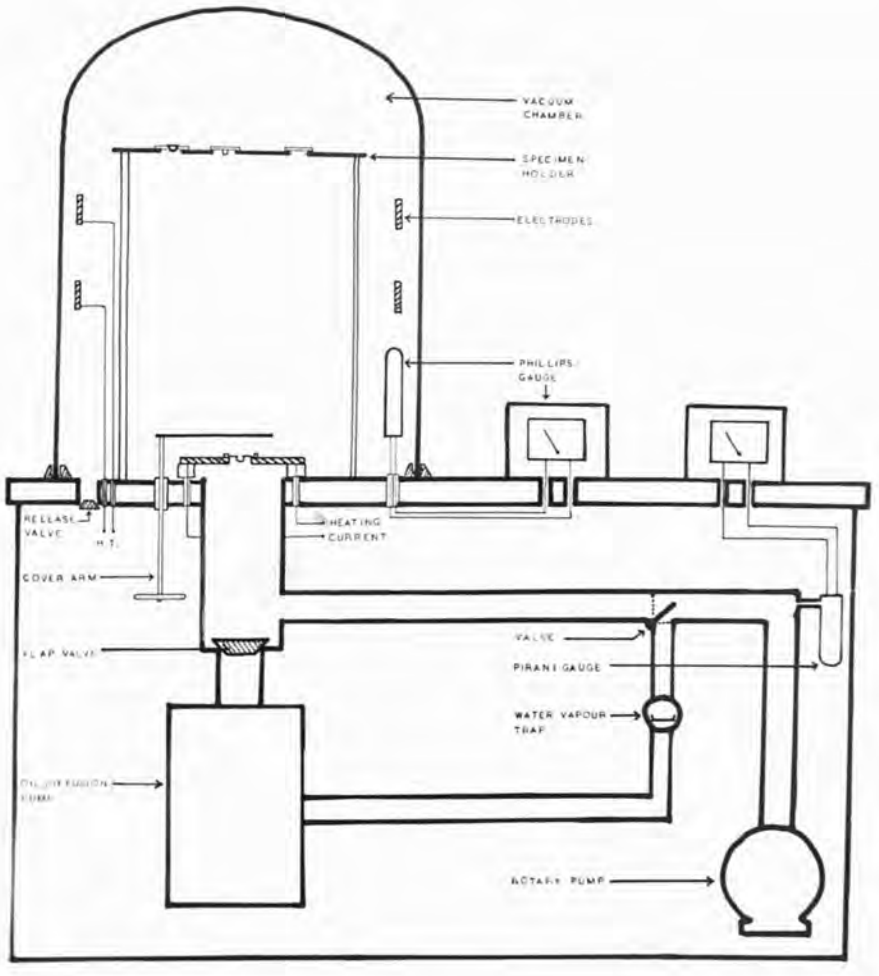

Fig.25. Coating Unit.

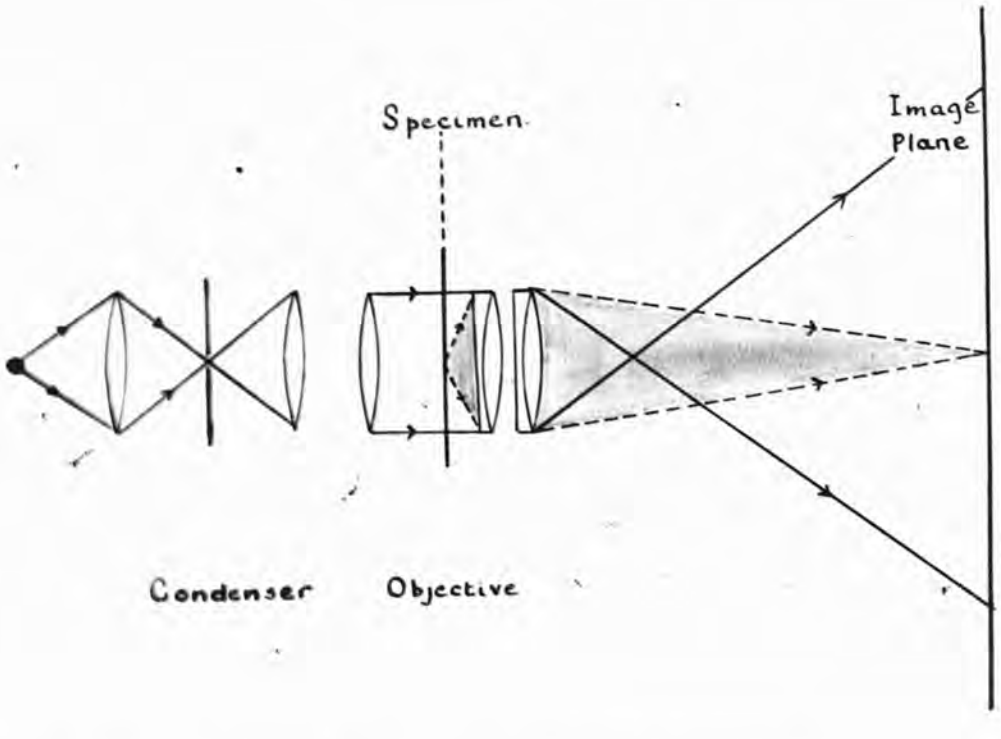

Fig.26. Transmission Phase Contrast Microscope.

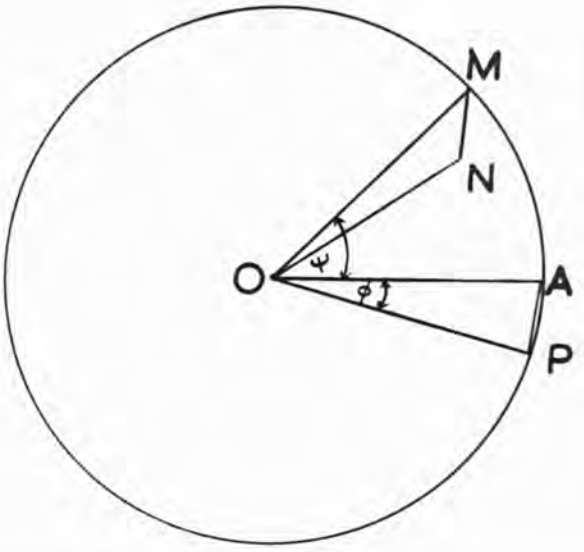

Fig.27.

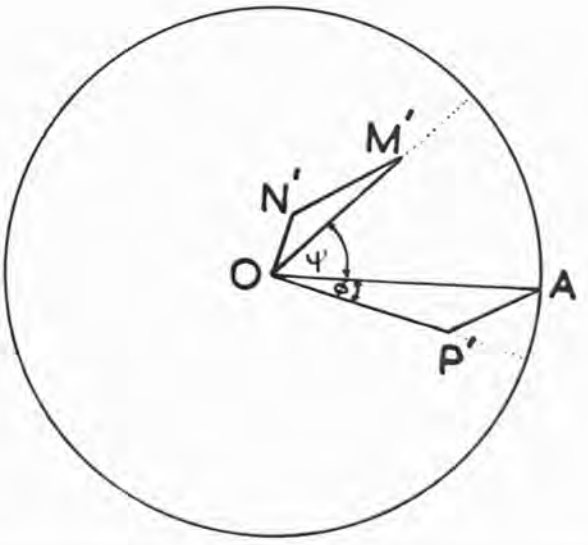

Fig.28.

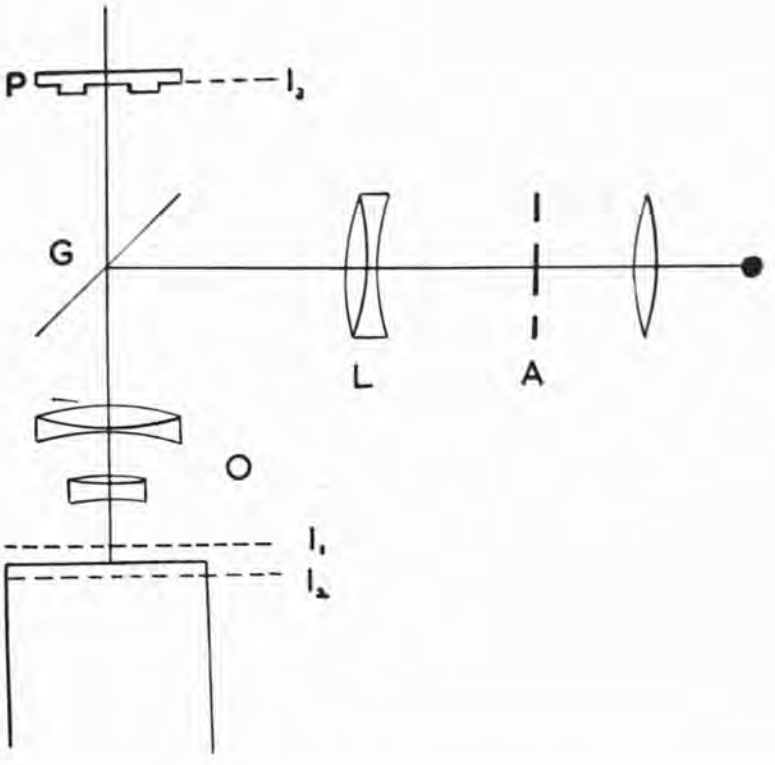

Fig.29. Reflexion Phase Contrast Microscope.

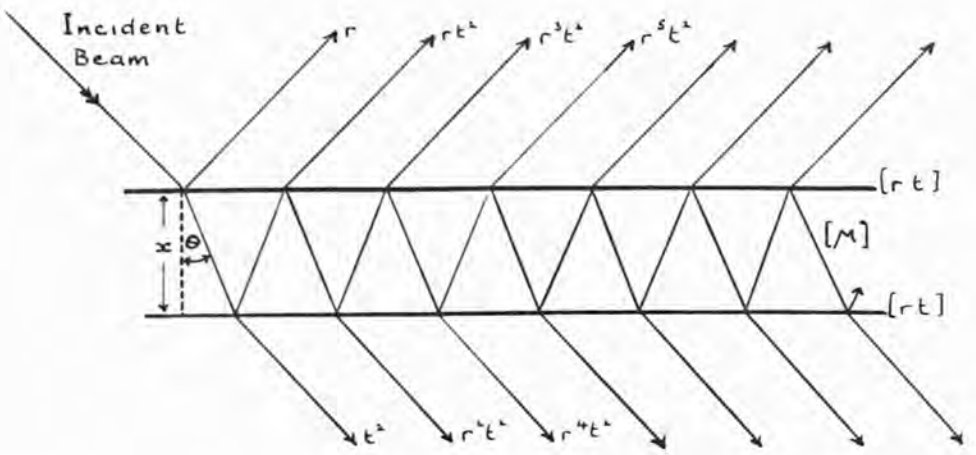

Fig.30. Parallel Plate Interferometer.

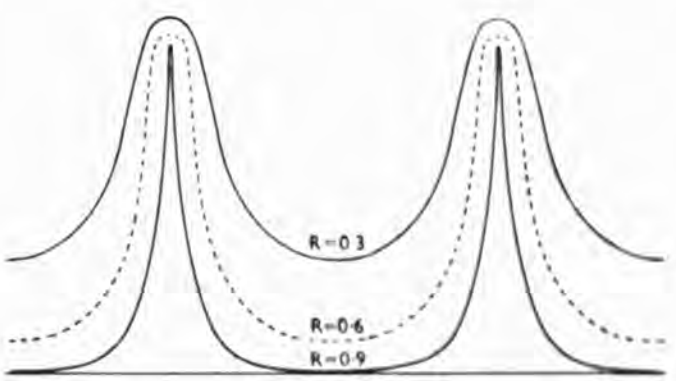

Fig.31. Variation of Fringe Shape with Reflectivity, r^2.

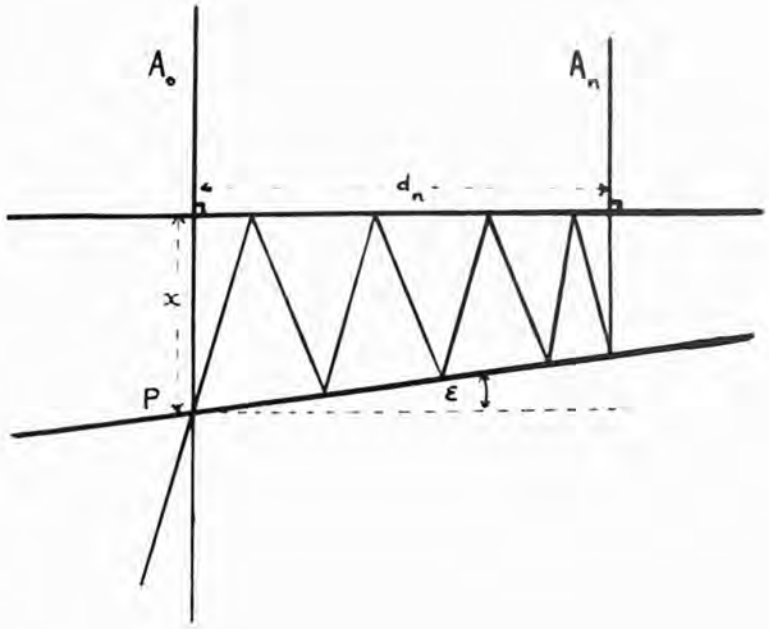

Fig.32. The Wedge Interferometer.

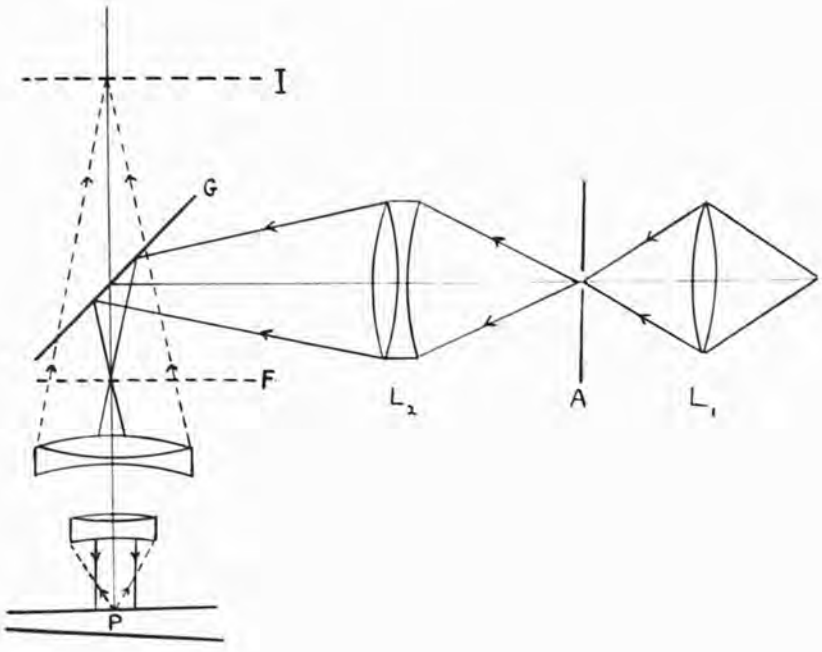

Fig.33. Optical System for Reflexion Fringes.

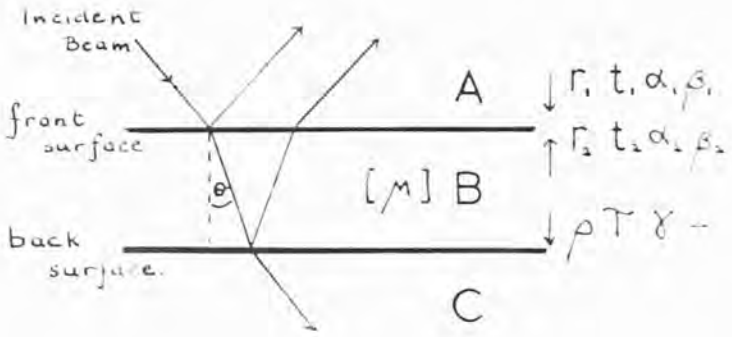

Light incident from:	A to B	B to A	B to C.
Amplitude reflexion coefficient.	r_1	r_2	ρ
Reflexion phase change.	α_1	α_2	γ
Amplitude transmission coefficient.	t_1	t_2	τ
Transmission phase change.	β_1	β_2	—

Fig.34.

Fig.35. Internal Interference Fringes. x350.

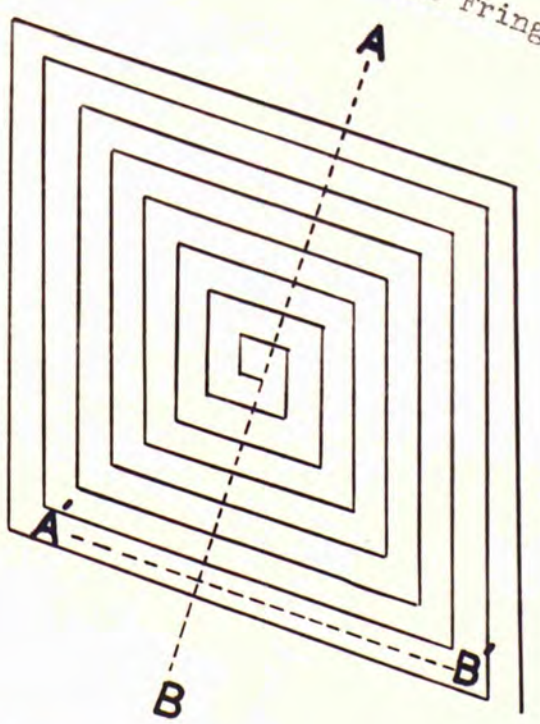

Fig.36.

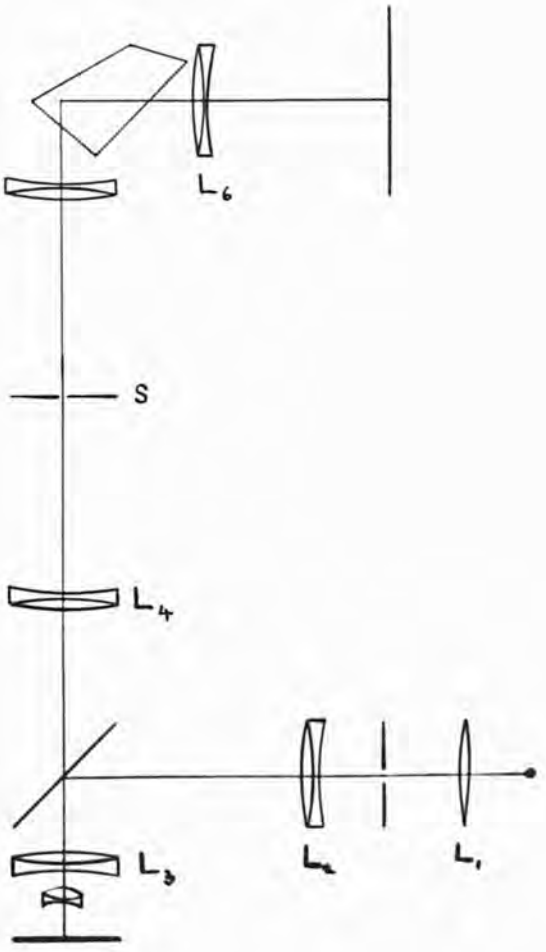

Fig.37. Optical Arrangement for Fringes of Equal Chromatic Order.

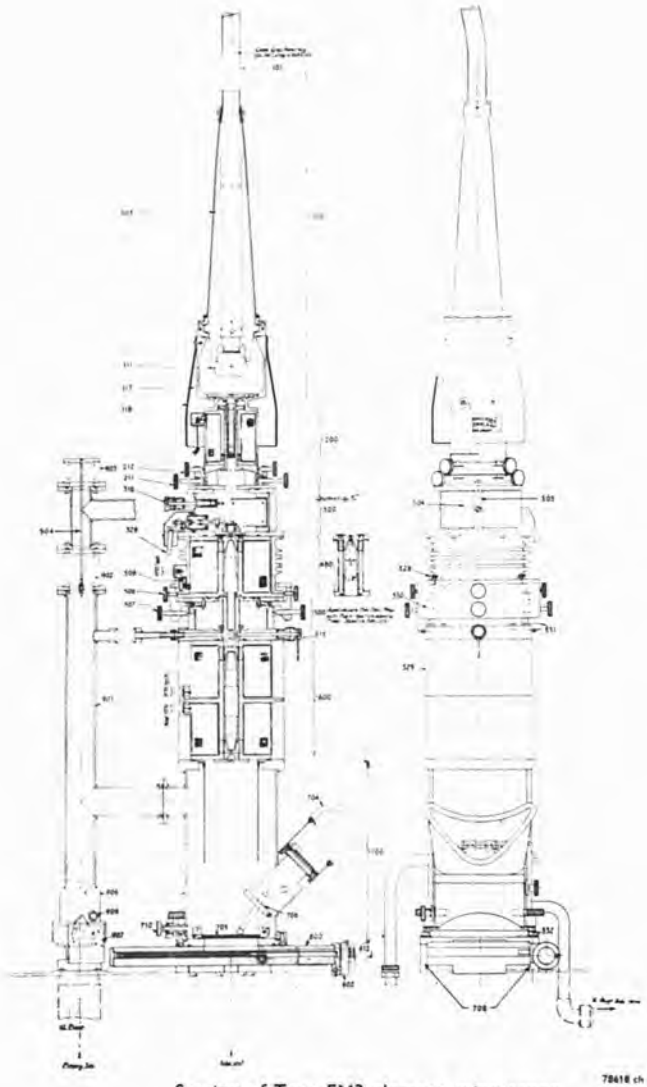

78618 ch

Section of Type EM3 electron microscope

Key to numbers on main stack—

100	Electron Gun	500	Intermediate Alignment Section
200	Condenser Lens	600	Projector Lenses
300	Specimen Stage	700	Viewing Chamber
400	Objective Lens	800	Camera

Fig.38.

Ray diagram, normal operation

Fig.39a.

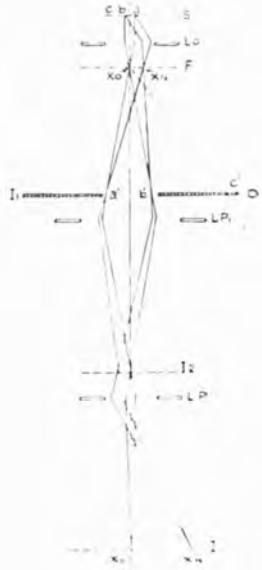

Ray diagram, electron diffraction

Fig.39b.

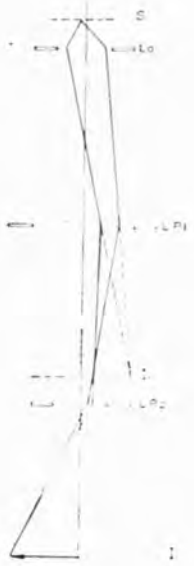

Ray diagram, operation at low magnifications

Fig.39c.

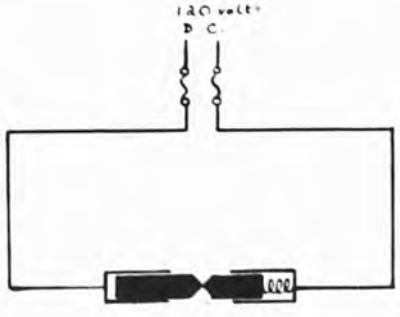

Fig.40. Circuit Supplying Carbon Electrodes.

Fig.4la. Shadowed Polystyrene Latex Particles

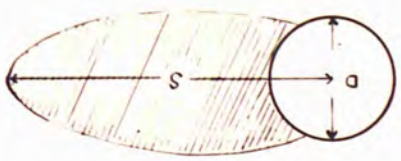

Fig.4lb.

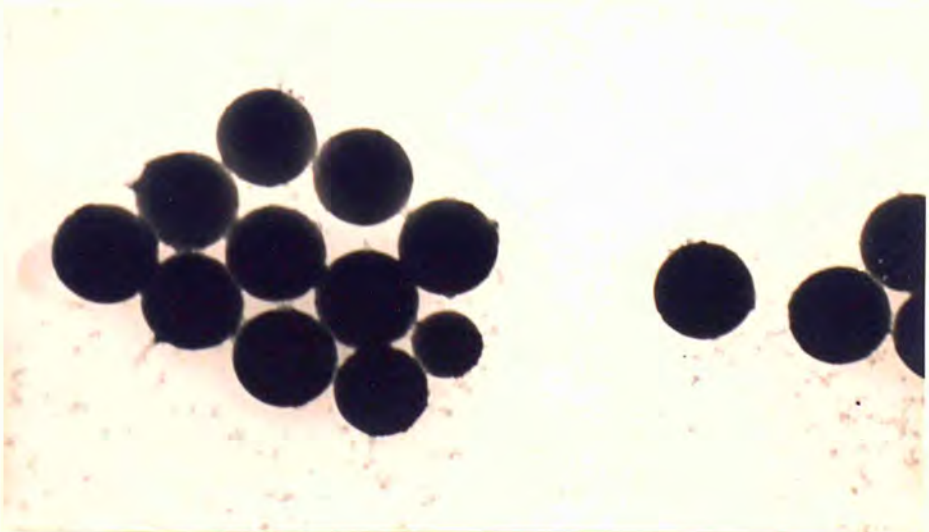

Fig.4lc. Polystyrene Latex Particles.
Diameter 0.54μ (Mean).

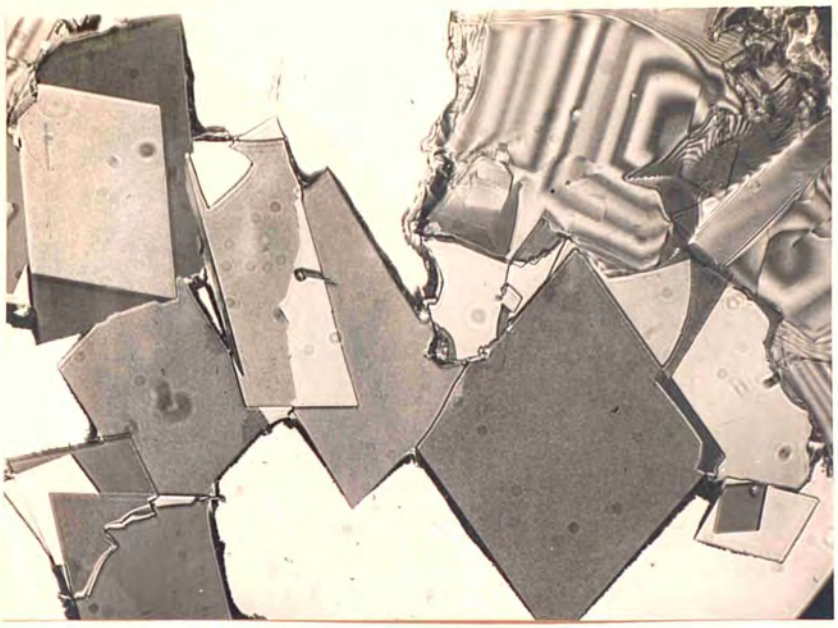

Fig.42. Areas of Uniform Tint.
Reflexion Internal Interference. x130.

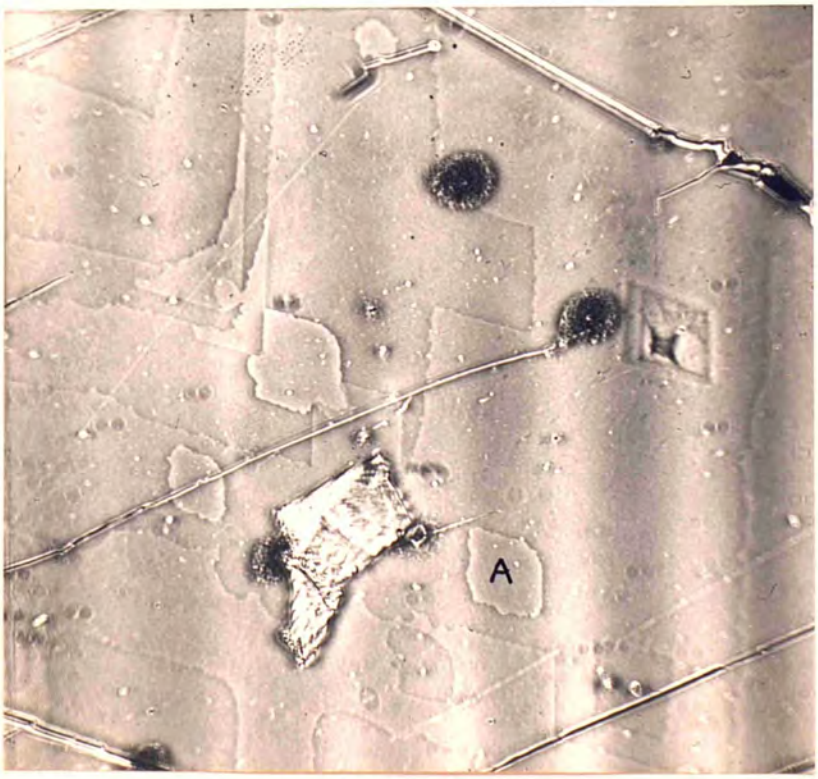

Fig.43. Two-dimensional Nuclei.
Phase Contrast. x135.

Fig.44. Behenic Acid.Elementary Spiral.
Electronmicrograph. x20,500.

Fig.45. Stearic Acid. Complex Spiral.
Reflexion Bright-field. x780.

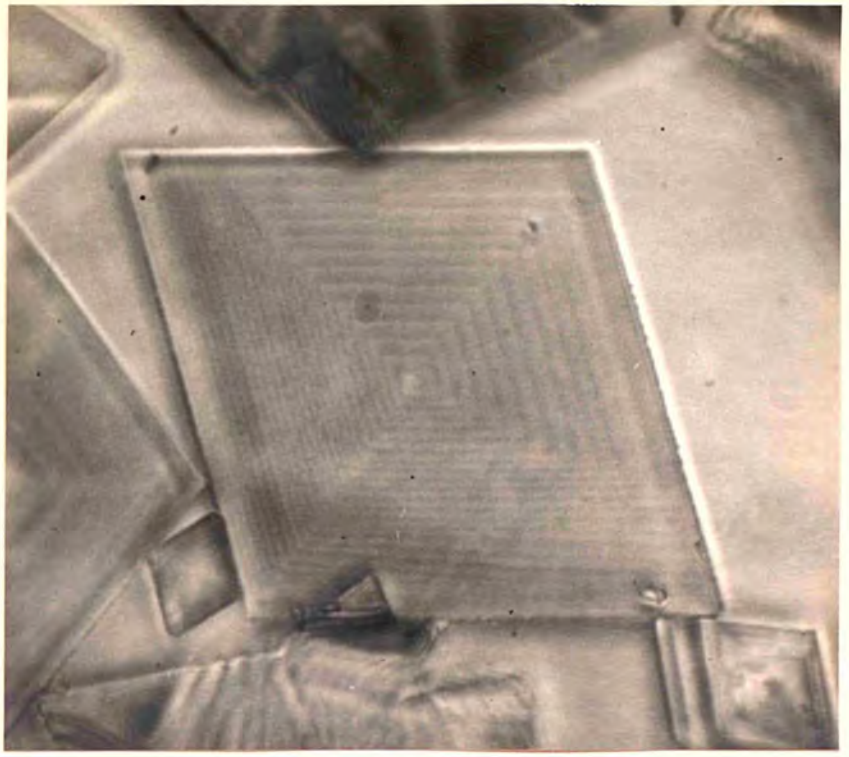

Fig.46. Behenic Acid. Single Spiral.
Reflexion Phase Contrast. x540.

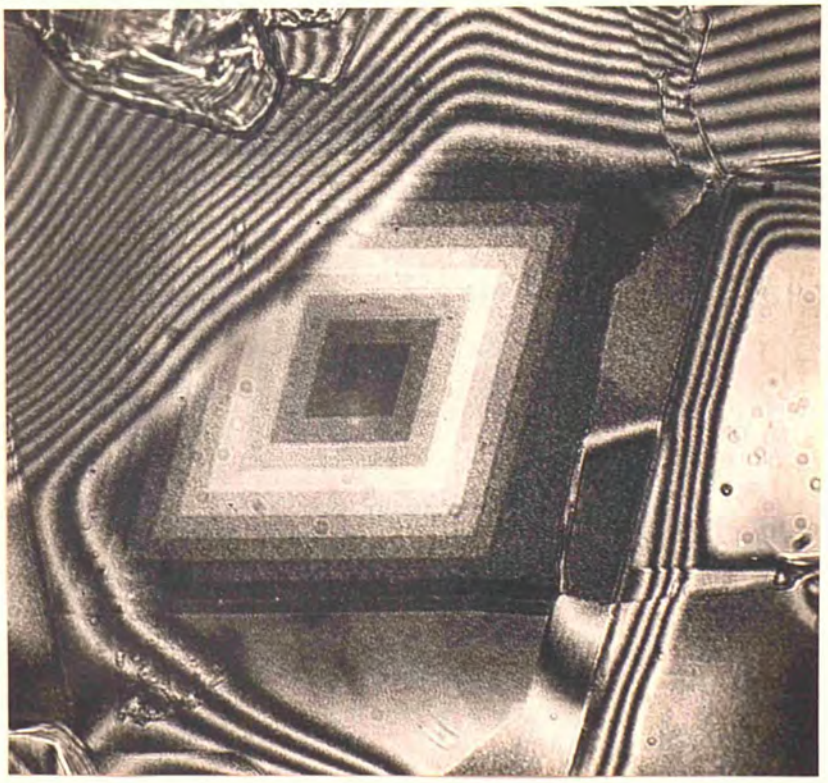

Fig.47. Stearic Acid. Single Spiral.
Reflexion Internal Interference.
x550.

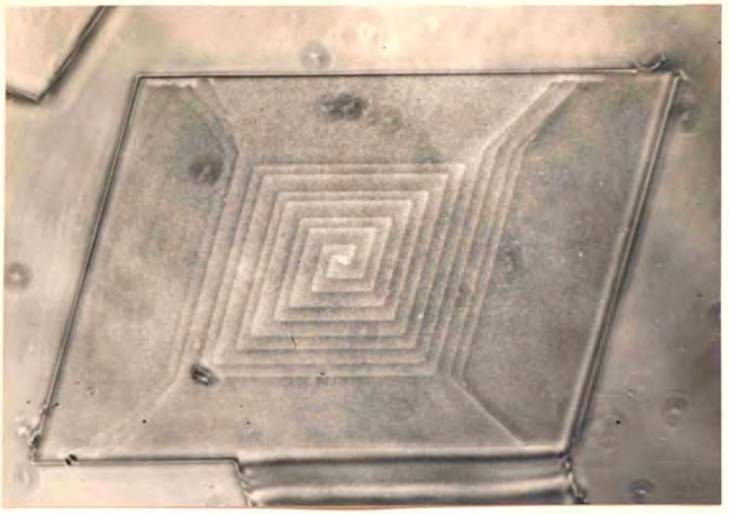

Fig.48. Behenic Acid. Two Spirals of Same Sense, $d < 2\pi\rho_c$.
Reflexion Phase Contrast. x610.

Fig.49. Behenic Acid. Two Spirals of Same Sense, $d < 2\pi\rho_c$.
Electronmicrograph. x5300.

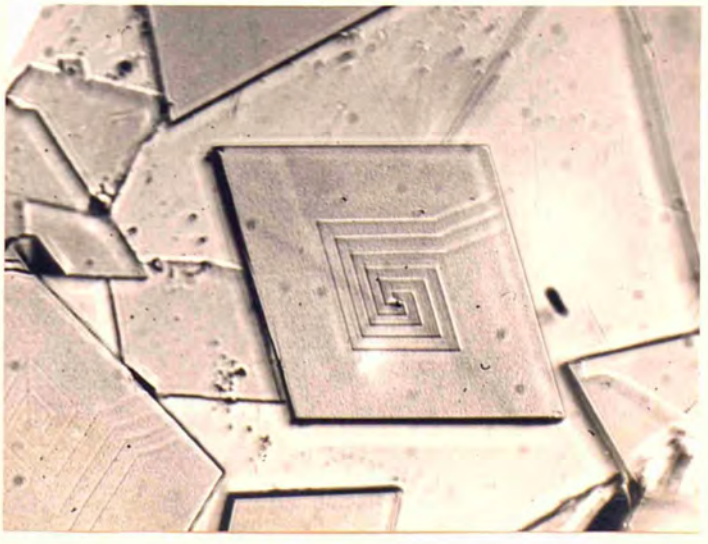

Fig.50. Stearic Acid. Three Co-operating Spirals.
Reflexion Bright-field. x520.

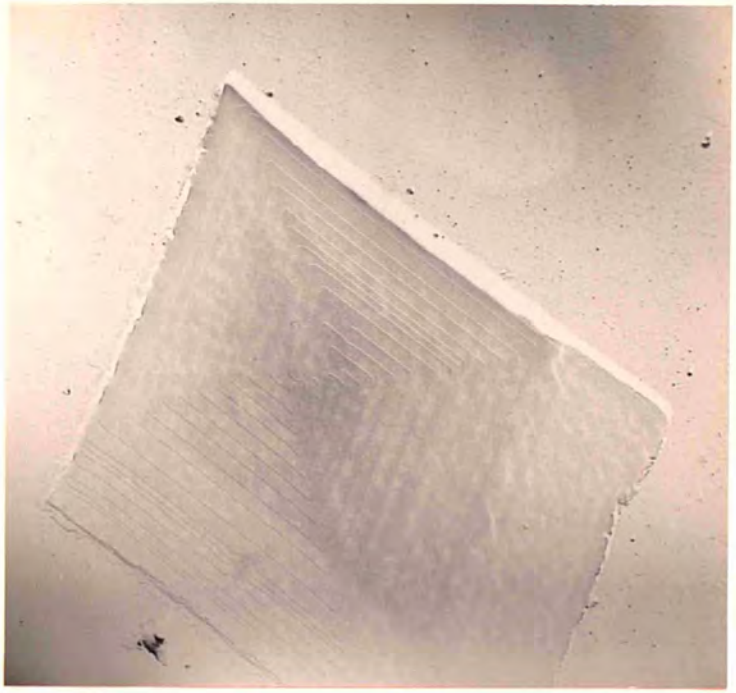

Fig.51. Behenic Acid. Group of Co-operating Spirals.
Electronmicrograph. x6600.

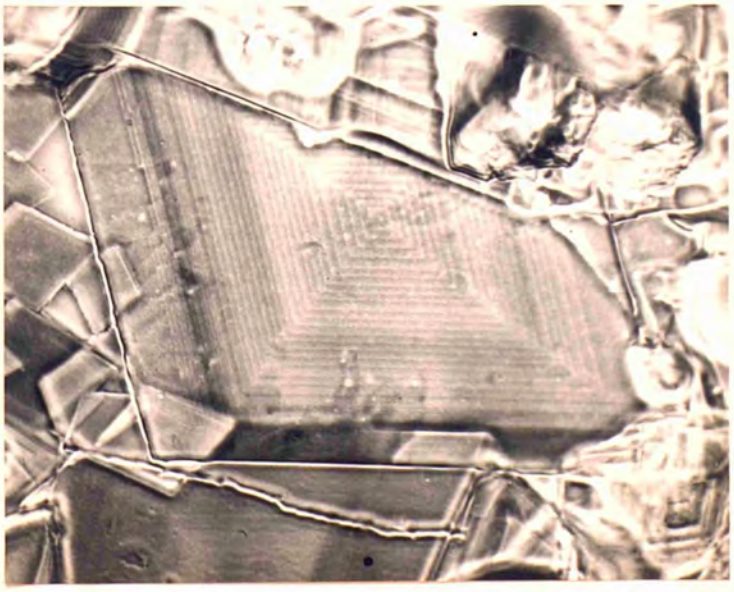

Fig.52. Behenic Acid. Two Co-operating Spirals of
Opposite Sense,
Reflexion Phase Contrast. x650.

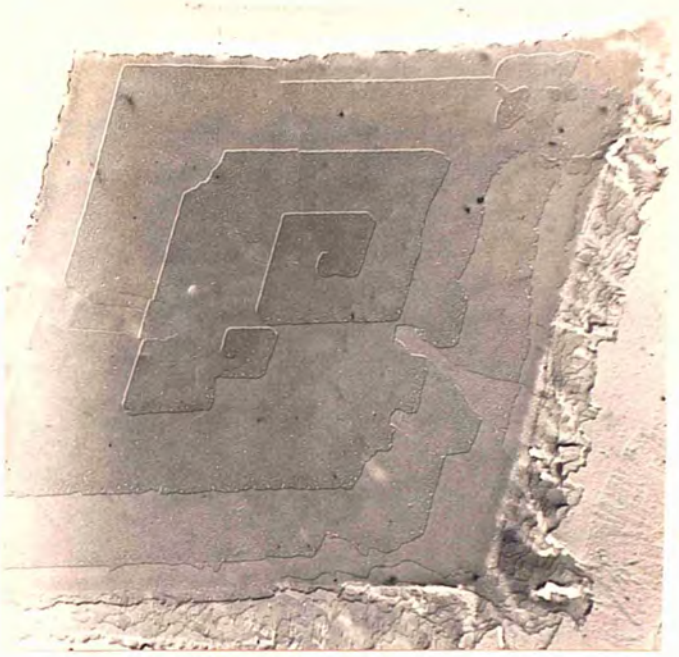

Fig.53. Behenic Acid. Two Co-operating Spirals of Opposite Sense,
Electronmicrograph. x6200.

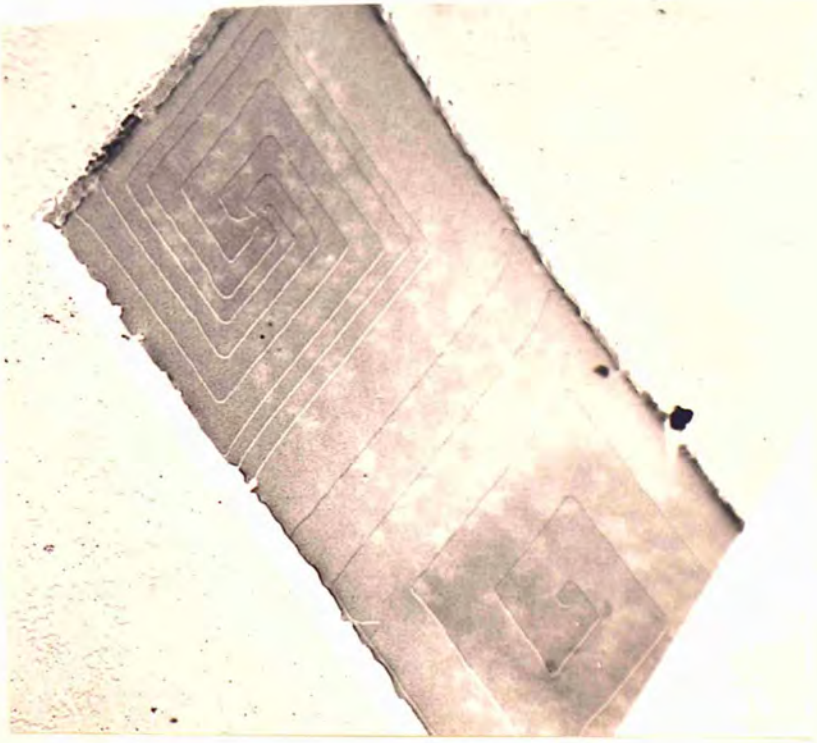

Fig.54. Behenic Acid. Group of Growth Spirals.
Electronmicrograph. x6300.

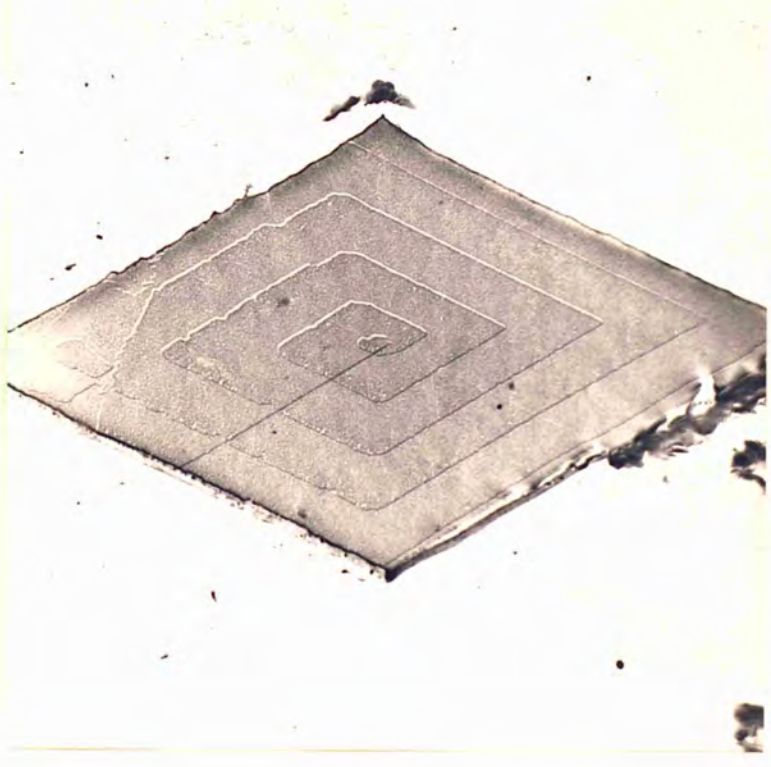

Fig.55. C-Form of Behenic Acid.
Electronmicrograph. x7700.

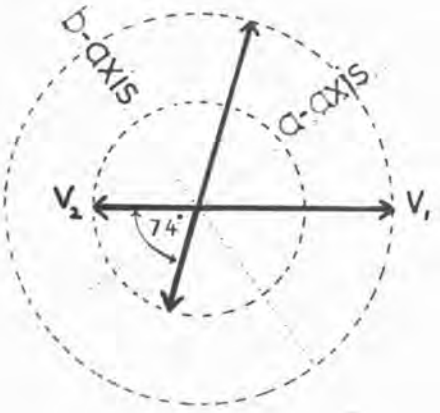

Fig.56. B-Form of Fatty Acid. Vector Diagram for Velocities of Advance of Growth-edges.

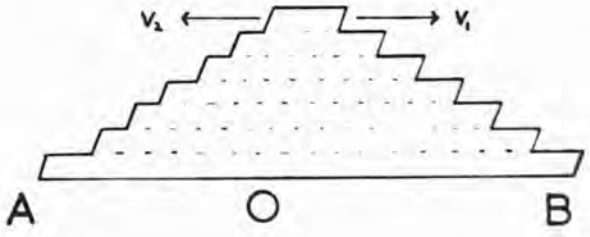

Fig.57. Section Through Crystal Perpendicular to Growth-edges.

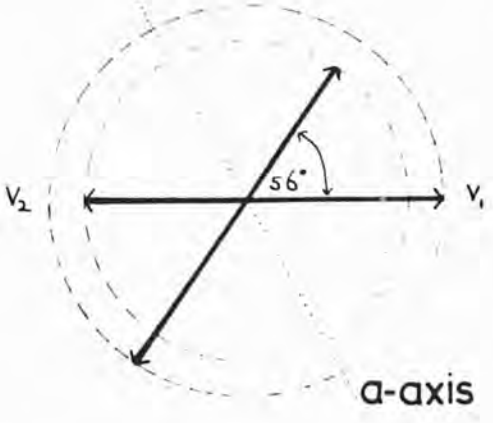

Fig.58. C-Form of Fatty Acid. Vector Diagram for Velocities of Advance of Growth-edges.

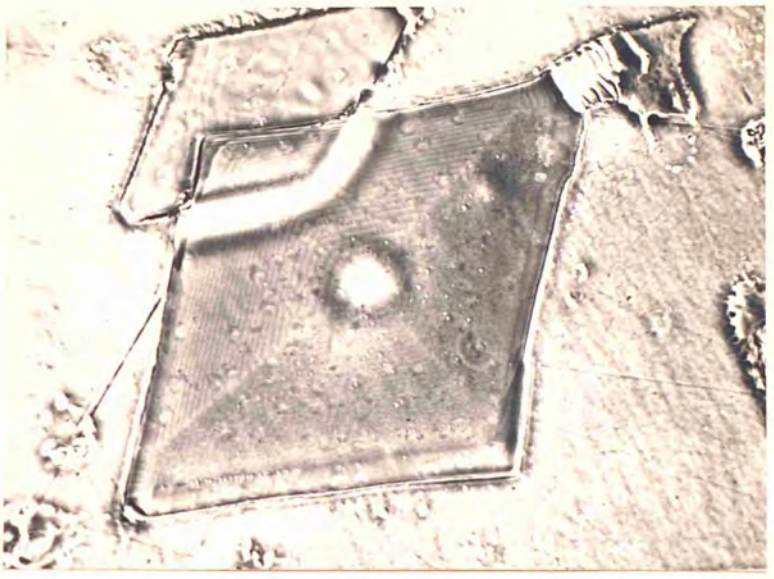

Fig.59. Crystal of Stearic Acid Grown at about 276° K.
Reflexion Phase Contrast. x820.

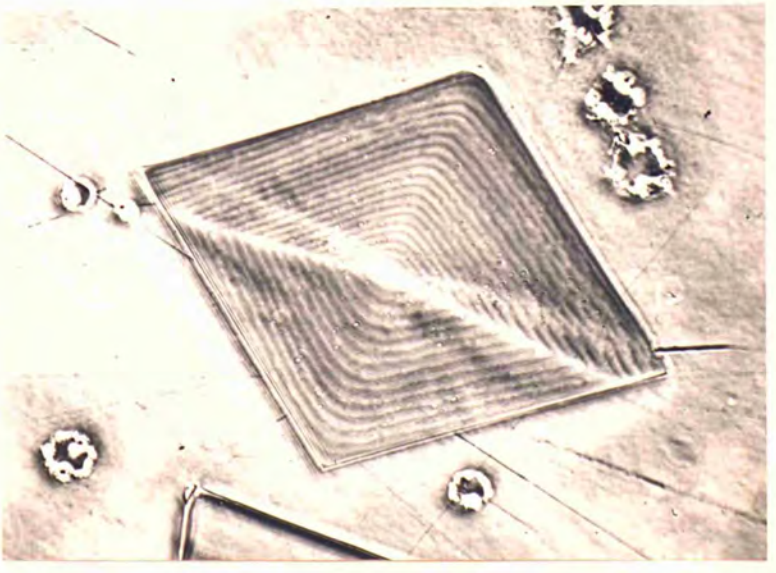

Fig.60. Crystal of Stearic Acid Grown at about 276° K.
Reflexion Phase Contrast. x770.

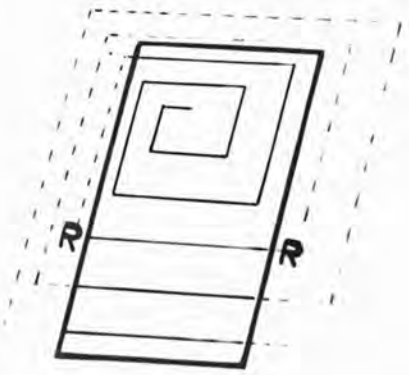

Fig.61a.

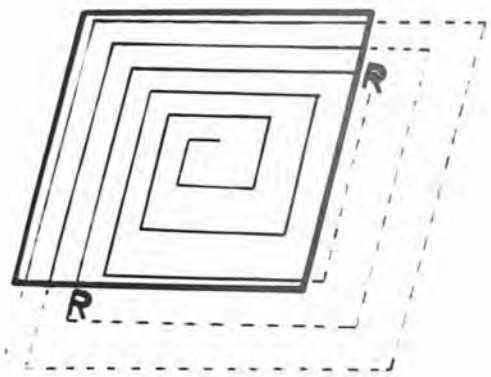

Fig.61b.

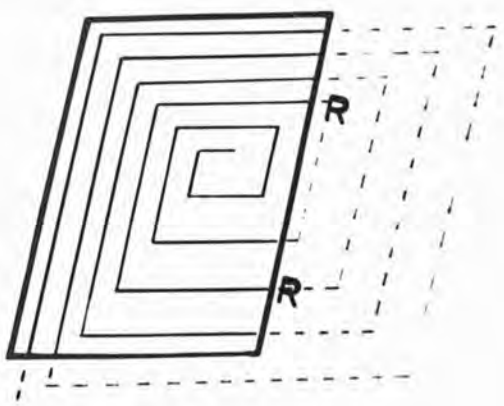

Fig.61c.

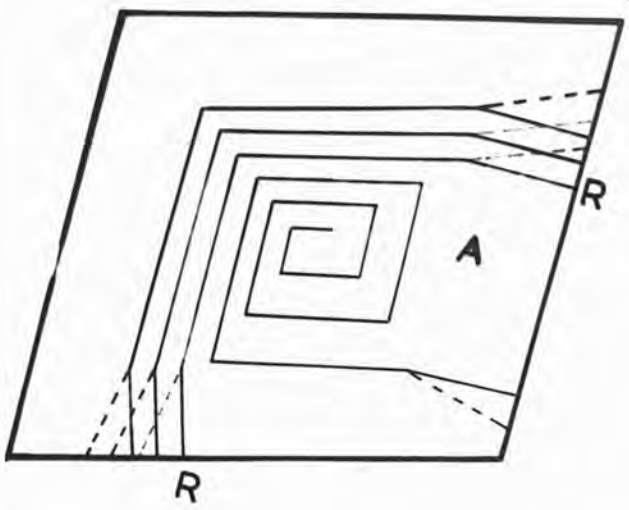

Fig.62.

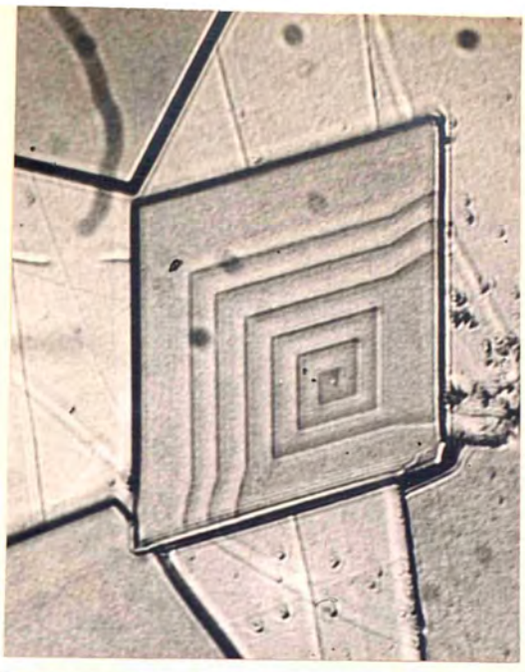

Fig.63. Stearic Acid. Single Spiral and Related Steps.
Reflexion Bright-field. x980.

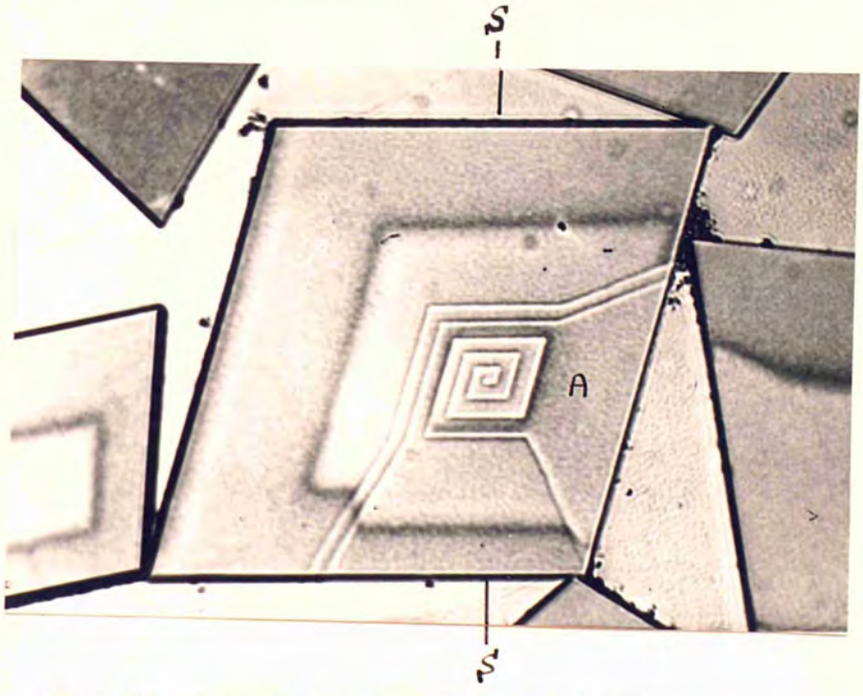

Fig.64. Stearic Acid. Internal Interference. x780.

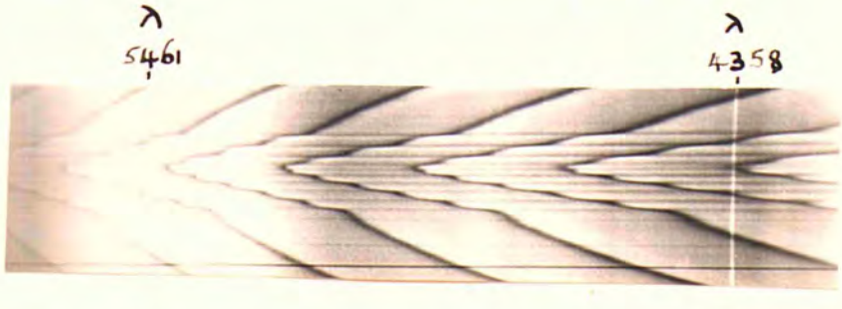

Fig.65. Fringes of Equal Chromatic Order for Section across above Crystal.

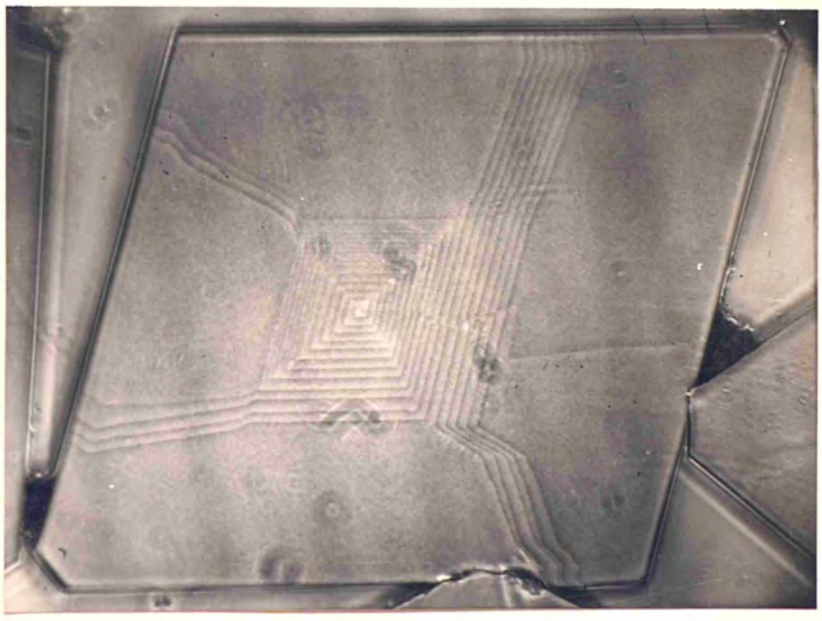

Fig.66. Stearic Acid. Interlaced Spiral with
Related Steps.
Reflexion Phase Contrast. x630.

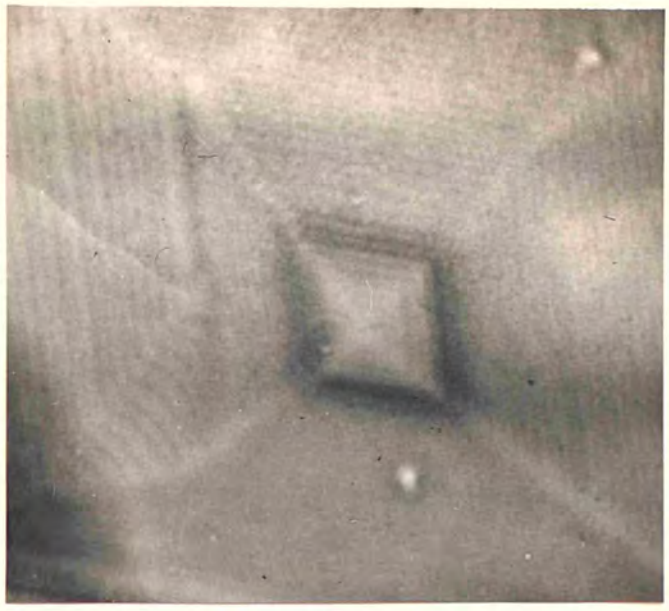

Fig.67a. Behenic Acid. Central Region of Fig.67b.
Reflexion Phase Contrast. x1190.

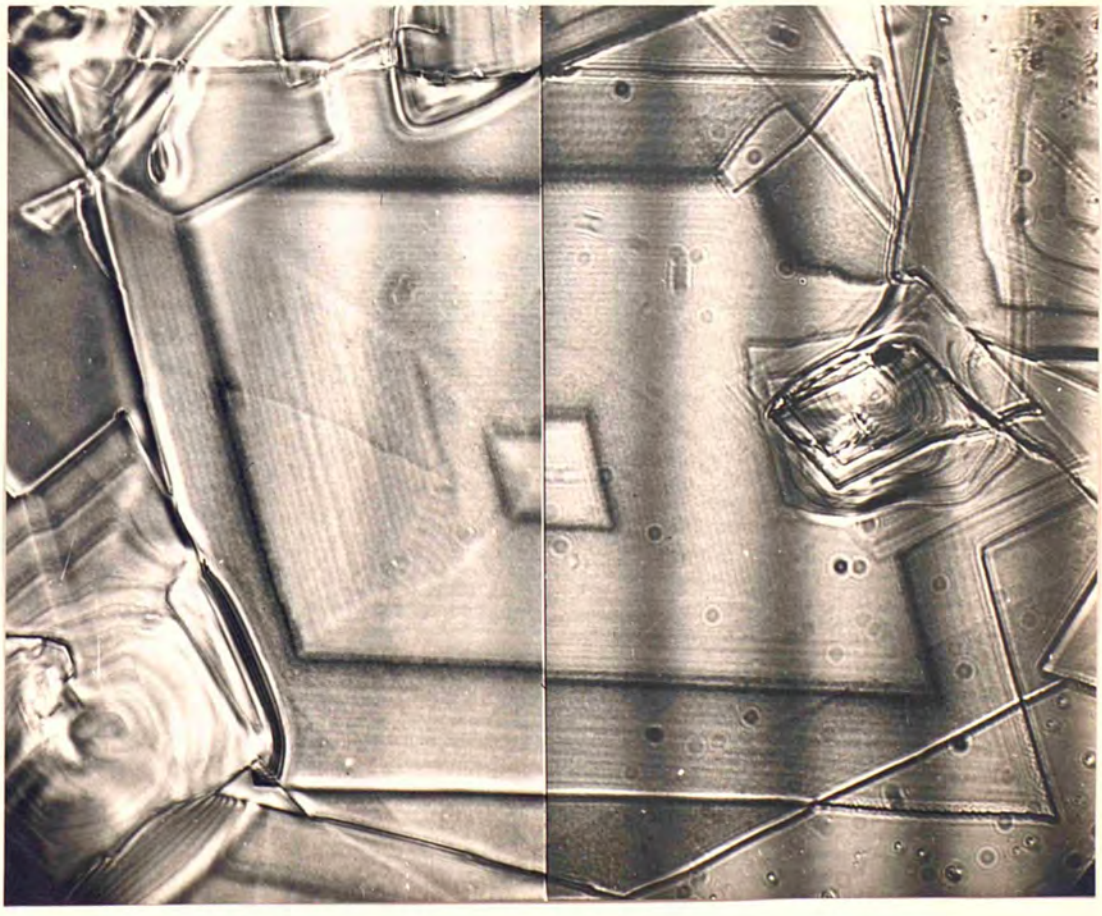

Fig.67b. Behenic Acid.
Reflexion Phase Contrast. Internal Interference. Hg. Yellow. One Component of Fringes. x680.

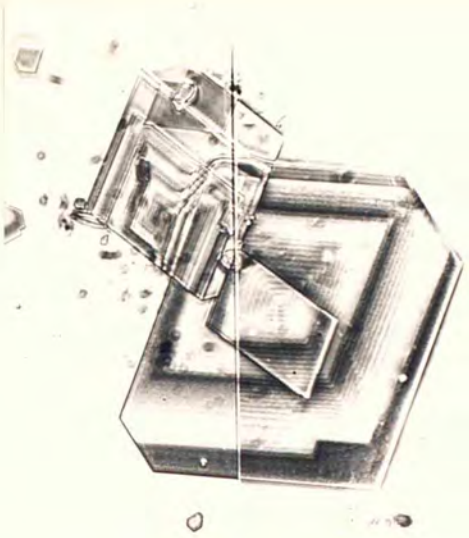

Fig.68. Stearic Acid.
Internal Interference. Reflexion Phase Contrast. x200.

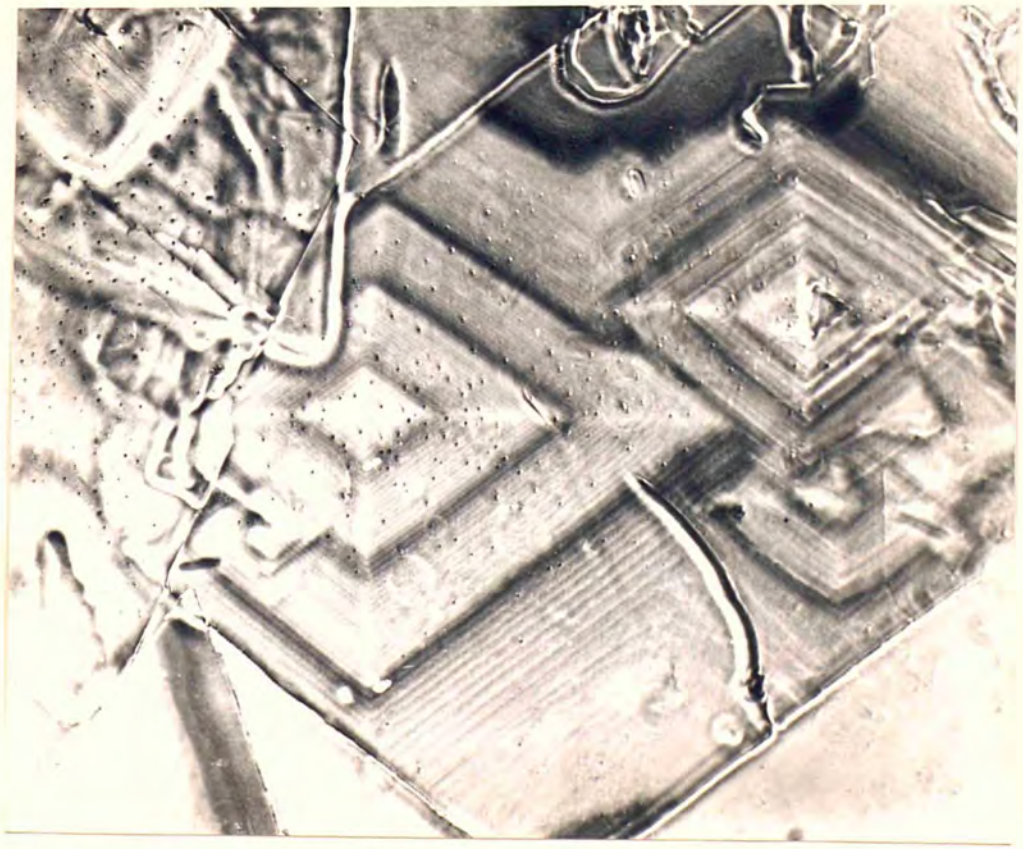

Fig.69. Stearic Acid.
Reflexion Phase Contrast with Superimposed Internal Interference Fringes. x680.

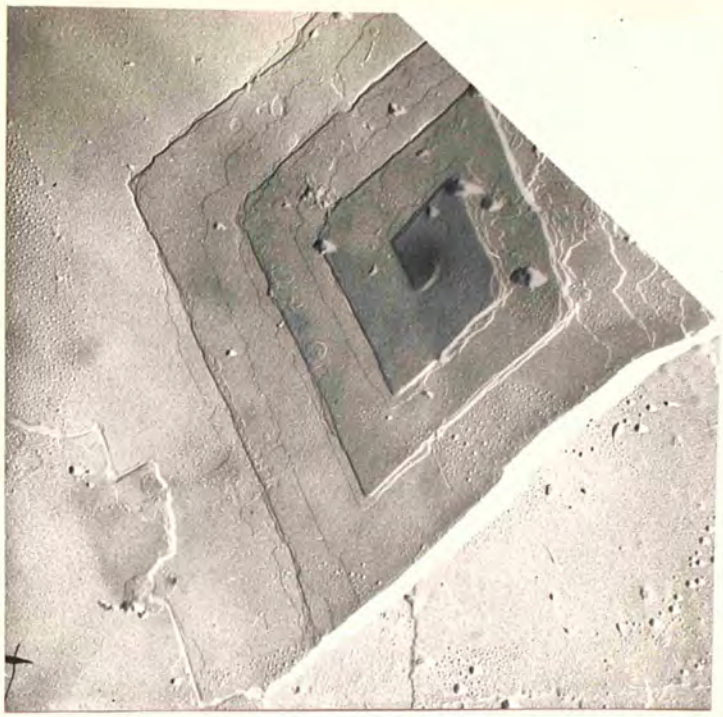

Fig.70. Behenic Acid. Multiple Growth Step.
Electronmicrograph. x7160.

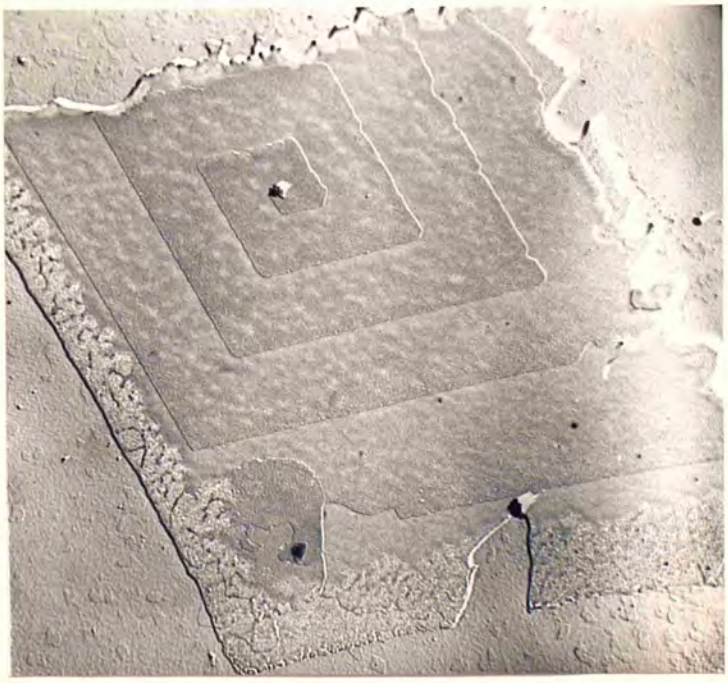

Fig.71. Behenic Acid. Bimolecular Growth Step.
Electronmicrograph. x7160.

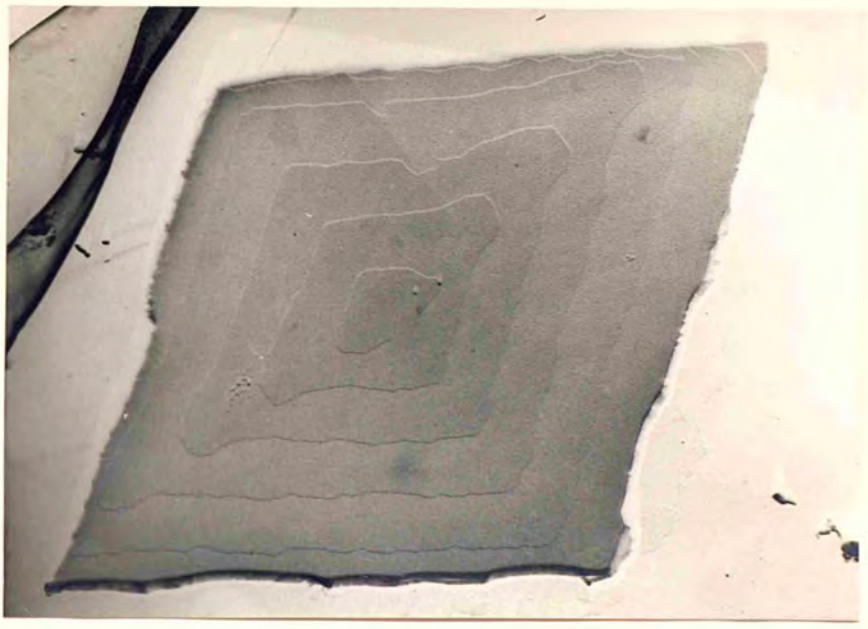

Fig.72. Behenic Acid. Trimolecular Growth Step.
Electronmicrograph. x 8200.

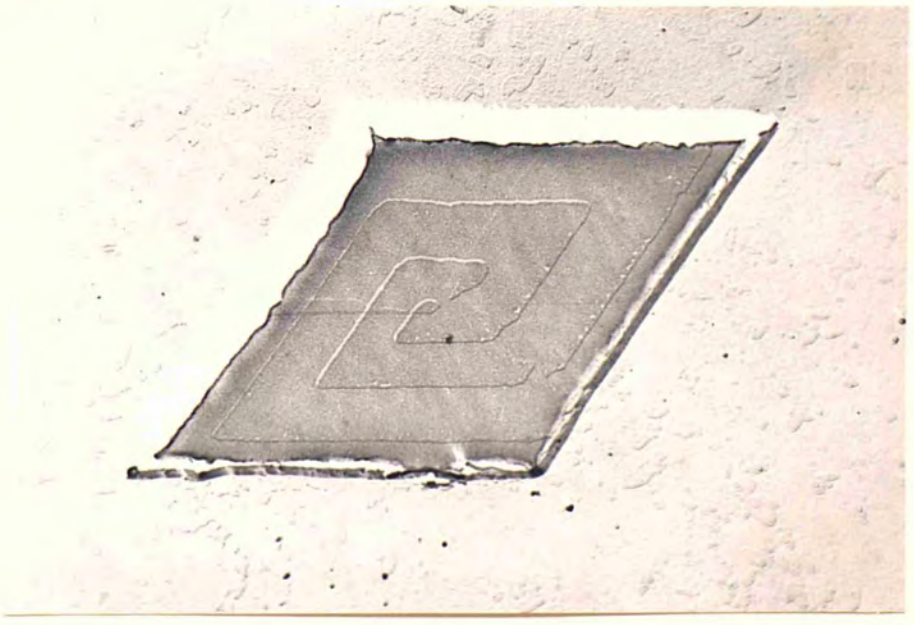

Fig.73. β-Form of Behenic Acid. Trimolecular
Growth Steps and Residual Steps.
Electronmicrograph. x9940.

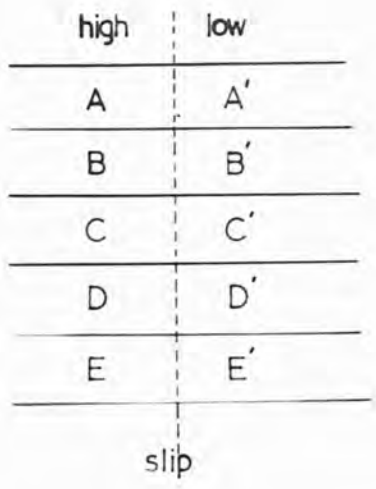

Fig.74.

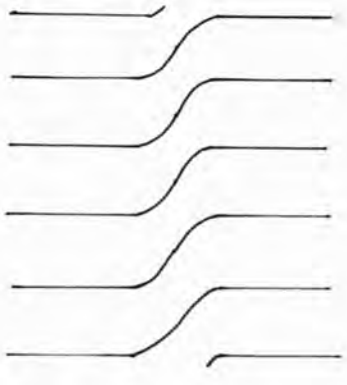

Fig.75.

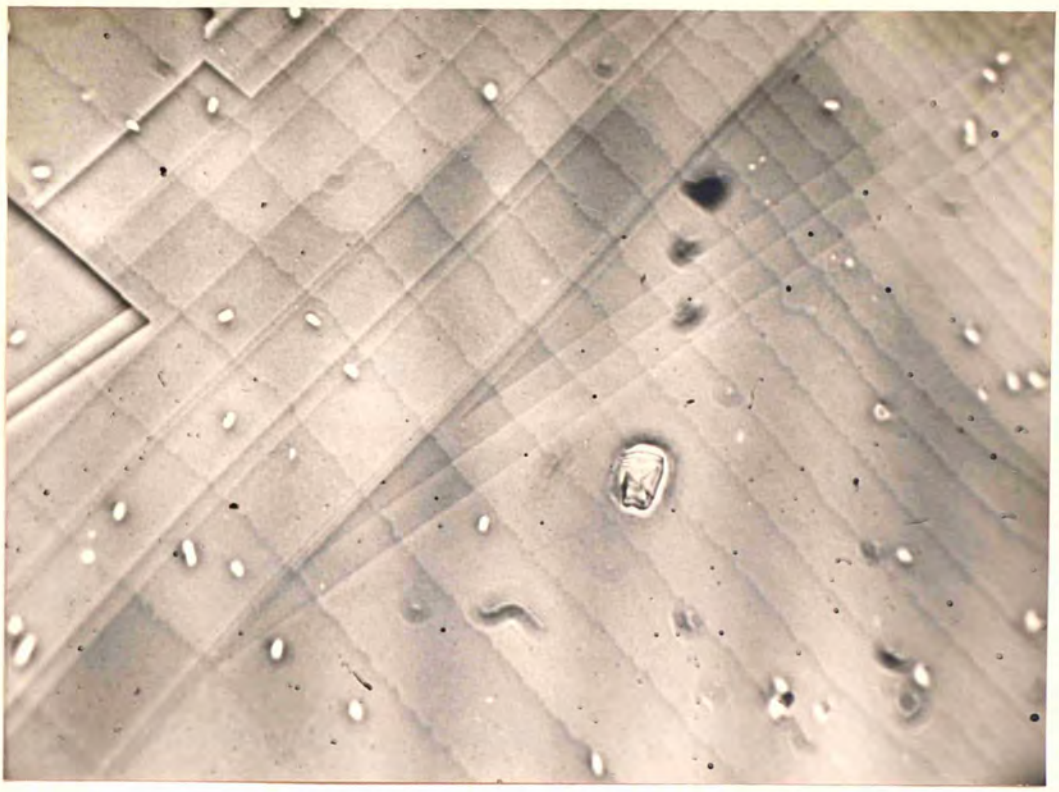

Fig.76. Stearic Acid. Reflexion Phase Contrast.
White Light. x240.

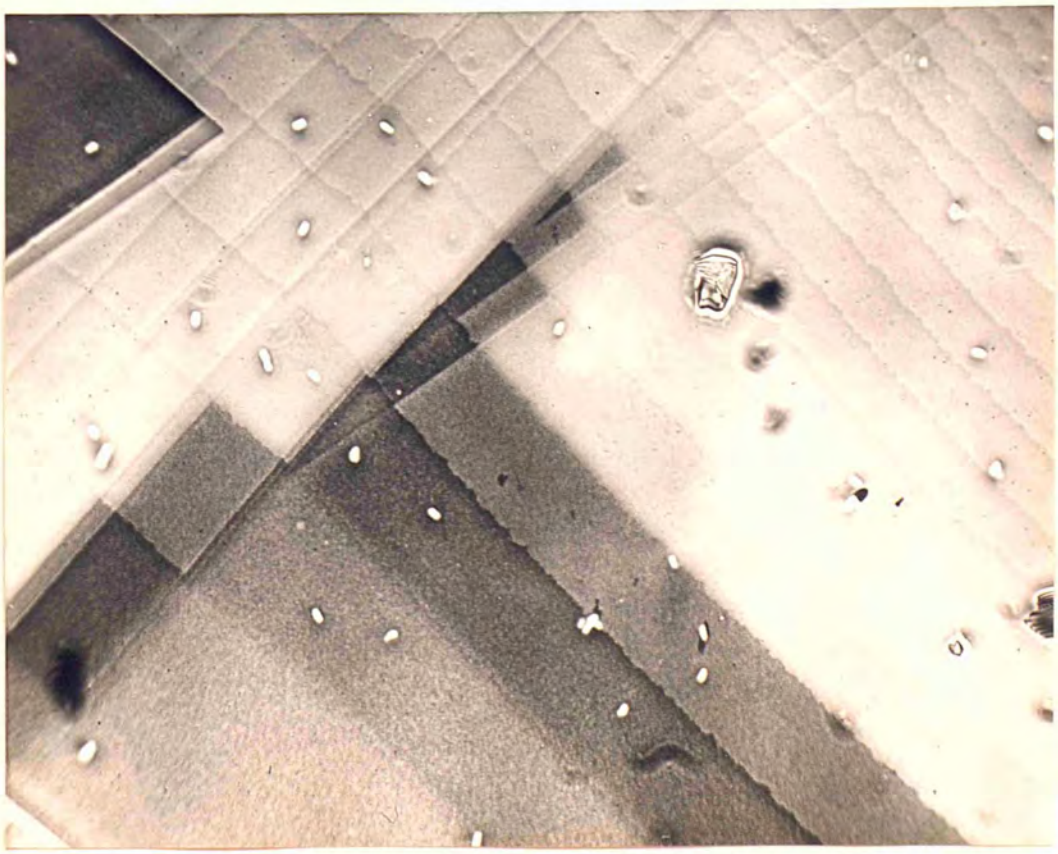

Fig.77. Stearic Acid. Phase Contrast with Superimposed
Internal Interference Fringes. Hg. Yellow.
One Component of Fringes. x240.

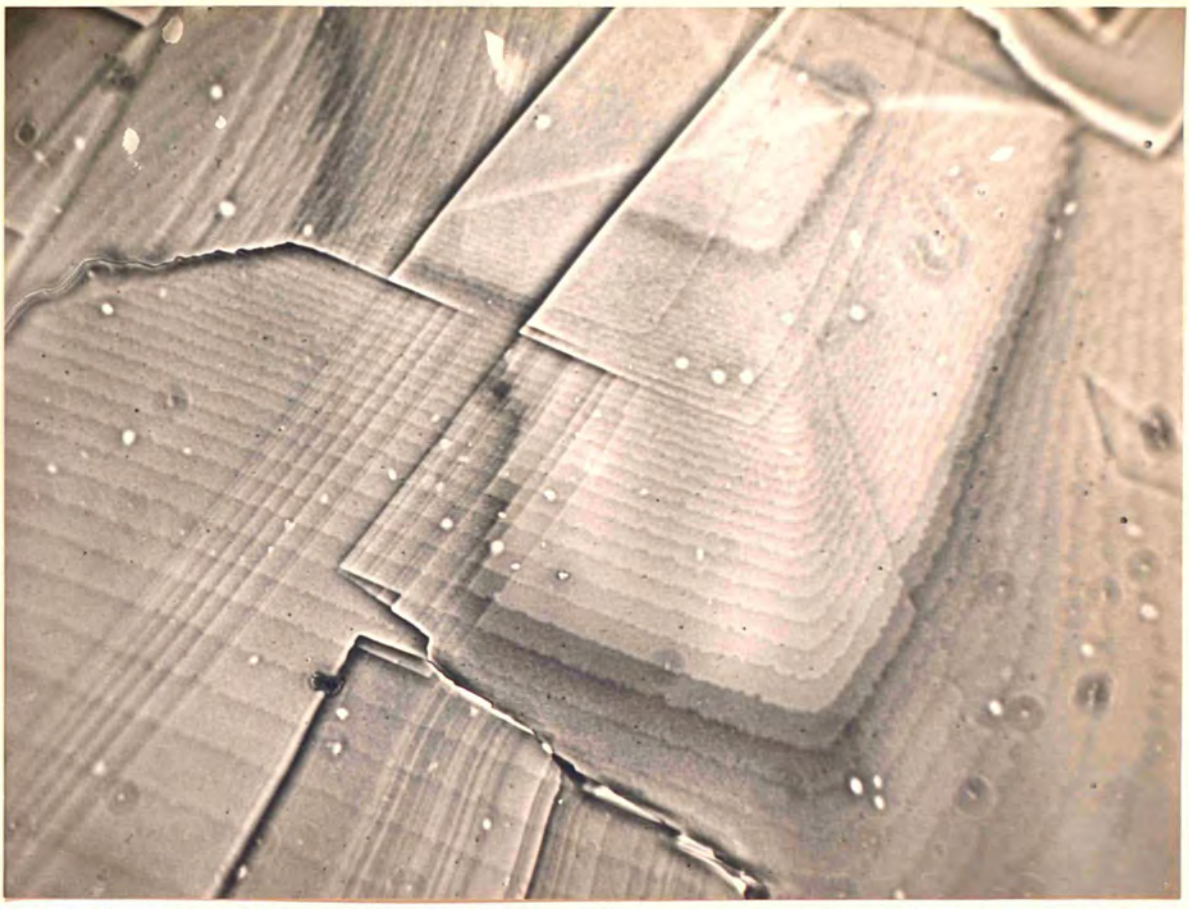

Fig.78. Stearic Acid. Reflexion Phase Contrast with Superimposed Internal Interference Fringes. Hg. Yellow. One Component of Fringes. x310.

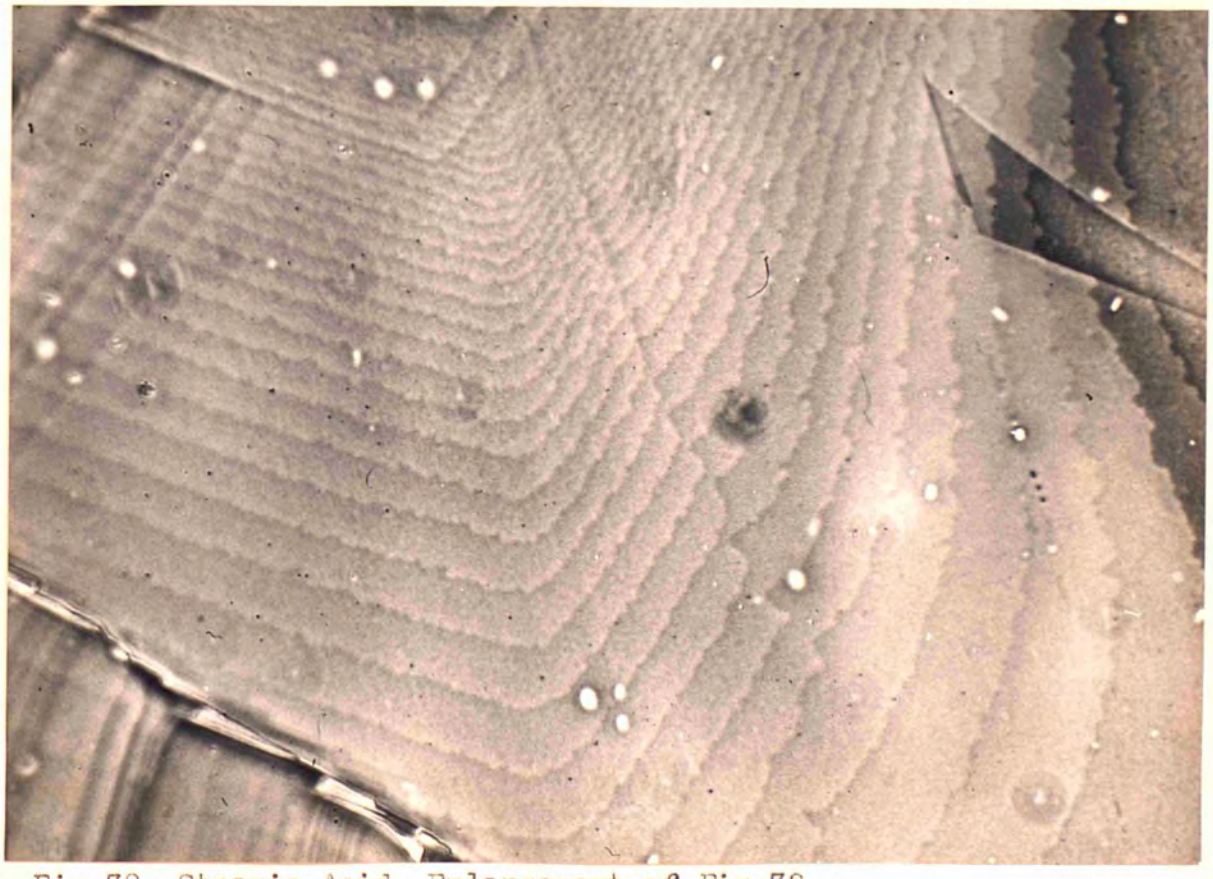

Fig.79. Stearic Acid. Enlargement of Fig.78. Reflexion Phase Contrast. x460.

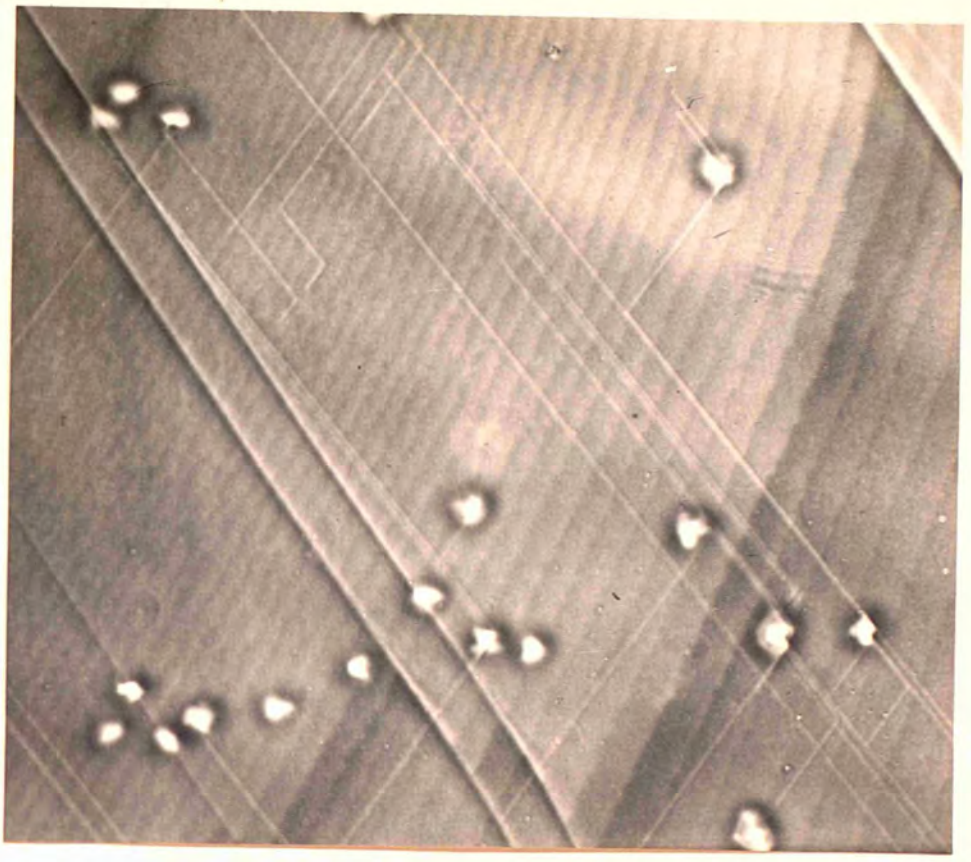

Fig.80. Stearic Acid. Terminated Slip Lines.
Reflexion Phase Contrast. x370.

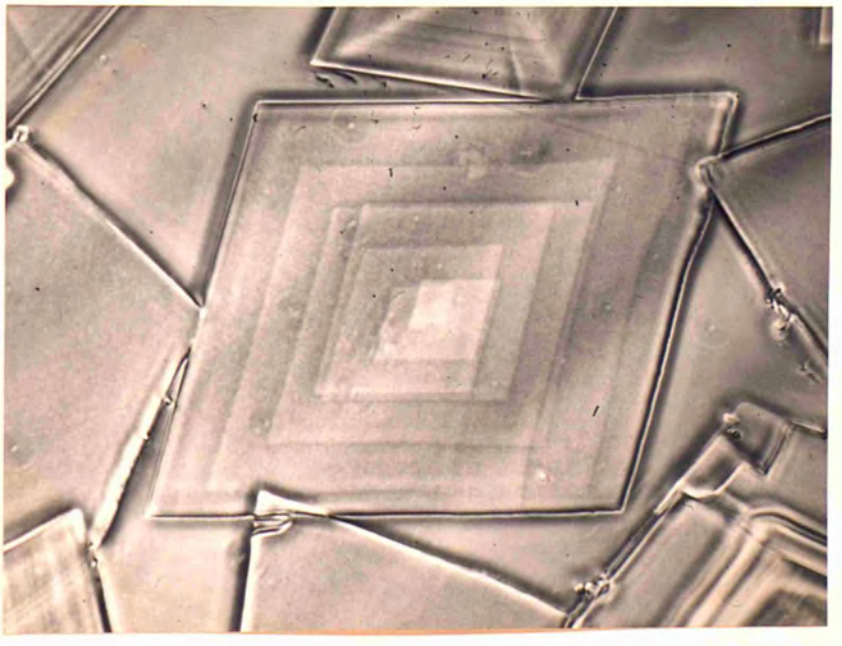

Fig.81. Behenic Acid. Internal Slip.
Reflexion Phase Contrast. x780.

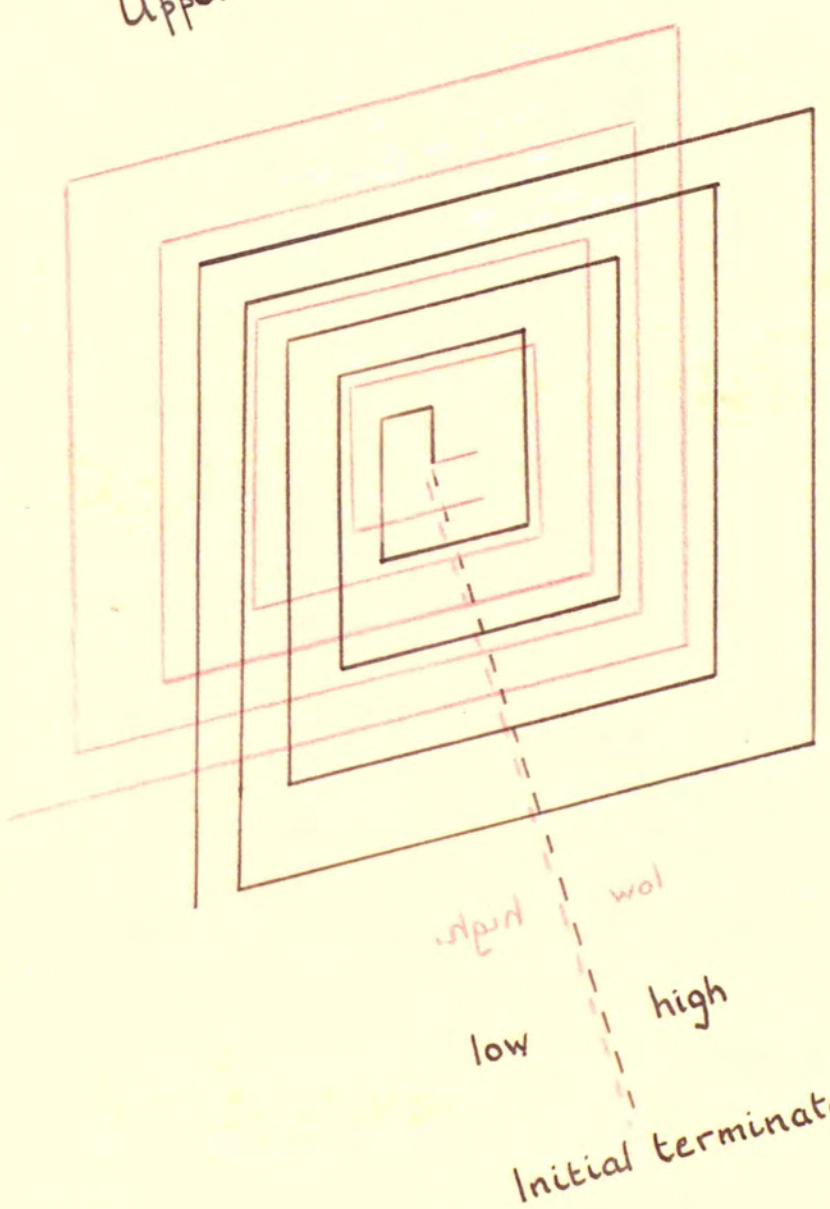

Fig. 82.

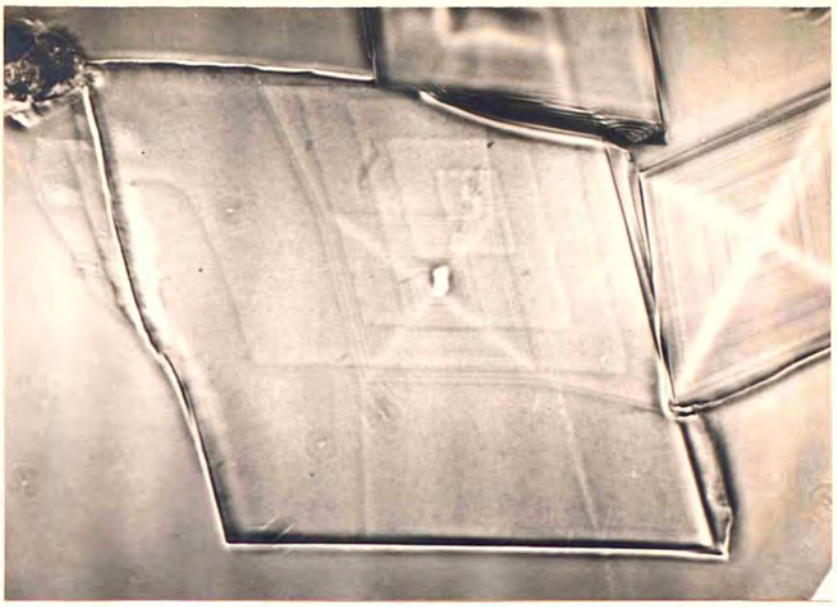

Fig.83. Behenic Acid. Internal Slip, Growth Centres Non-coincident. Reflexion Phase Contrast. x680.

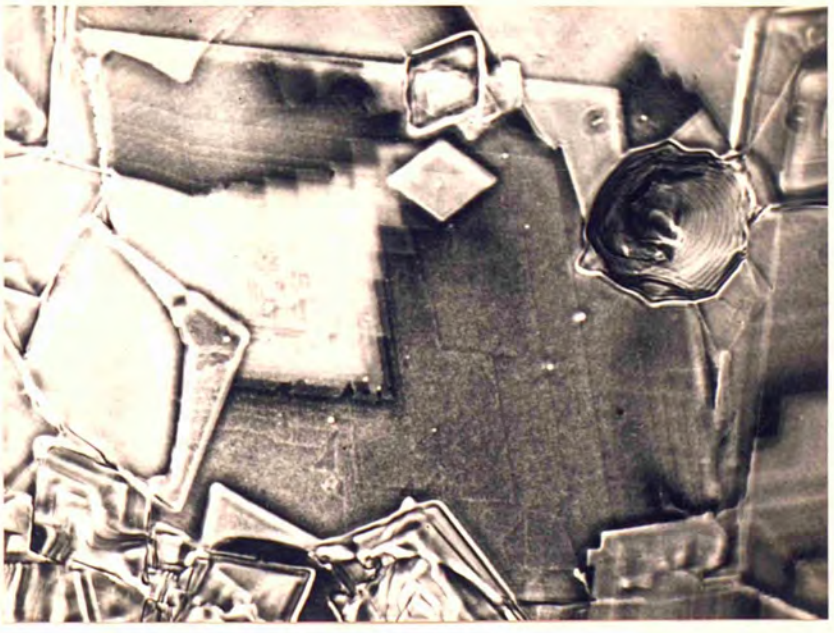

Fig.84. Behenic Acid. Internal Slip, Growth Centres Non-coincident. Reflexion Phase Contrast with Superimposed Internal Interference Fringes. Hg. Green. One Component of Fringes. x630.

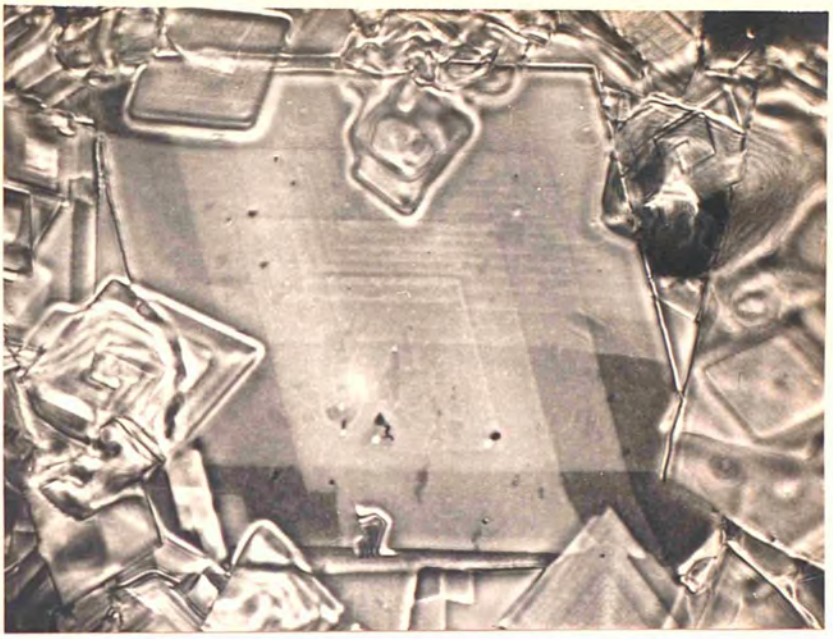

Fig.85. Behenic Acid. Internal Slip, Growth Centres Non-coincident.
Reflexion Phase Contrast with Superimposed Internal Interference Fringes. Hg. Yellow.
One Component of Fringes. x700.

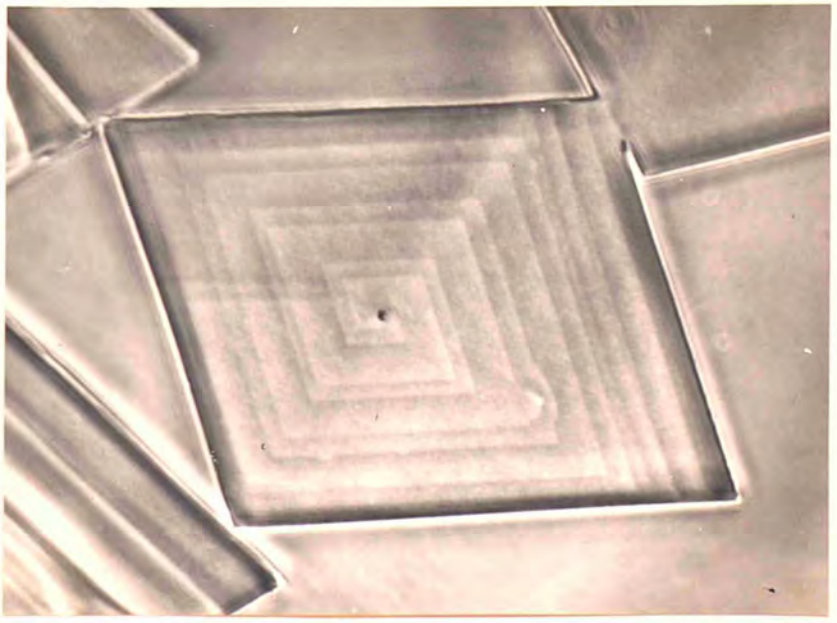

Fig.86. Behenic Acid. Internal Slip.
Reflexion Phase Contrast. x1090.

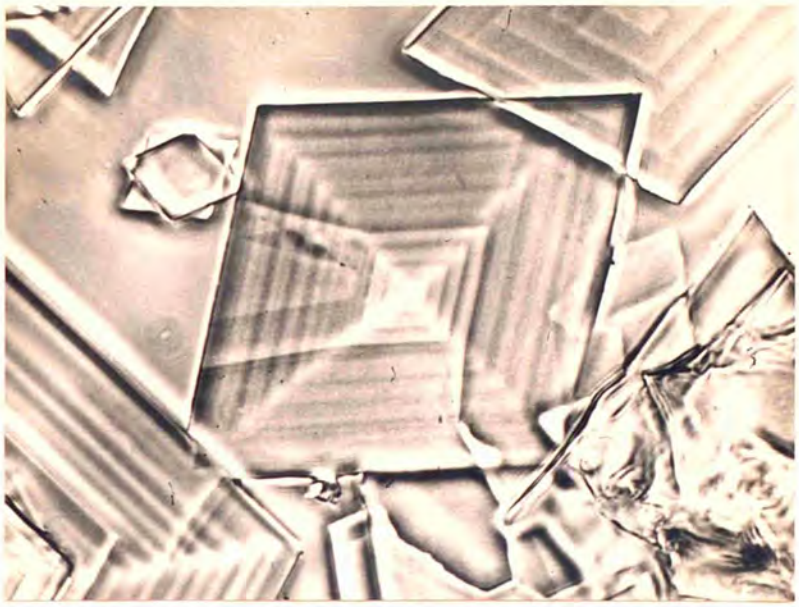

Fig.87. Behenic Acid. Internal Slip after Growth on one Face was arrested.
Reflexion Phase Contrast. x920.

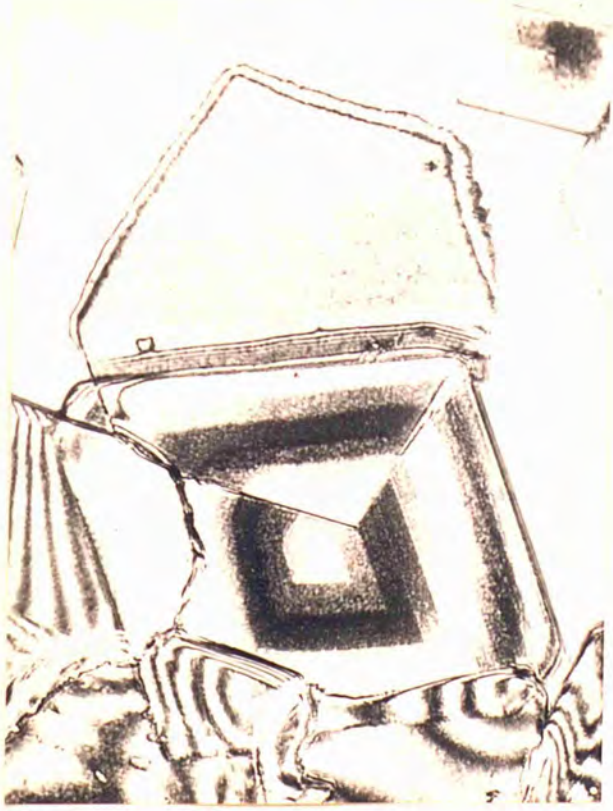

Fig.88. Stearic Acid.
Internal Interference.
Hg. Green (one component).
x650.

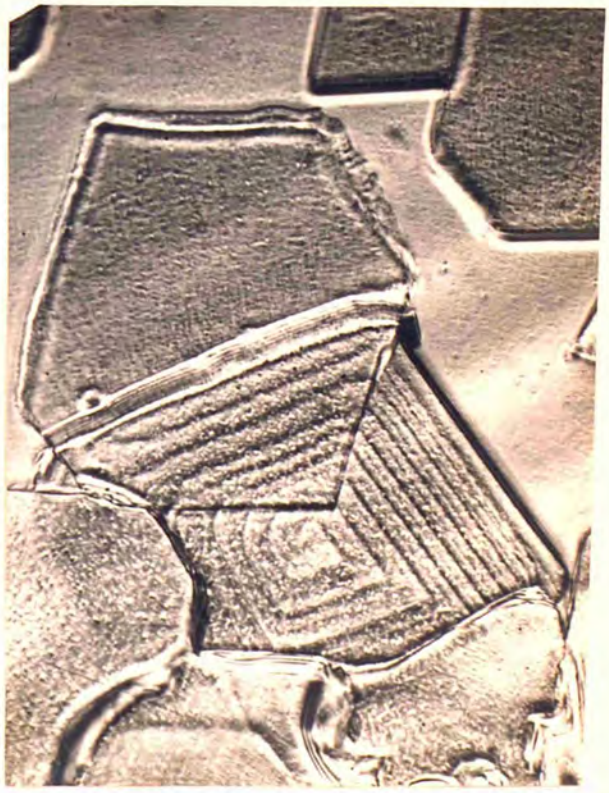

Fig.89. Stearic Acid. Crystal Opaquely Silvered.
Reflexion Phase Contrast.
x650.

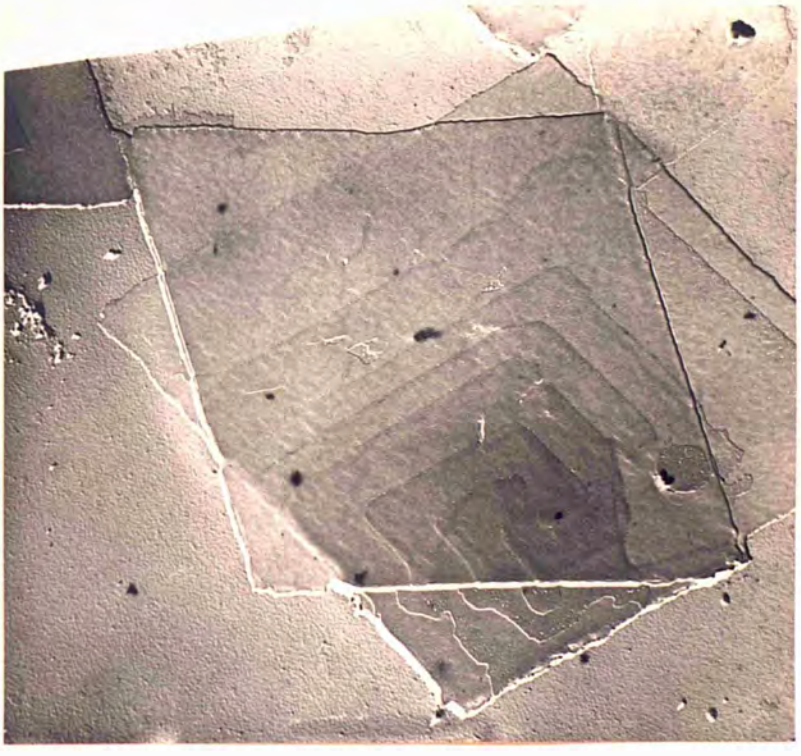

Fig.90. Behenic Acid. Internal Slip.
Electronmicrograph. x5600.

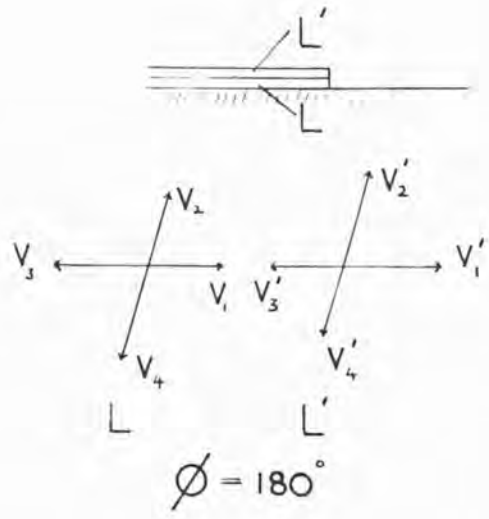

Fig.91. Vector Diagrams for the Velocities of Advance of Component Layers.

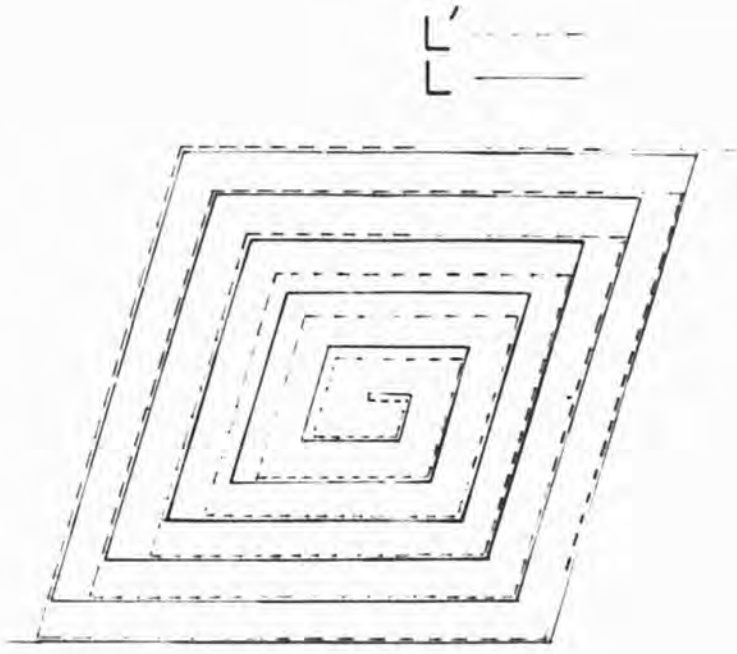

Fig.92. The Resultant Growth Pattern.

Fig.93. Stearic Acid. Interlaced Spiral.
Reflexion Phase Contrast. x530.

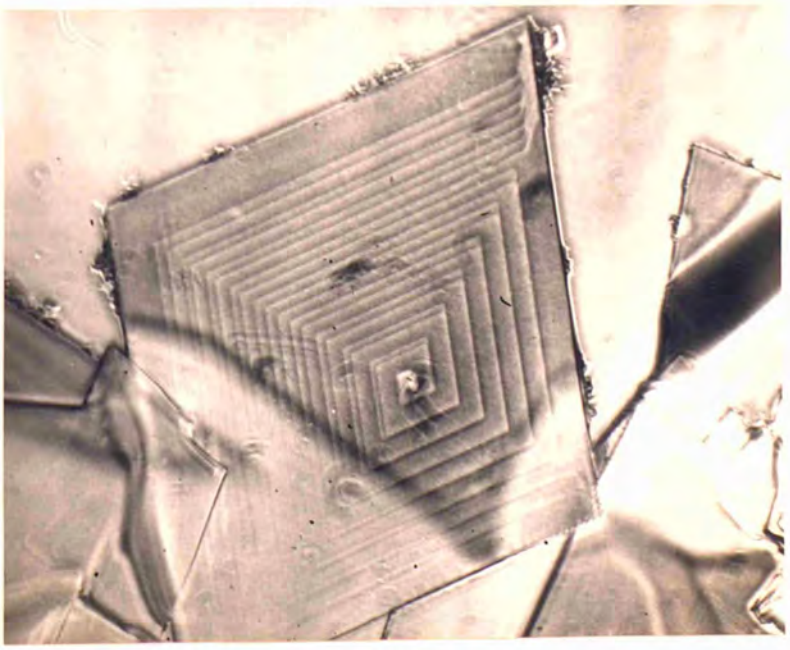

Fig.94. Stearic Acid. Interlaced Spiral.
Reflexion Phase Contrast. x530.

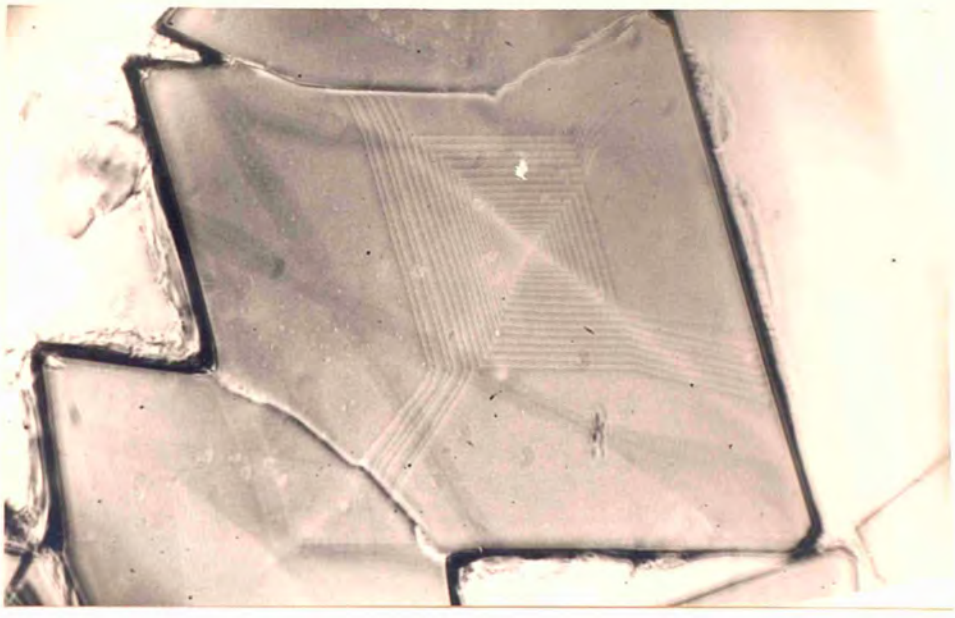

Fig.95. Stearic Acid. Interlaced Spiral.
Reflexion Phase Contrast. x220.

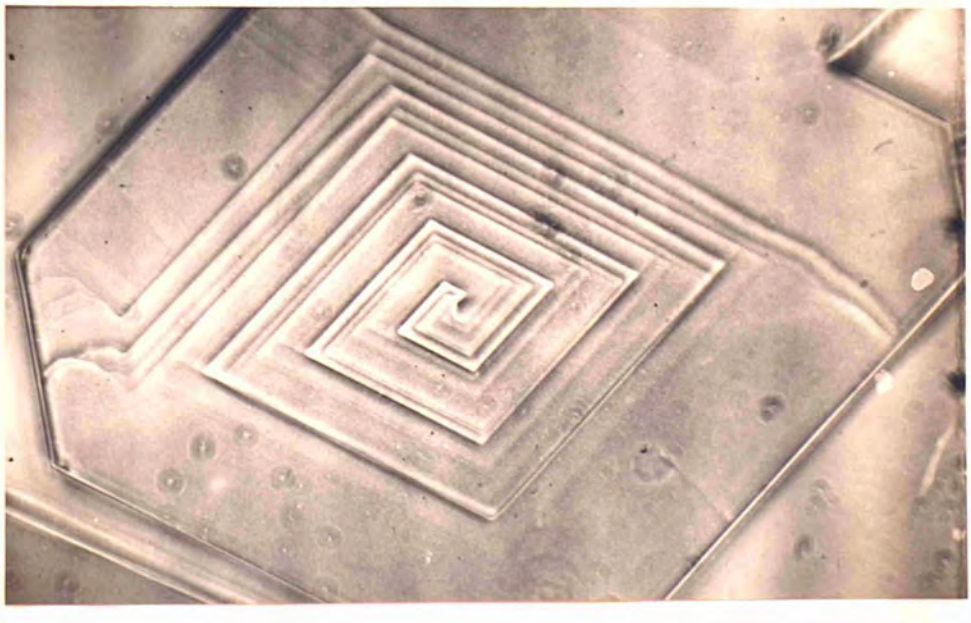

Fig.96. Group of Interlaced Spirals.
Stearic Acid.
Reflexion Phase Contrast. x530.

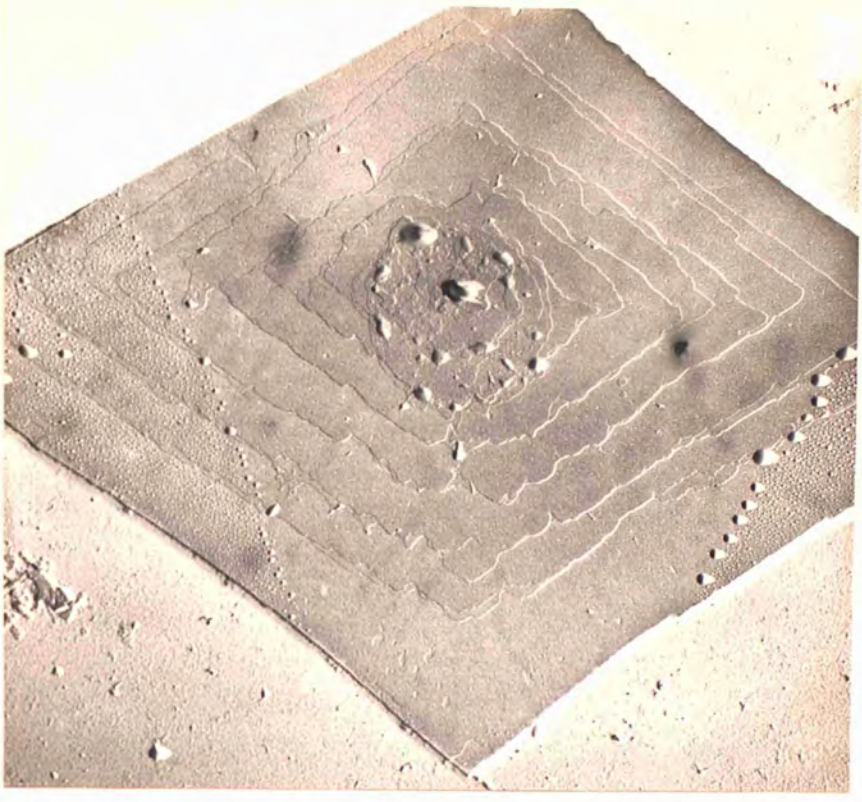

Fig.97. Behenic Acid. Interlaced Spiral.
Electronmicrograph. x6100.

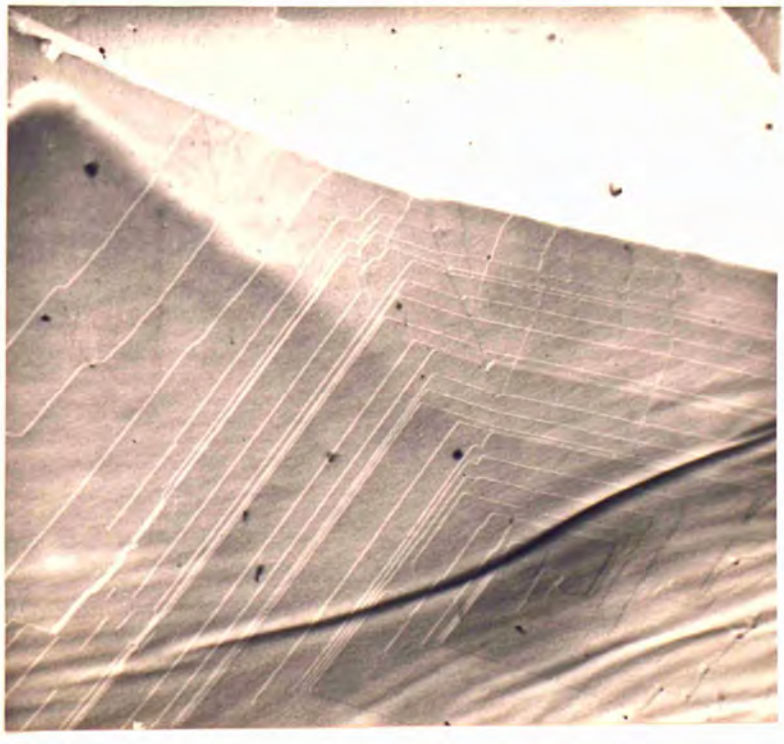

Fig.98. Behenic Acid. Step Grouping.
Electronmicrograph. x 6800.

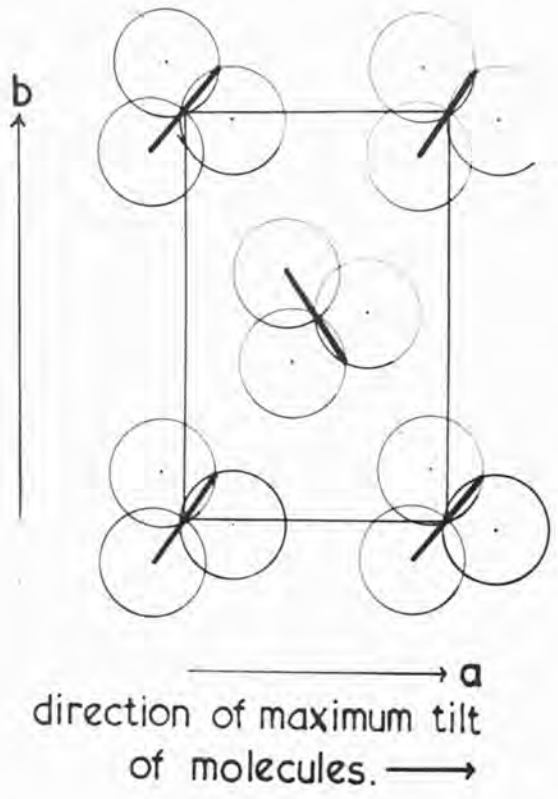

Fig.99a. Diagrammatic Representation of Packing of Molecules in Basal Plane.

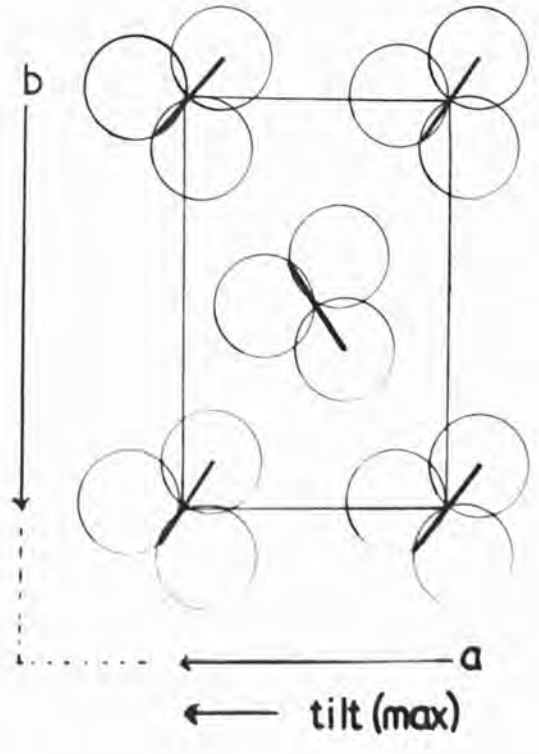

Fig.99b. Packing after Rotation $\phi = 180°$.

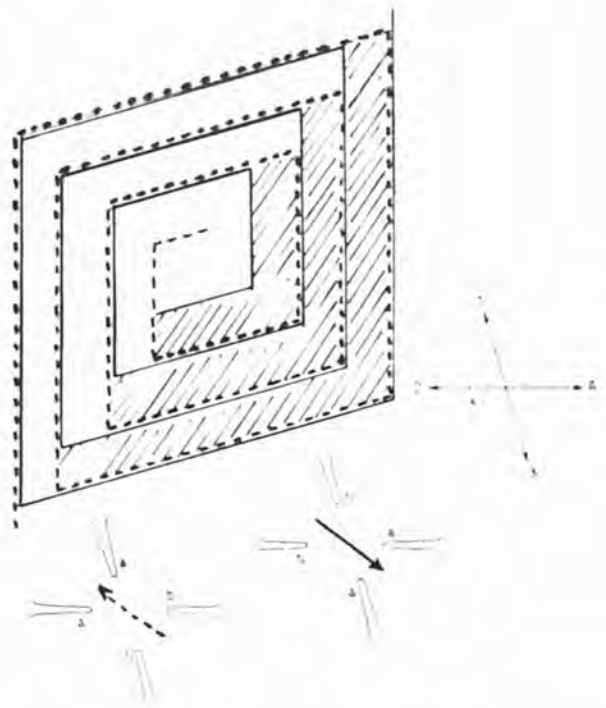

Fig.100. Interlaced Monomolecular Layers.
(Amelinckx).

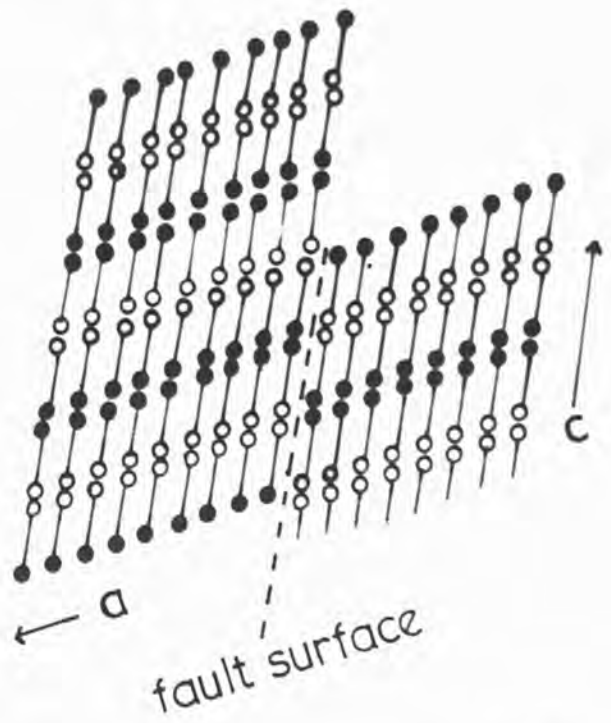

Fig.101. An Imperfect Dislocation.

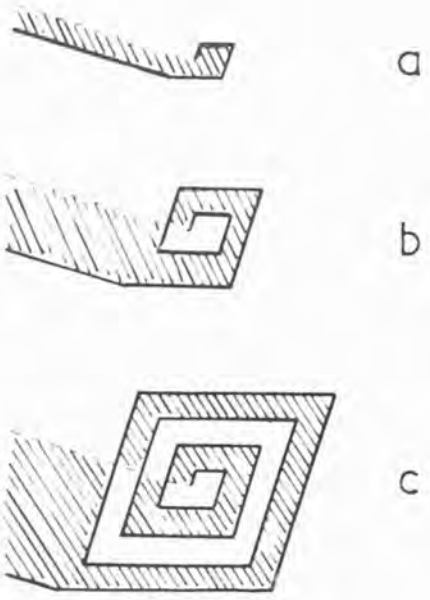

Fig.102. Growth from an Imperfect Dislocation when Stacking in Growth Edge is determined by Substrate.

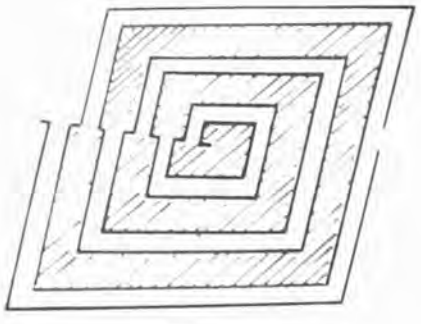

Fig.103. Growth Pattern from an Imperfect Dislocation when Velocity of Advance depends on Bonding to Substrate.

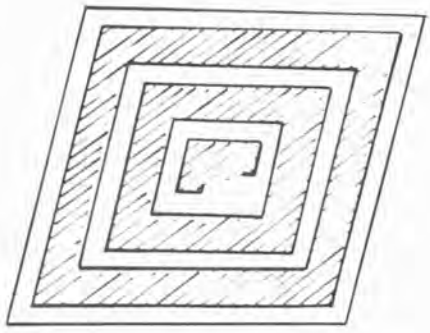

Fig.104. Growth from Two Imperfect Dislocations of Opposite Sense.

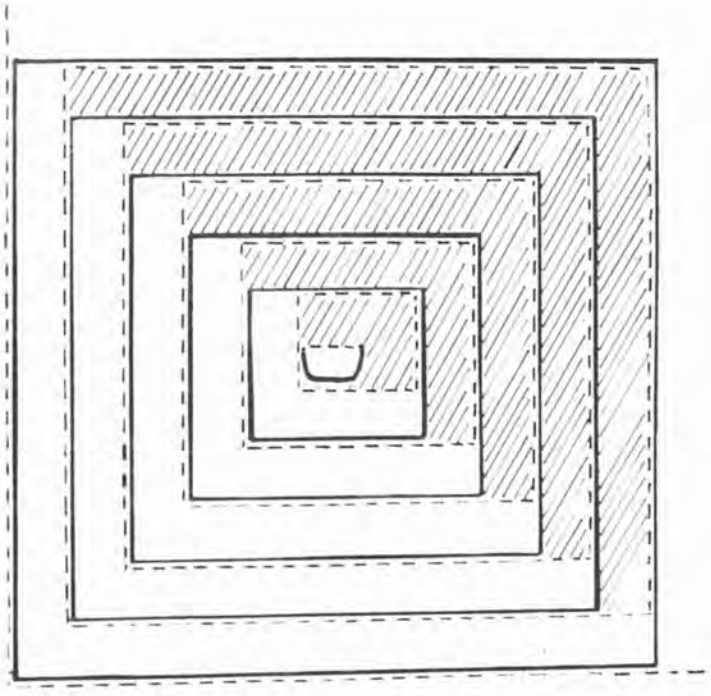

Fig.105. Interlacing due to Two Imperfect Dislocations of Opposite Sense. (Amelinckx).

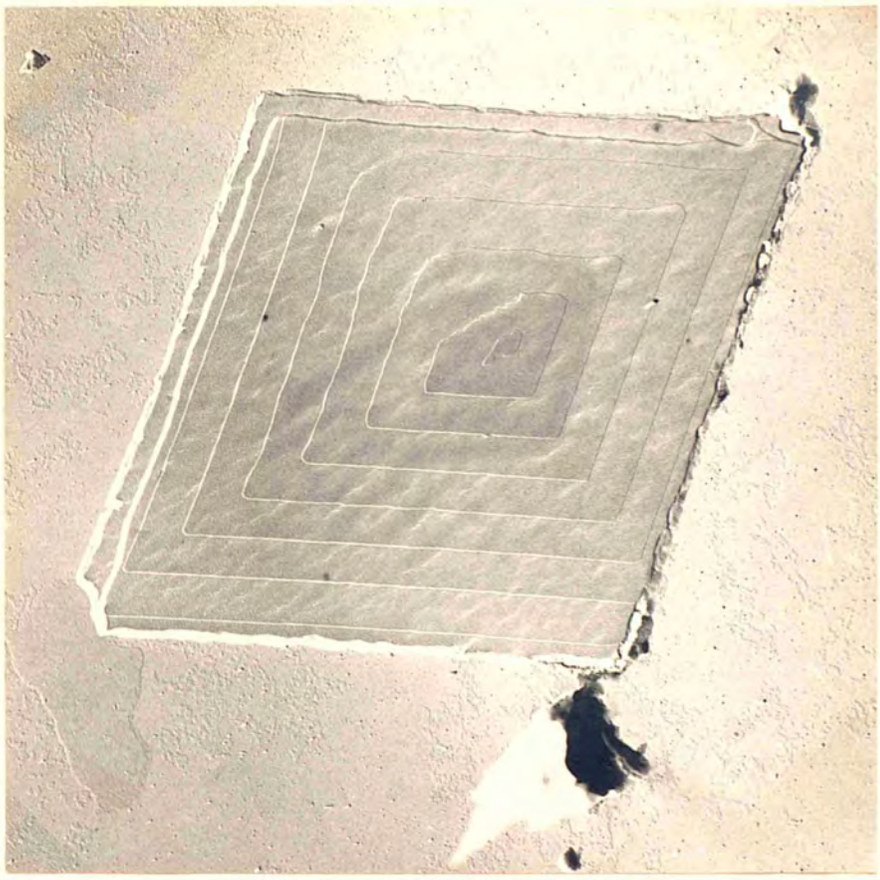

Fig.106. Growth from an Imperfect Dislocation.
Electronmicrograph. x6700.
Behenic Acid.

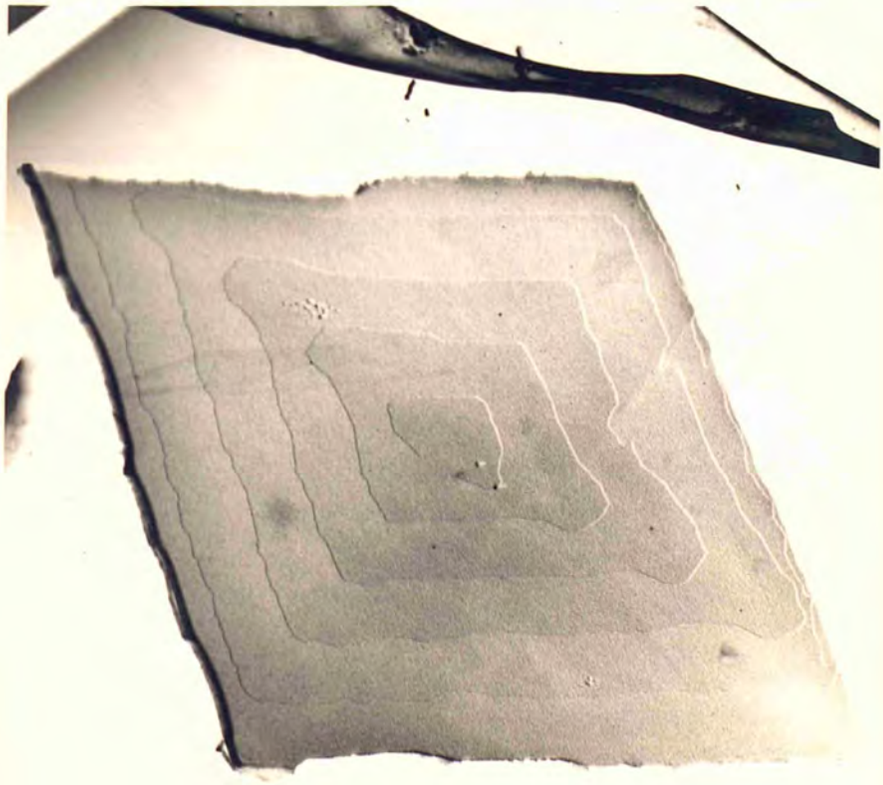

Fig.107. Growth from an Imperfect Dislocation.
Electronmicrograph. x7700.
Behenic Acid

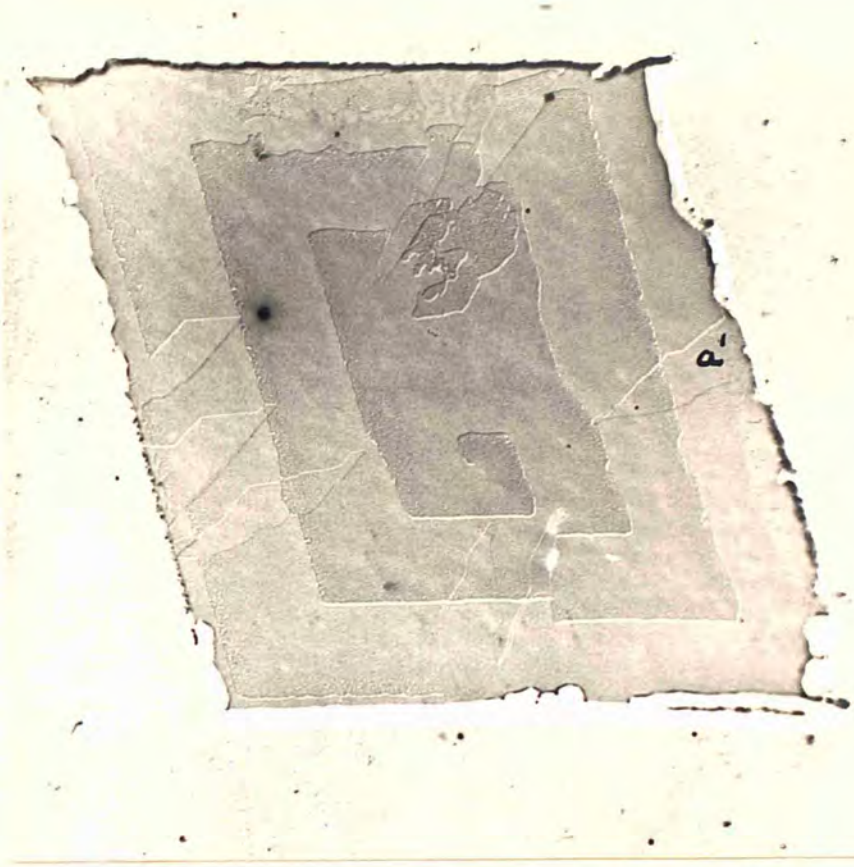

Fig.108. Growth from an Imperfect Dislocation.
Electronmicrograph. x8400.
Behenic Acid.

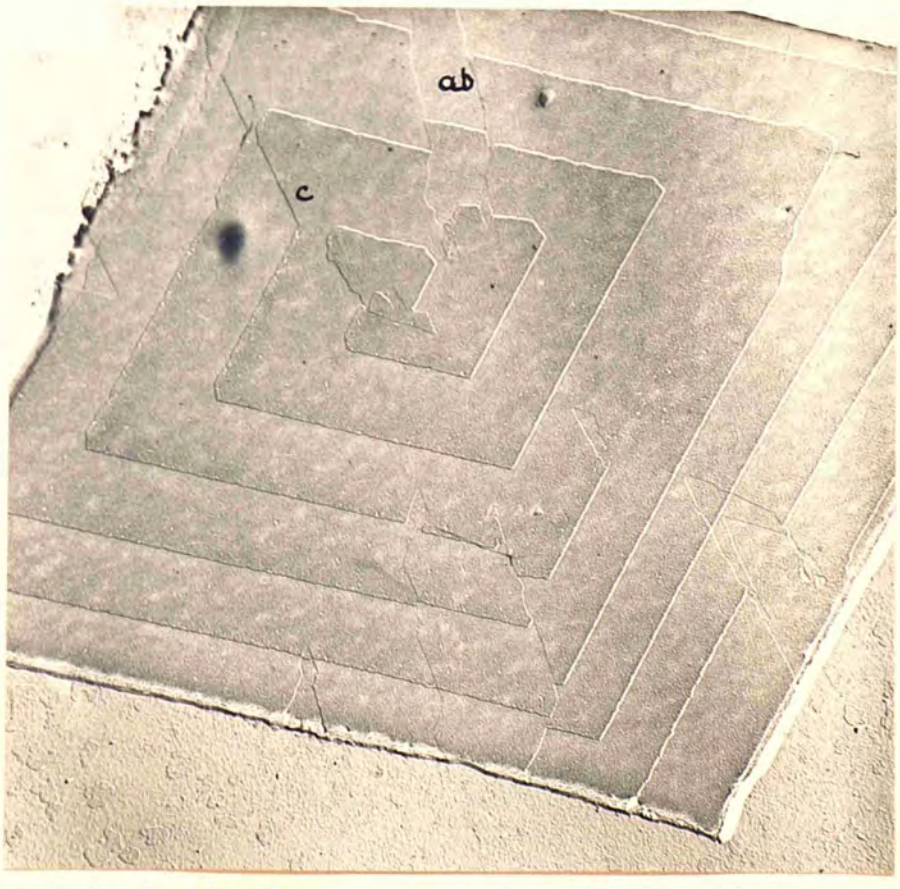

Fig.109. Growth from an Imperfect Dislocation.
Electronmicrograph. x9000.
Behenic Acid.

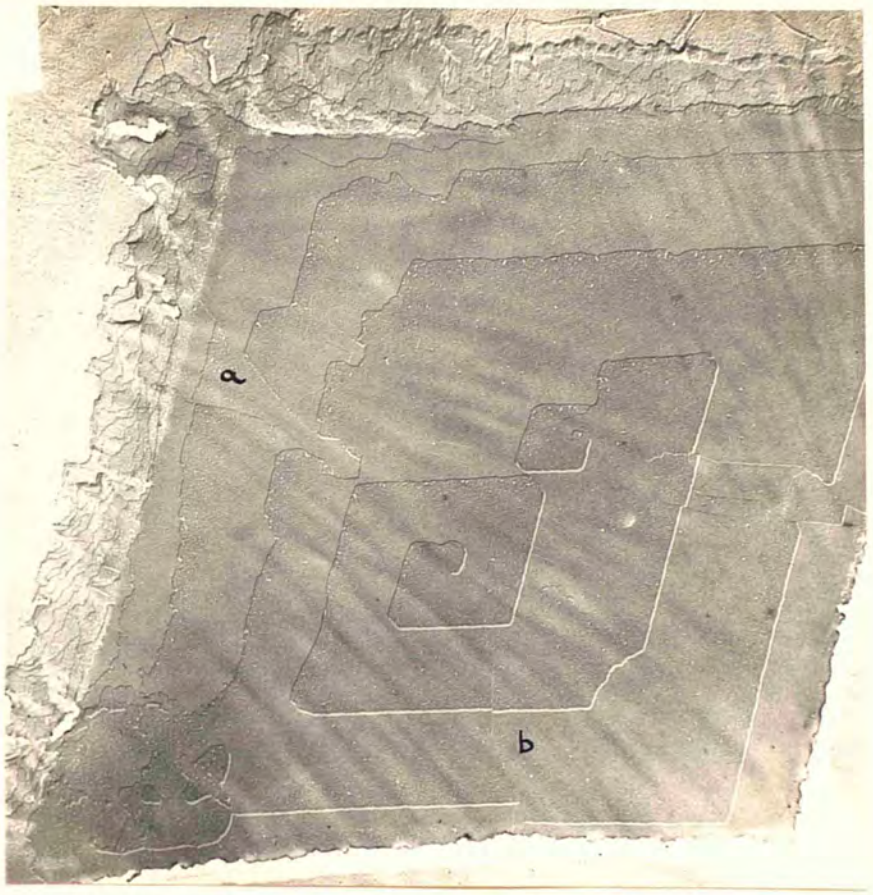

Fig.110. Growth from an Imperfect Dislocation.
Electronmicrograph. x9200.
Behenic Acid.

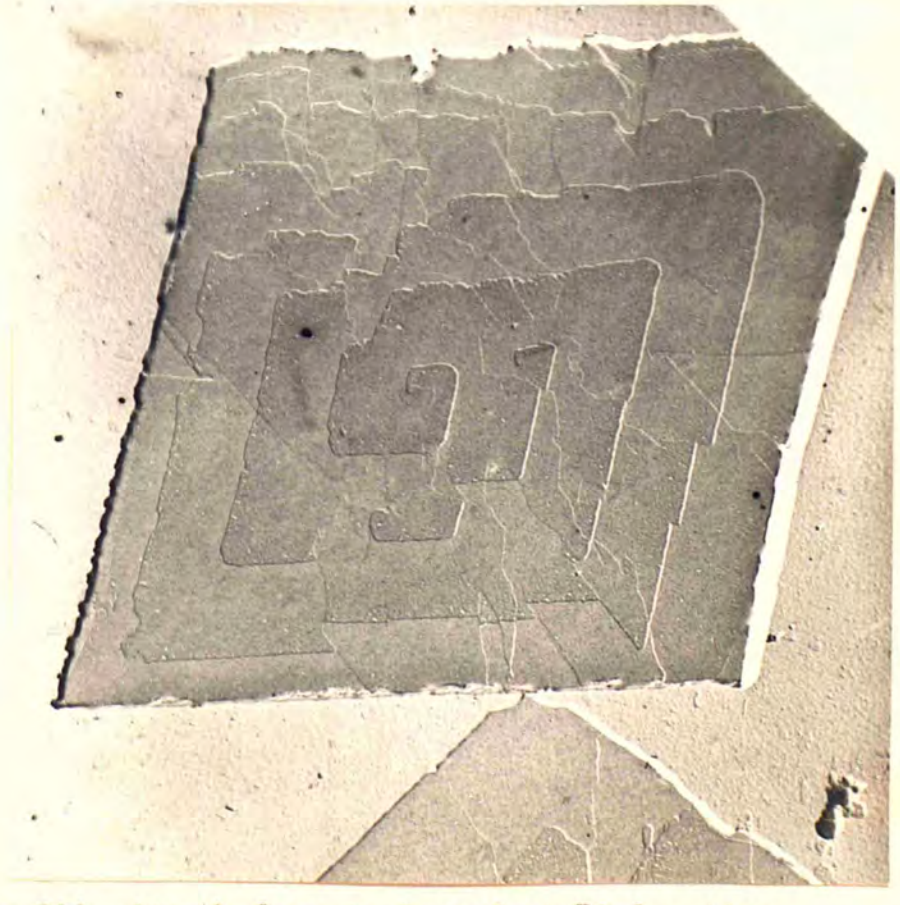

Fig.111. Growth from an Imperfect Dislocation.
Electronmicrograph. x8300.
Behenic Acid.

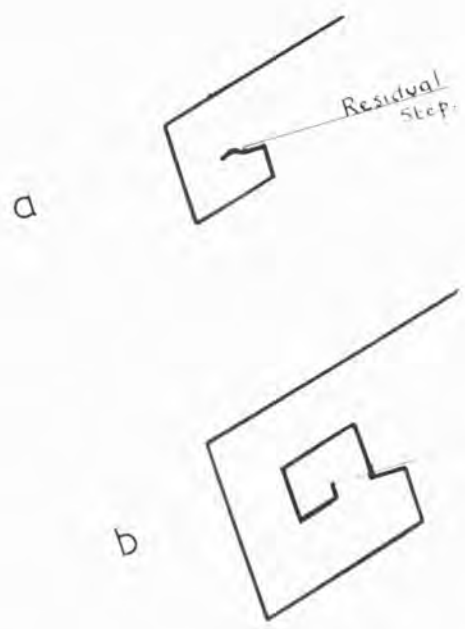

Figs.112a,b. Spiral Growth Layers Crossing a Residual Step.

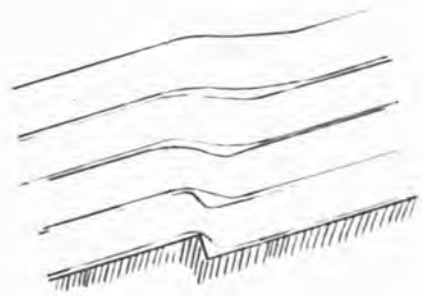

Fig.112c. Decrease in Sharpness of Residual Step as Growth proceeds.

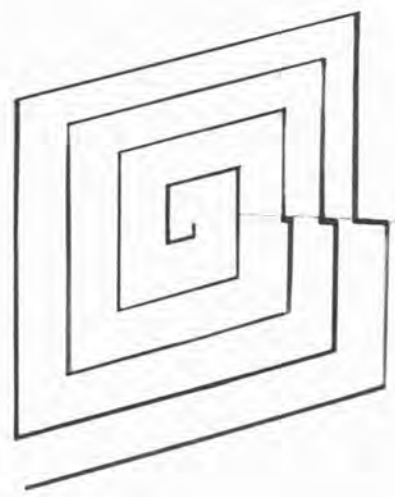

Fig.113. The Resultant Growth Pattern.

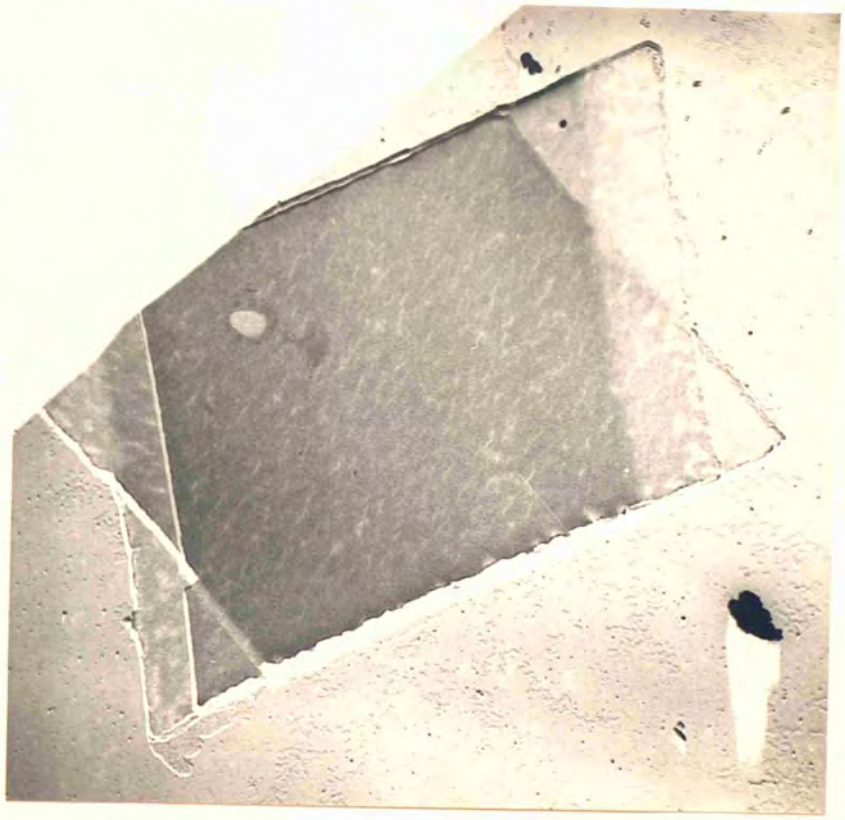

Fig.114. Behenic Acid. Contact Twins.
Electronmicrograph. x5700.

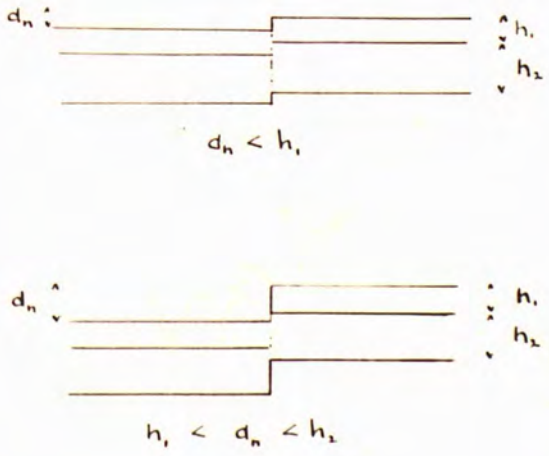

Fig.115.

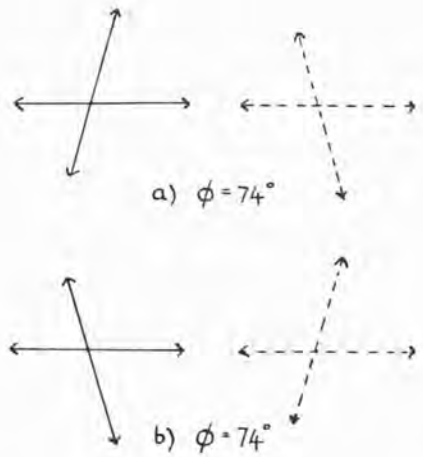

Fig.116. Vector Diagrams for the Velocities of Advance of Growth Edges.

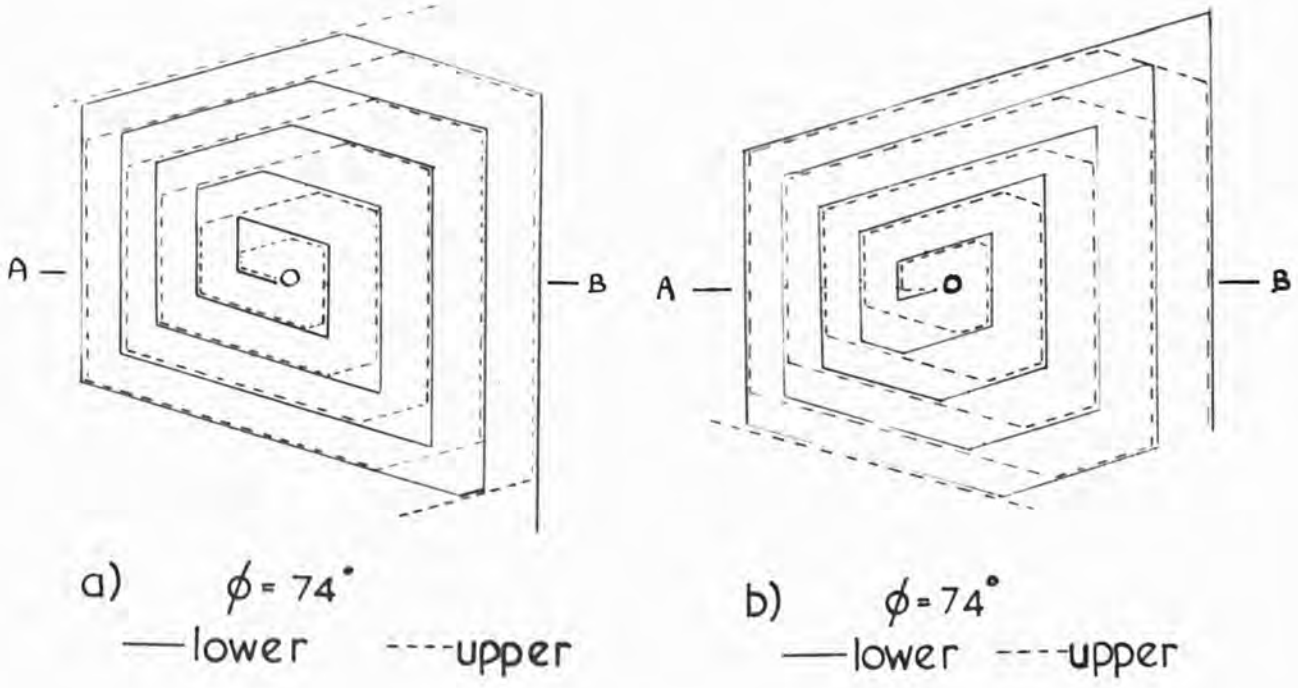

Fig.117. The Resultant Growth Patterns.

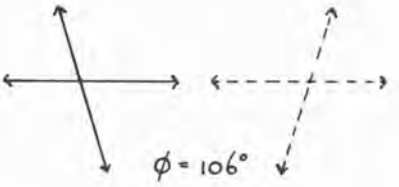

Fig.118a. Vector Diagrams for Velocities of Advance of Growth Edges.

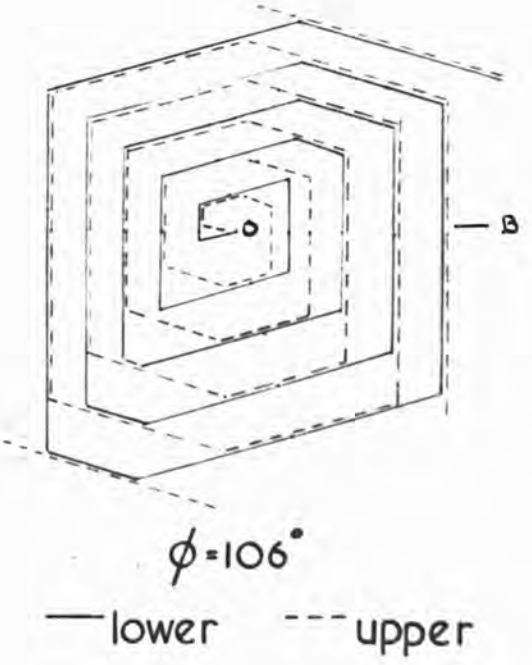

Fig.118b. The Resultant Growth Pattern.

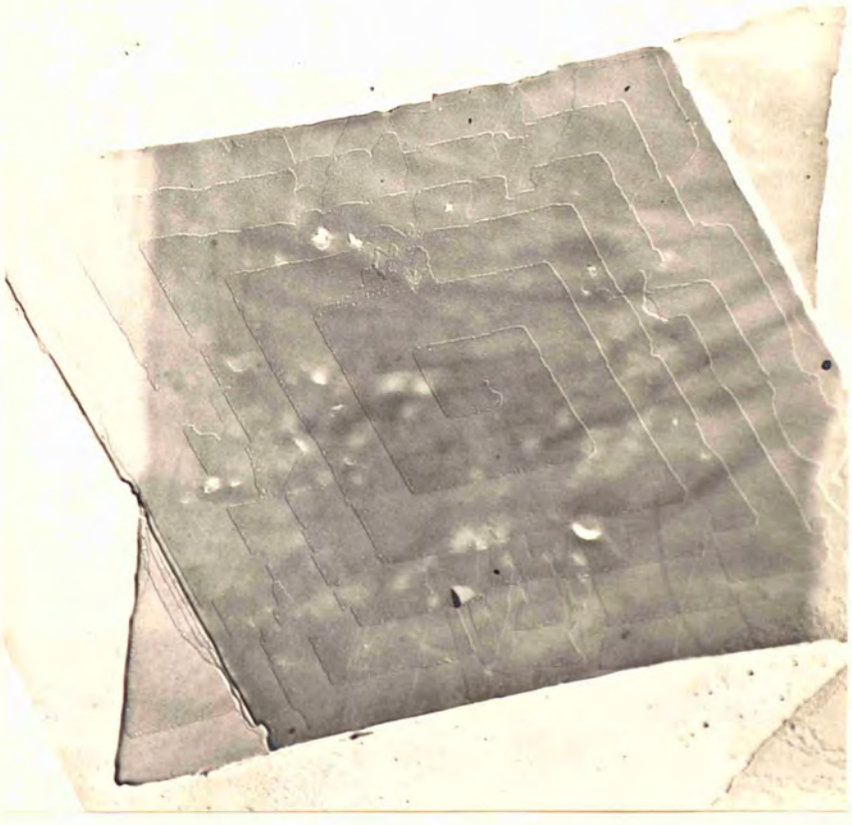

Fig.119. Behenic Acid. Spiral Growth on a Twinned Crystal. $d_n < h_1$. Electronmicrograph. x5900.

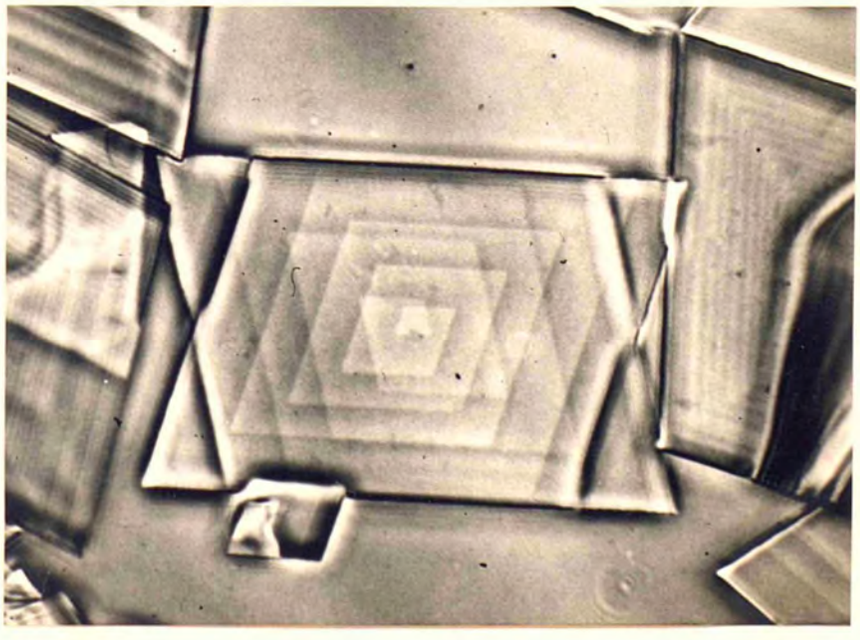

Fig.120. Behenic Acid. Two Spirals in Twinned Orientation revealed by Internal Slip. Crystal Opaquely Silvered. $d_n < h_1$. Reflexion Phase Contrast. x1100.

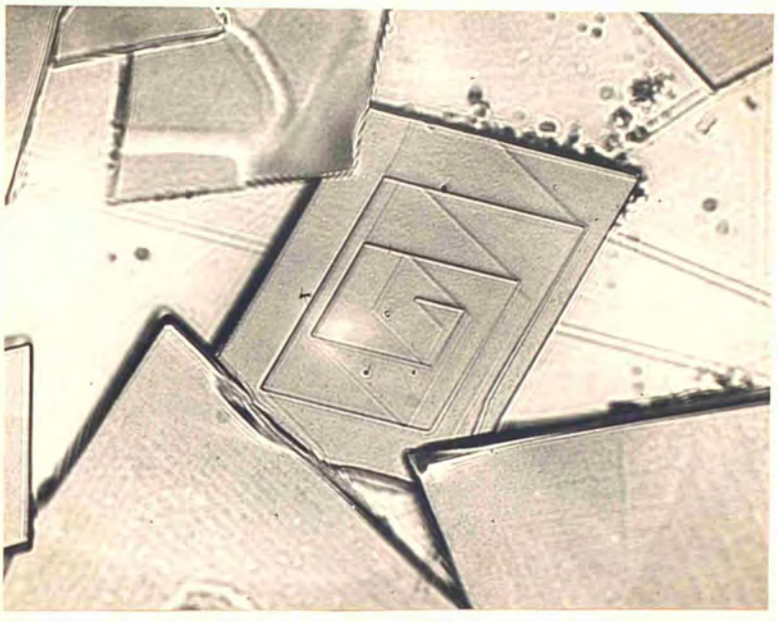

Fig.121. Stearic Acid. Two Spirals in Twinned Orientation. $h_2 > d_n > h_1$.
Crystals Opaquely Silvered.
Reflexion Bright-field. x680.

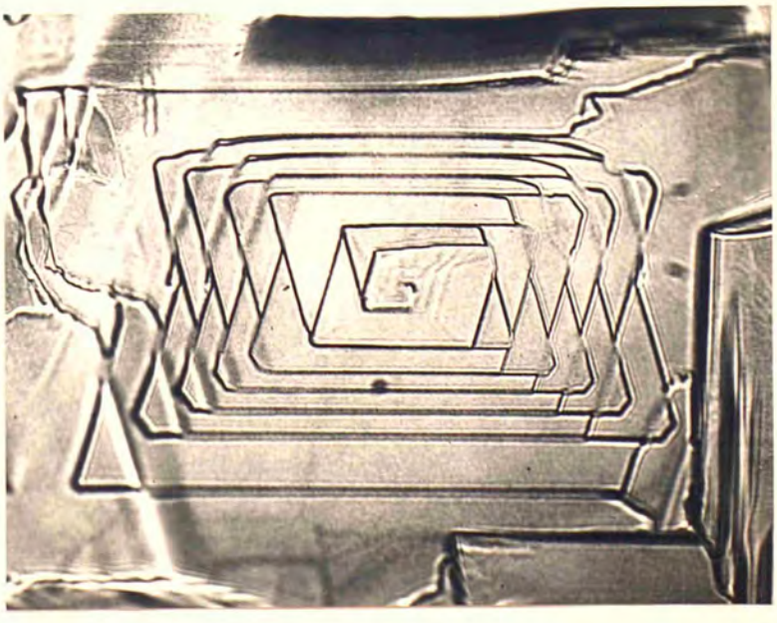

Fig.122. Stearic Acid. Two Spirals in Twinned Orientation. $h_2 > d_n > h_1$. $\phi = 106°$.
Crystals Opaquely Silvered.
Reflexion Bright-field. x700.

Fig.123. Stearic Acid. Two Spirals in Twinned Orientation. $h_2 > d_n > h_1$. $\phi = 74°$ Reflexion Bright-field. x660.

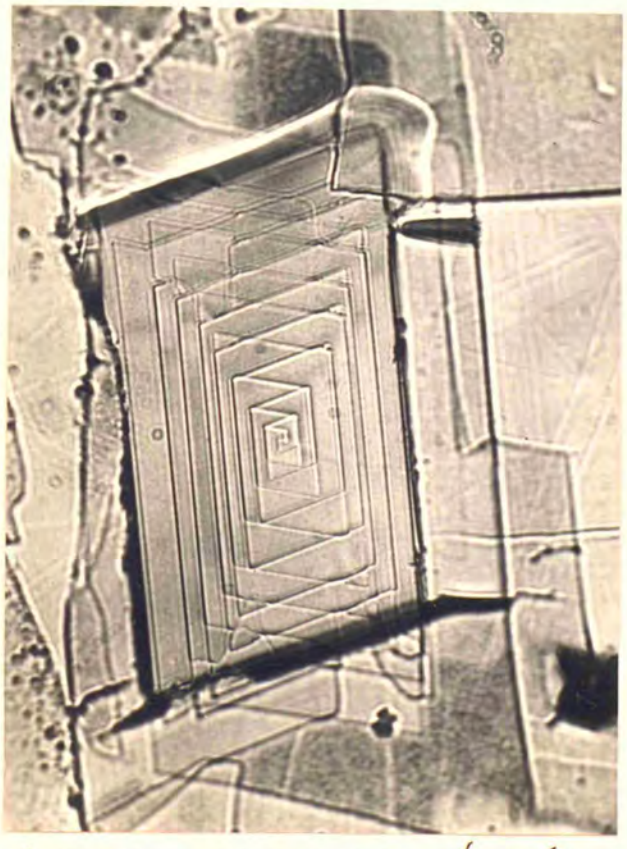

Fig.124. Stearic Acid. $\phi = 106°$ Upper Surface Silvered, Reflectivity ~85%. Reflexion Bright-field. x480.

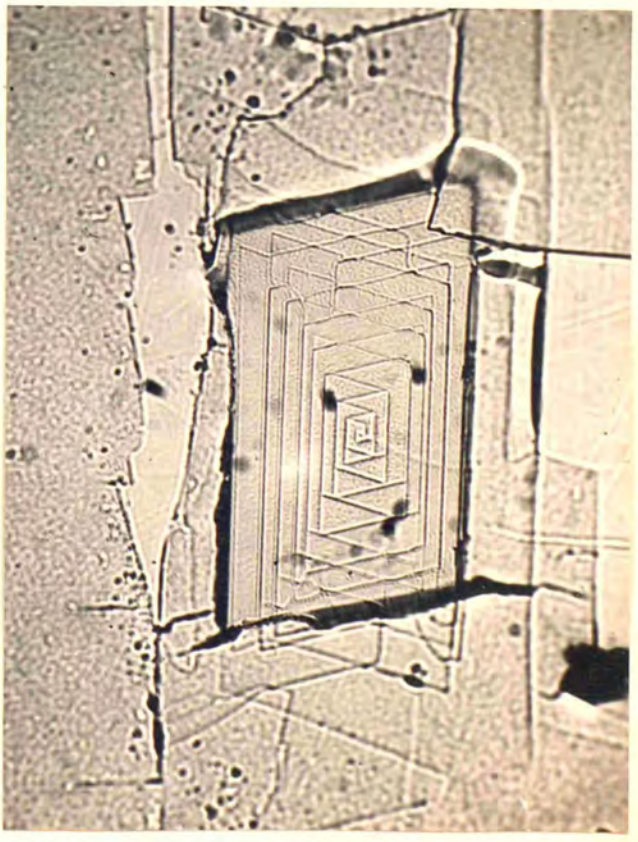

Fig.125. Stearic Acid. Crystal Opaquely Silvered. Reflexion Bright-field.

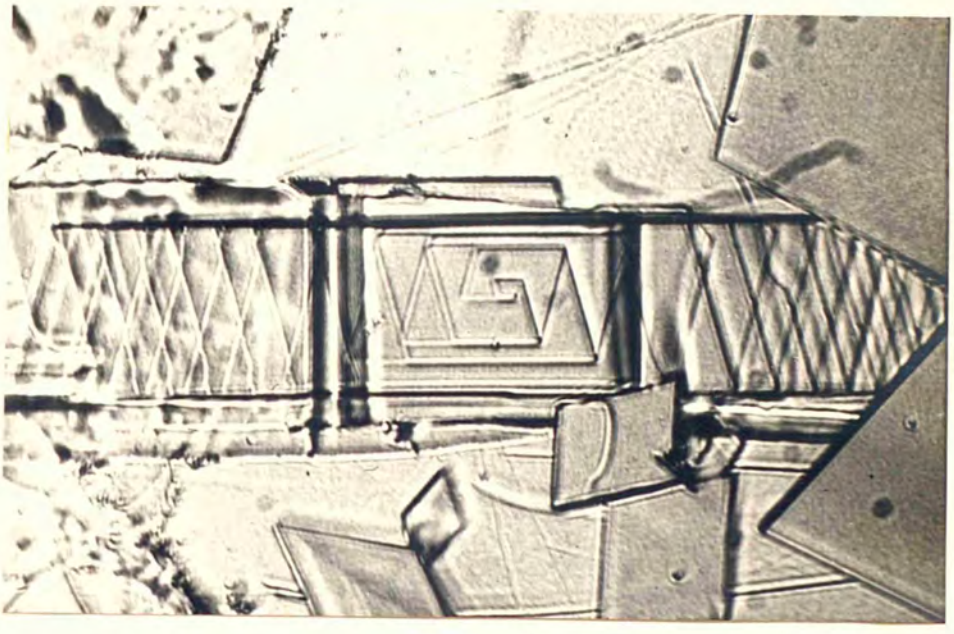

Fig.126. Stearic Acid. Two Spirals in Twinned Orientation. $h_2 > d_n > h_1$. $\phi = 106°$
Crystal Opaquely Silvered.
Reflexion Bright-field. x870.

Fig.127. Behenic Acid. Twinned Crystal.
Electronmicrograph. x3800.

Fig.128. Behenic Acid. Transmission Electron Diffraction Pattern. Incident Beam Normal to Basal Plane.

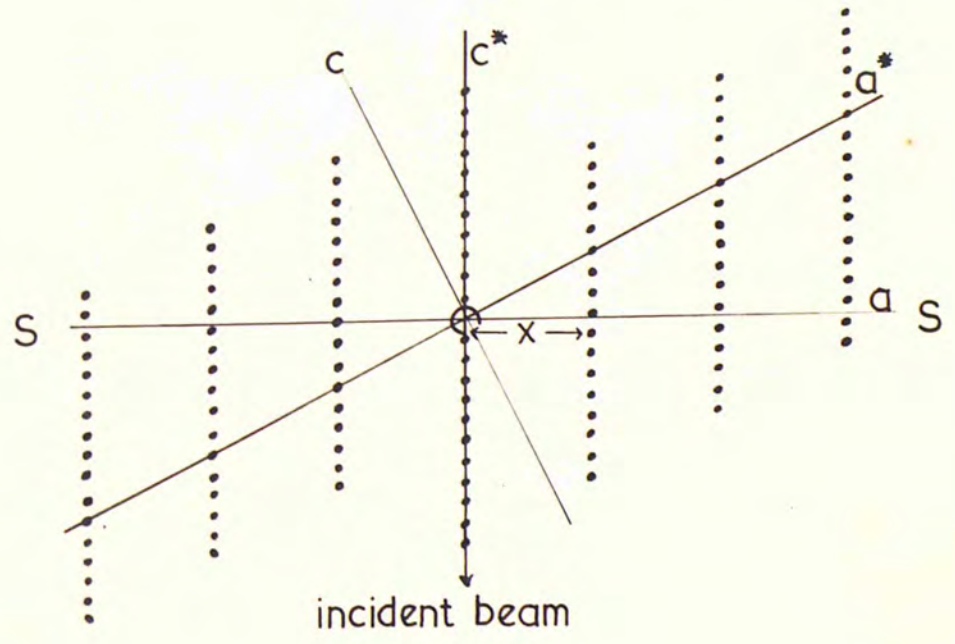

Fig.129. Reciprocal Lattice and Sphere of Reflexion.

a)

b)

c)

d)

Fig.130. Behenic Acid. Transmission Electron Diffraction Patterns. Photographs taken at 10sec. intervals.

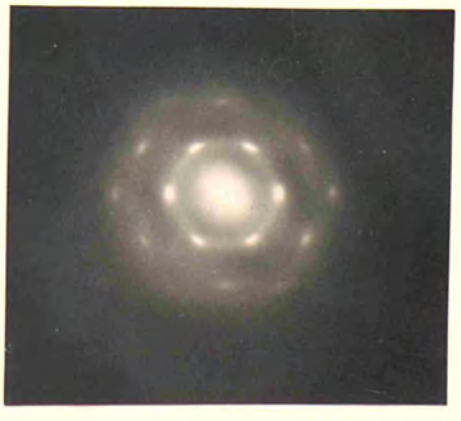

Fig.131. Behenic Acid. The Final Stage of the Diffraction Pattern.

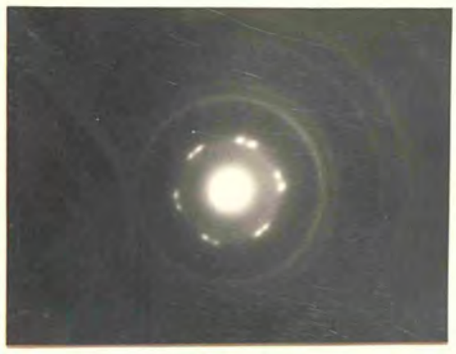

Fig.132. Behenic Acid. Transmission Electron Diffraction Pattern from the Twinned Crystal shown in Fig.133..

Fig.133. Behenic Acid. Twinned Crystal. Electronmicrograph. x31000.

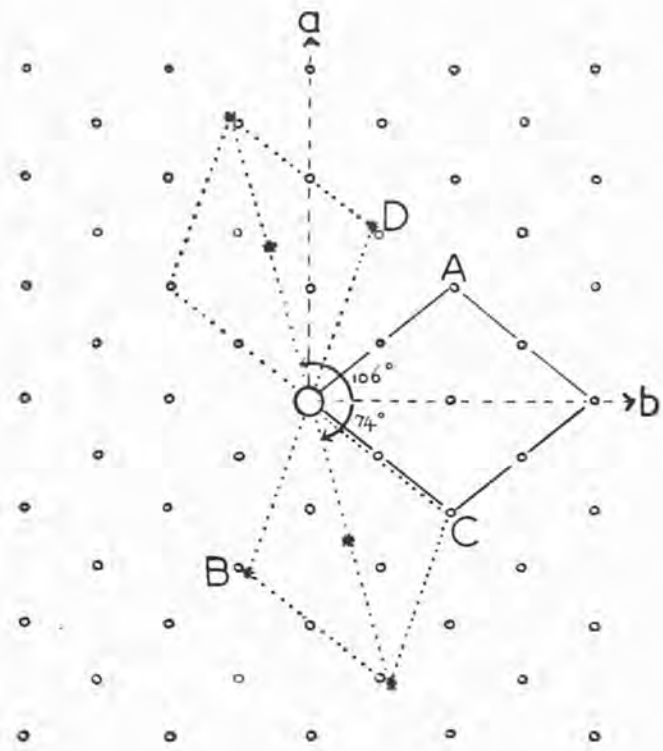

Fig.134. The Packing in the Plane of Contact.

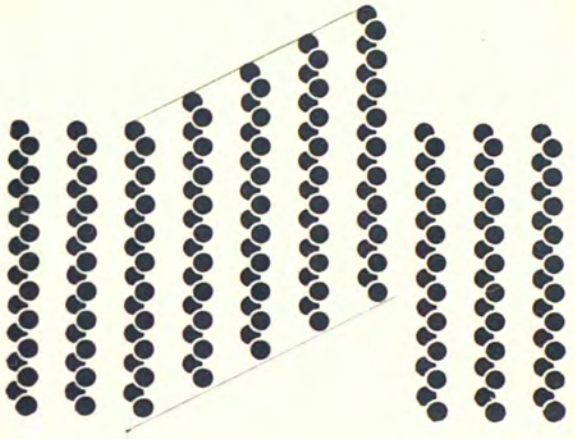

Fig.135. A Succession of Small Stacking Faults in an Orthorhombic Paraffin. (Anderson and Dawson).

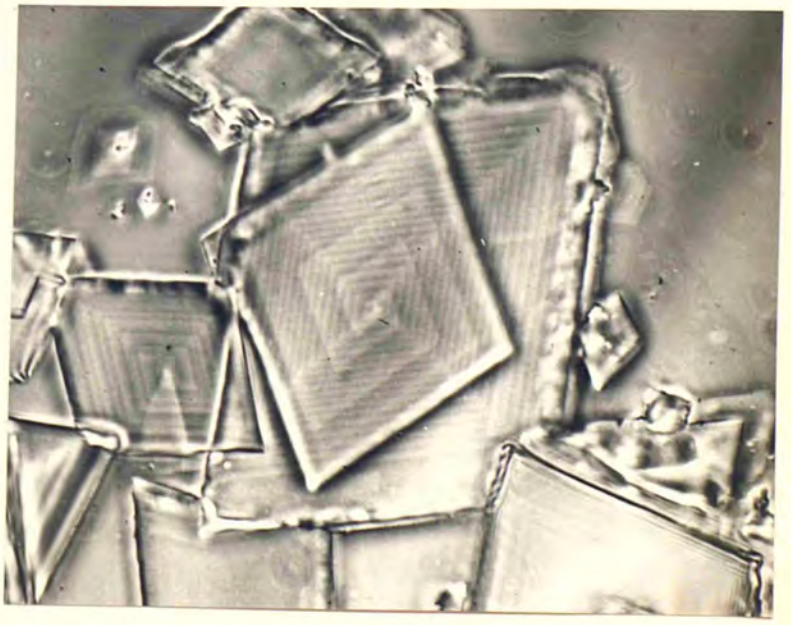

Fig.136. Behenic Acid. Spiral Growth on Randomly Misoriented Crystals. Crystals Opaquely Silvered. Reflexion Phase Contrast. x820.

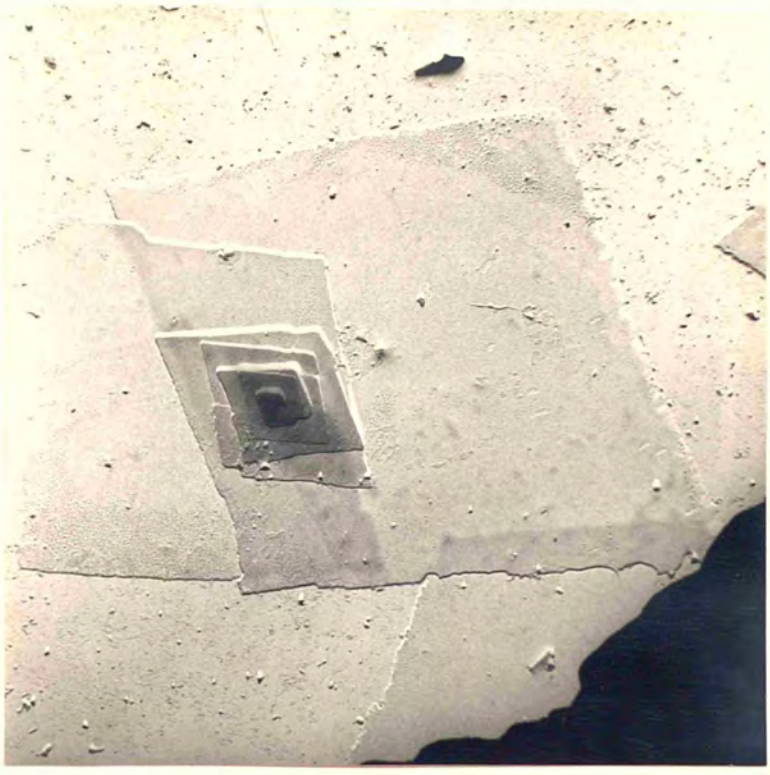

Fig.137. Behenic Acid. Interleaved Growth Spirals
in Random Orientation.
Electronmicrograph. x4000.

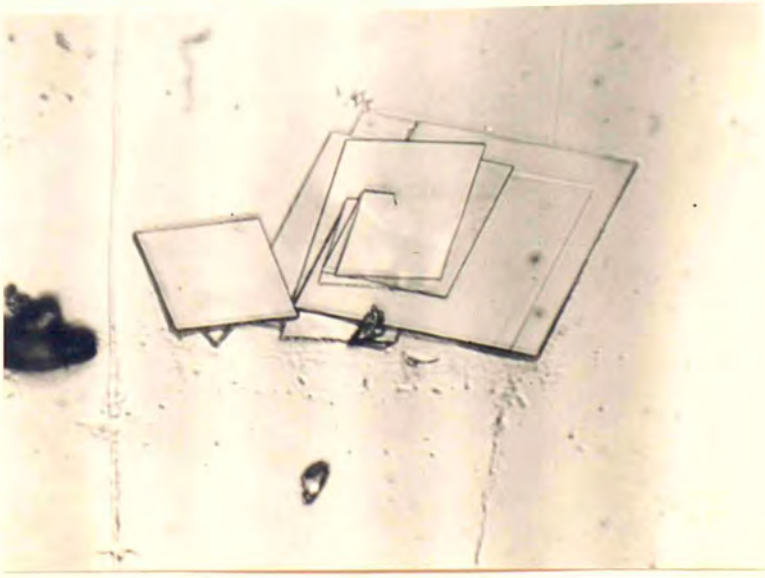

Fig.138. Stearic Acid. Interleaved Growth Spirals
in Random Orientation.
Crystals Opaquely Silvered.
Reflexion Bright-field. x510.

Fig.139. Behenic Acid. Interleaved Growth Spirals
in Random Orientation.
Electronmicrograph. x5900.

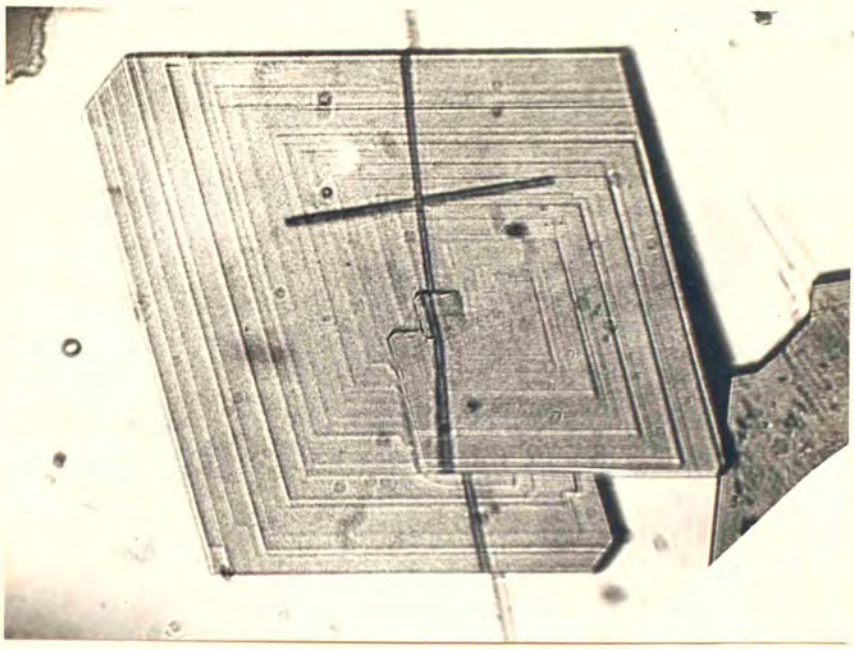

Fig.140. Stearic Acid. Spiroidal Crystal.
Oblique Reflexion Bright-field.
x560.

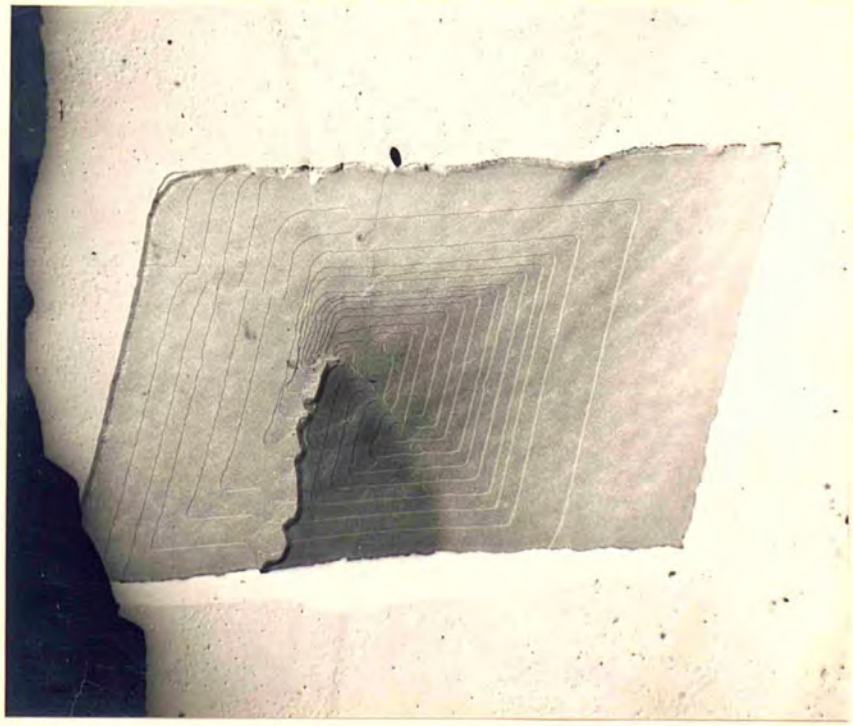

Fig.141. Behenic Acid. Spiroidal Crystal.
Electronmicrograph. x5500.